CLIMATE ASSESSMENT FOR 2001

BY A. M. WAPLE, J. H. LAWRIMORE, M. S. HALPERT, G. D. BELL, W. HIGGINS, B. LYON, M. J. MENNE, K. L. GLEASON, R. C. SCHNELL, J. R. CHRISTY, W. THIAW, W. J. WRIGHT, M. J. SALINGER, L. ALEXANDER, R. S. STONE, AND S. J. CAMARGO

TABLE OF CONTENTS

AFFILIATIONS: Waple—NOAA/National Climatic Data Center and STG Inc., Asheville, North Carolina; Lawrimore, Menne, and Gleason—NOAA/National Climatic Data Center, Asheville, North Carolina; Halpert, Bell, Higgins, and Thiaw—Climate Prediction Center, NOAA/NWS/NCEP, Washington, D.C.; Lyon and Camargo—International Research Institute for Climate Prediction, Lamont–Doherty Earth Observatory, Palisades, New York; Schnell—Climate Monitoring and Diagnostics Laboratory, NOAA, Boulder, Colorado; Christy—University of Alabama at Huntsville, Huntsville, Alabama; Wright—National Climate Center, Australian Bureau of Meteorology, Melbourne, Australia; Salinger—National Institute for Water and Atmospheric Research, Auckland, New Zealand; Alexander—Hadley Center for Climate Prediction and Research, Met Office, Bracknell, Berkshire, United Kingdom; Stone—Cooperative Institute for Research in Environmental Sciences, University of Colorado, Boulder, Colorado

CORRESPONDING AUTHOR: Anne M. Waple, STG Inc., National Climatic Data Center, NOAA/NESDIS, 151 Patton Avenue, Asheville, NC, 28801-5001
E-mail: Anne.Waple@noaa.gov

ABSTRACT

Global temperatures in 2001 were 0.51°C (0.92°F) above the long-term (1880–2000) average, which places 2001 as the second warmest year in the 122-year instrumental record. Land temperatures were 0.75°C (1.35°F) above average and ocean temperatures were 0.40°C (0.72°F) above the 1880–2000 mean. This ranks them as the second and third warmest on record, respectively. The Northern Hemisphere temperature continued to average near record levels in 2001 at 0.60°C (1.08°F) above the long-term average. The Southern Hemisphere also reflects the globally warmer conditions, with a positive anomaly of 0.43°C (0.77°F).

Annual anomalies in excess of 1.0°C (1.8°F) were widespread across North America and much of Europe and the Middle East, while significantly cooler than average conditions were confined to western Australia, the northeast and northwest Pacific Ocean, and the far southeastern region of the Pacific, near coastal Chile.

Although no hurricanes made landfall in the United States for the second consecutive year, it was nonetheless an extremely active Atlantic hurricane season, the fourth most active on record. Tropical Storm Allison became the costliest tropical storm on record when it caused approximately $5 billion worth of damage in the southern and southeastern United States. The season was slow to start but quickly escalated in the last three months of the season and it was the first time in recorded history that three hurricanes formed in the Atlantic in the month of November.

The long-running La Niña episode finally came to an end in 2001. The La Niña, which began in mid-1998 persisted through the first half of the year but gave way to neutral ENSO conditions for the latter half.

Other notable events in 2001 include extreme cold and snow in Siberia during the 2000–01 boreal winter, ongoing drought in the Middle East and central Asia, drought in Central America and Brazil, near-record flooding in central/eastern Europe, an extremely wet austral spring in northeastern Argentina, severe moisture deficits in some regions of the United States, and the driest year on record in parts of western Australia.

1. INTRODUCTION

This is the twelfth year that the Climate Assessment has been written to summarize the state of the earth's climate. This assessment contains analyses of the global climate system for 2001 including significant events and their impacts, and atmospheric dynamics that have influenced weather and climate over the year. The report also seeks to place the climate of 2001 in historical perspective by analyzing the trends in temperature, precipitation, and trace gases over the last century, during which the instrumental record illustrates a variable and changing climate system.

The National Climatic Data Center has taken the lead in producing the assessment for the second consecutive year. However, it is a cooperative effort that includes contributions from scientists around the country and the world, including the Climate Prediction Center, the International Research Institute for Climate Prediction, the Climate Monitoring and Diagnostics Laboratory, the Australian Bureau of Meteorology, the U.K. Met Office, Rutgers University, the New Zealand National Institute for Water and Atmospheric Research, and the Cooperative Institute for Research in Environmental Sciences (CIRES). The analyses within this report rely on data from a number of different sources. These include 1) land surface temperature and precipitation data from the Global Historical Climatology Network (Peterson and Vose 1997; Vose et al. 1992), and the United States Historical Climate Network (Easterling 1996); 2) surface temperature data from a land–sea blended dataset (Jones et al. 2001); 3) gridded analyses from the National Centers for Environmental Prediction–National Center for Atmospheric Research (NCEP–NCAR) Climate Data Assimilation System/50-year reanalysis (Kistler et al. 2001); 4) satellite data; and 5) ship reports. Due to the large number of data sources used throughout this report, it is not possible to refer to one standard base period.

Section 2 includes a review of the global-scale climate in 2001. Surface temperature and upper-air temperatures are examined, as well as global precipitation and Northern Hemisphere snow cover. Section 3 addresses the global trends and impacts of trace gases, while conditions in the Tropics and polar regions are discussed in sections 4 and 5, respectively. Section 4 includes an assessment of ENSO, which began the year in its cold phase, and transitioned to neutral conditions by midyear. The tropical storms of the Atlantic and Pacific are also reviewed in this section. Section 5 includes a review of the climate of the Arctic and Antarctic with a summary of sea ice conditions and stratospheric ozone. Section 6 addresses regional climate highlights throughout 2001 including extreme drought in parts of Asia and the United States, Central America, Brazil, East Africa, and Australia. Extreme winter temperatures in Siberia are discussed as well as flooding in Europe and Argentina. The climate of Australia, New Zealand, and the South Pacific are also reviewed in this section. The 2001 assessment

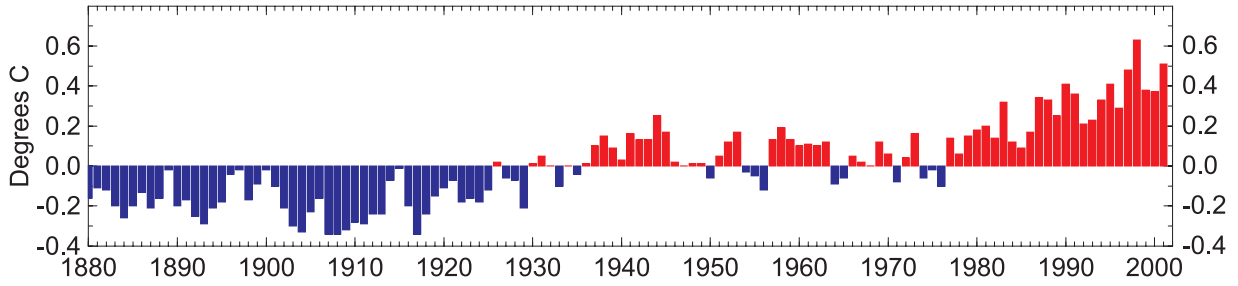

Fig. 1. Global mean annual surface temperature anomalies (°C) 1880–2001. Anomalies are departures from an 1880–2000 base period and include both land and SST observations.

concludes with a section illustrating surface and upper-air temperatures for each season over the globe. While each section is essentially self-contained, frequent cross-referencing between sections occurs throughout the text.

2. GLOBAL CLIMATE

a. Surface temperature

Mean annual surface temperature values for the globe are calculated by averaging gridded values of temperature anomalies based on a network of more than 1000 in situ observing stations (Peterson and Vose 1998) and a blended sea surface temperature dataset (Reynolds and Smith 1994; Smith et al. 1996). The blend of sea surface temperature values is produced from a combination of satellite observations and ship and ocean buoy measurements. Based on these land and ocean surface temperature observations, the mean global surface temperature for 2001 was 0.51°C above the 1880–2000 average (0.29°C above the 1971–2000 annual average). Consequently, 2001 ranks as second warmest in the 1880–2001 period, 0.12°C cooler than the record warmest year of 1998, and 0.14°C above the value for 2000.

Global mean annual surface temperature anomalies for the period 1880–2001 are shown with respect to the long-term (1880–2000) base period in Fig. 1. The top five warm years in the observed record now include, in descending order: 1998, 2001, 1997, 1995, and 1990. Eight of the 10 warmest years have occurred since 1990. In the 122-yr period of record, the most recent year to rank within the cold third of the historic distribution was 1956, a year in which the average temperature was −0.12°C below average. The most recent year to average below the 1880–2000 mean was 1976. While global mean surface temperatures have not increased monotonically over the period of record, when viewed as a linear trend, surface temperatures have warmed at a rate of 0.06°C per decade since 1900. Since 1977, however, the rate of increase has been closer to 0.2°C decade^{-1}.

Two calendar-month record high temperature departures were set in October and November 2001 when global land and sea surface temperatures averaged 0.37° and 0.42°C above the 1971–2000 October and November means, respectively. Serial monthly global mean temperature anomalies for the period

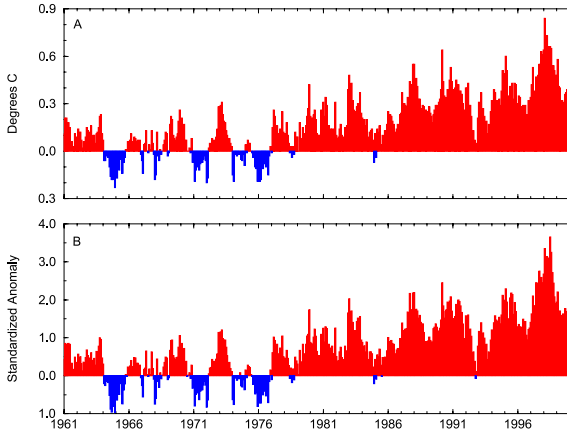

Fig. 2. Global mean monthly surface temperature anomalies, 1961–2001, expressed as (a) the departure from the 1880–2000 monthly mean, and (b) as a standardized anomaly (z score) based on the mean and variance for each calendar month.

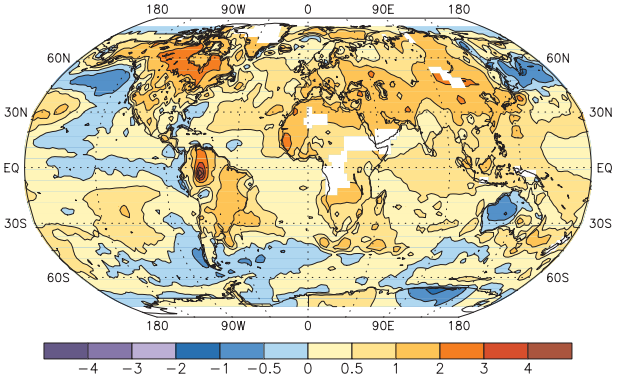

Fig. 3. Mean annual surface temperature (°C) for 2001. Anomalies are departures from a 1971–2000 base period.

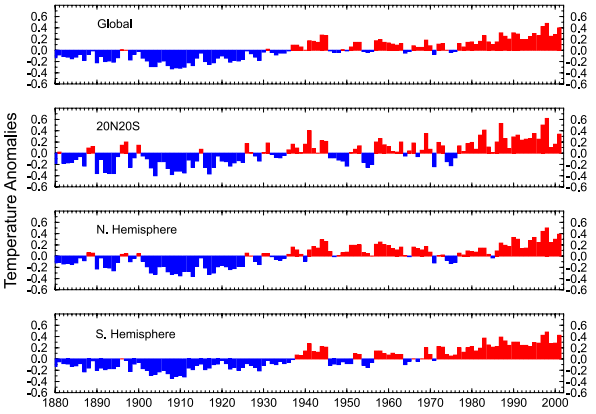

Fig. 4. Mean annual SST anomalies (°C): (a) Global, (b) 20°S–20°N, (c) Northern Hemisphere, (d) Southern Hemisphere. Anomalies are departures from an 1880–2000 base period.

1961–2001 are shown with respect to a 1880–2000 base period in Fig. 2a. The record high temperature anomaly for any month in the 1880–2001 period of record was set in February 1998 when surface temperatures averaged 0.84°C above the 1971–2000 February mean. Since there is a distinct annual cycle to monthly temperature variance, global monthly surface temperature departures are also shown as standardized anomalies (*z* scores) in Fig. 2b. The largest *standardized* anomaly for any month occurred in July 1998, followed by the February 1998 standardized value. Eight of the current monthly global surface temperature records were established during January–August 1998; the September and December monthly records occurred in 1997, and the October and November records occurred in 2001 (the October anomaly equaled that of October 1997). The record high global monthly temperatures observed in 2001 for October and November were set during the very warm boreal autumn (September–November) season when nearly all of the land surface areas of the world averaged above the 1971–2000 mean (see Fig. 86).

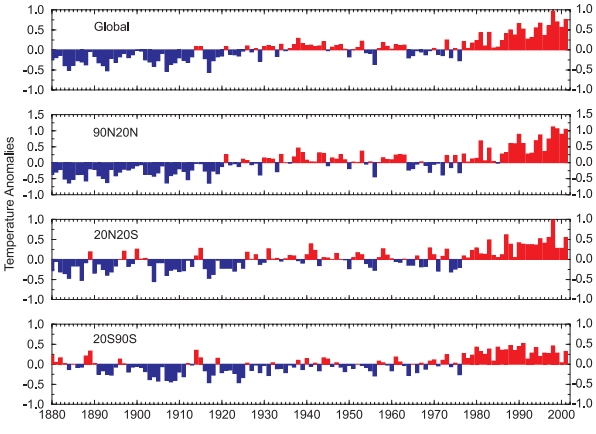

Fig. 5. Mean annual land surface temperature anomalies (°C): (a) Global, (b) 20°–90°N, (c) 20°S–20°N, (d) 90°–20°S. Anomalies are departures from an 1880–2000 base period.

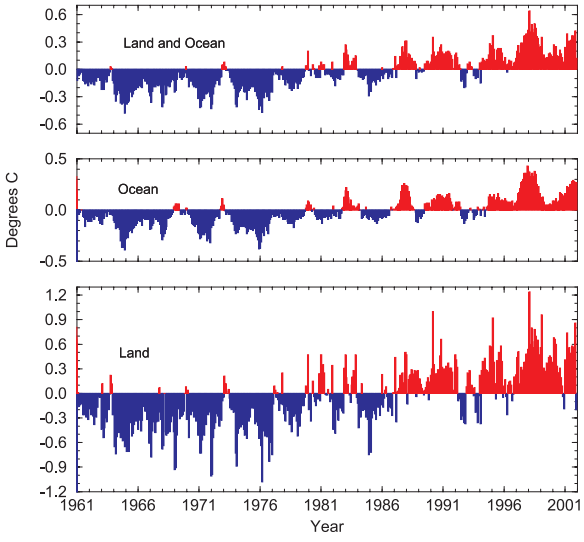

Fig. 6. Mean monthly surface temperature anomalies (°C), 1961–2001. (a) Global, (b) sea surface only, (c) land surface only. Anomalies are departures from a 1971–2000 base period.

The geographic distribution of mean annual global surface temperature anomalies for 2001, with respect to a 1971-2000 base period, is shown in Fig. 3. While ENSO neutral conditions were giving way to indications of a developing El Niño by year's end, negative annually averaged anomalies are evident in the eastern tropical Pacific (see section 4a). Cooler-than-average annual SSTs also were present across portions of the Southern Ocean and the North Pacific. Notwithstanding the presence of these negative anomalies, globally averaged SSTs in 2001 ranked as third warmest over the 122-yr period of record (Fig. 4a), the top five warm years being (in descending order): 1998, 1997, 2001, 1987, and 2000. Sea surface temperatures in the Tropics (Figs. 4b–d) ranked as eighth warmest, but temperatures south and north of the equator ranked as second and third warmest on record, respectively.

The majority of the earth's land surface averaged above the 1971–2000 mean in 2001, most notably across much of Canada [see section 6a(4)], where positive anomalies exceeded 2°C in many areas. Below average surface anomalies were largely confined to Australia where persistent negative anomalies, espe-

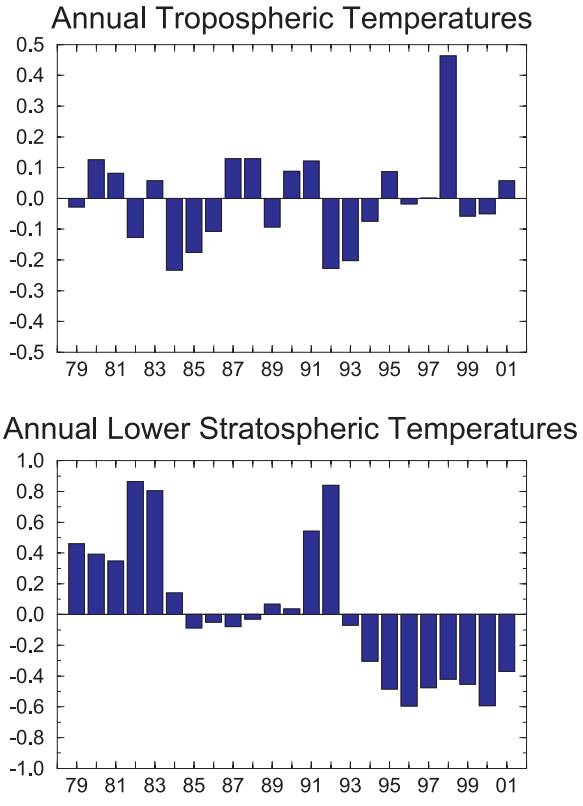

FIG. 7. Annual global temperature anomalies derived from MSU/AMSU lower-troposphere retrieval (top) and MSU channel 4 (and AMSU channel 9) for the stratosphere (bottom). Anomalies are departures from the 1979–98 base period means (top) and from the 1984–90 base period (bottom). (Data provided by the University of Alabama in Huntsville.)

cially in western regions, were found throughout much of 2001 (Figs. 80, 82, 84, 86, and section 6g). Land surface temperatures, averaged globally, ranked as second warmest over the period of record with a departure from the 1880–2000 mean of 0.75°C (Fig. 5a). The five warmest years for land areas are 1998, 2001, 1999, 1995, and 1990.

Land surface temperature anomalies, with respect to a 1880–2000 base period and stratified by latitude band, are shown in Figs. 5b–d. Land surface temperatures averaged across the mid- and high latitudes of the Southern Hemisphere were characterized by smaller anomalies than those for higher latitudes. Between 20° and 90°S, the land surface temperature for 2001 ranks as twelfth warmest, while across the latitude bands 20°–90°N and 20°N–20°S average temperatures ranked as third warmest. The return of record or near-record near-surface temperature anomalies in 2001 can be seen in Fig. 6, which depicts serial monthly anomalies for the period 1961–2001.

b. Upper-air temperature

Annual anomalies of the globally averaged, bulk atmospheric temperatures for the troposphere and lower stratosphere are shown in Fig. 7. These temperatures are derived from the microwave emission of atmospheric molecular oxygen and monitored by Microwave Sounding Units (MSUs) and the Advanced MSUs (AMSUs since 1998) that are flown as part of the instrument suite on the National Oceanic and Atmospheric Administration's (NOAA) polar-orbiting satellites (Christy et al. 2000). Biases and errors due to spacecraft orbital drift (in both time and space) and on-orbit calibration changes have been identified and removed. Though the MSUs and the AMSUs measure slightly different bandpass widths, a linear combination of the data from various AMSU viewing angles produces the necessary representation of the original MSU weighting functions.

1) TROPOSPHERE

The global tropospheric anomaly (roughly the mean temperature from the surface to 8-km altitude) was slightly warmer than the 20-yr (1979–1998) average at +0.08°C, the eighth warmest of the 23-yr series (Fig. 7, top). The overall trend since 1979 is +0.05°C decade^{-1}.

The geographical distribution of the 2001 tropospheric anomalies for each half of the year is shown in Fig. 8. The influence of La Niña conditions during the first half of 2001 is evident as negative anomalies in the tropical eastern Pacific. Extensive regions in the midlatitudes of both hemispheres were warmer than average. This midlatitude warmth was even more intense and generally more widespread in the second half of the year, particularly over North America and the Argentine Basin. The globally averaged anomaly was 0.03°C in January–June and 0.13°C in July–December.

The difference in temperature trends over the past 23 years between the surface and the troposphere in the Tropics continued in 2001 with divergence relative to 1979–80 amounting to a statistically significant temperature difference of about 0.5°C (Christy et al. 2001). These findings have been supported by comparisons using other upper-air datasets based on radiosondes and meteorological analyses (Hurrell et al. 2000; Stendel et al. 2000) and by a radiosonde-based calculation of steepening lapse rates (Gaffen et al. 2000). However, trend differences between the troposphere and surface in some continental regions, such as North America and Europe, are virtually zero (Houghton et al. 2001; Lawrimore et al. 2001).

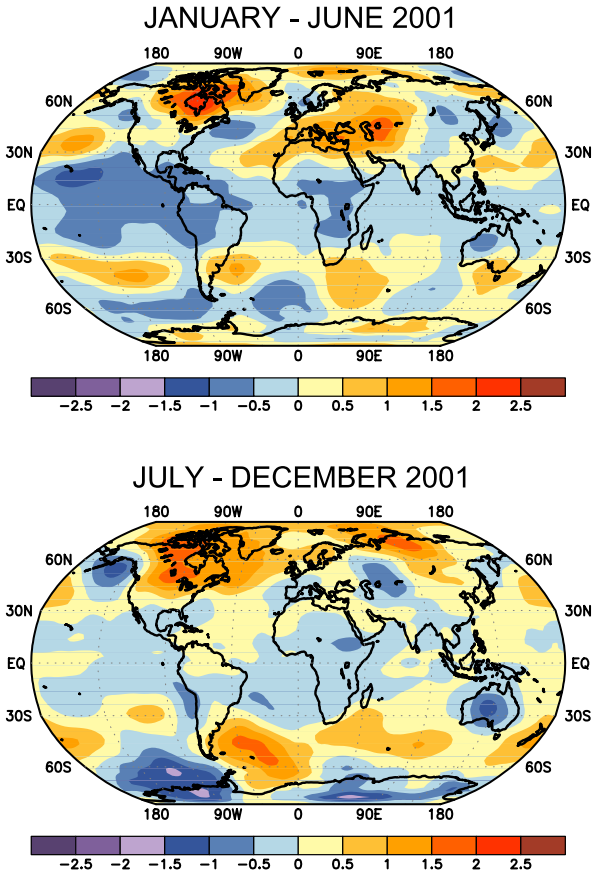

Fig. 8. Mean tropospheric temperature anomalies (°C) for (a) Jan–Jun 2001 and (b) Jul–Dec 2001 derived from the MSU/AMSU lower-troposphere retrieval. Anomalies are departures from the 1979–98 base period means. (Data provided by the University of Alabama in Huntsville.)

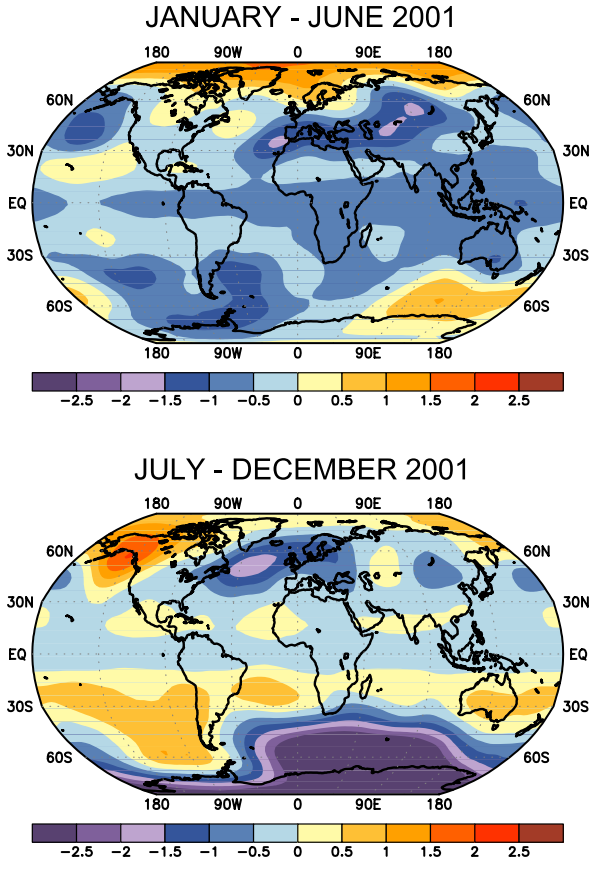

Fig. 9. Mean stratospheric temperature anomalies (°C) for (a) Jan–Jun 2001 and (b) Jul–Dec 2001 derived from the MSU channel 4 (and AMSU channel 9). Anomalies are departures from the 1984–90 base period means. (Data provided by the University of Alabama in Huntsville.)

2) Lower Stratosphere

Lower stratospheric temperatures, which represent the temperature in the layer 16–23 km above the surface, have remained below average since 1993. The warm anomalies in 1991 and 1992 are a result of the aerosol loading of the stratosphere due to Mt. Pinatubo in 1991 (Fig. 7, bottom). For the year as a whole, there were widespread negative anomalies, peaking in Antarctica, east of the Weddell Sea to the South Pole. This prominent cold region was the dominant feature in the second half of the year when the ozone concentration reached its minimum near the end of September (Fig. 9) In examining the seasonal and geographic distribution of the negative stratospheric temperature anomalies it is clear that they are consistent with the depletion of ozone (Chanin and Ramaswamy 1999).

The stratosphere began the year in the easterly or cold phase of the quasi-biennial oscillation (QBO), thus producing substantial negative anomalies in the equatorial band. The winds began shifting to a more westerly phase in the latter half of 2001, reducing the cooling signature for July–December as shown in Fig. 9.

A North Polar sudden stratospheric warming in February 2001 produced a monthly anomaly of +15°C at those high latitudes that impacted the 6-month average (Fig. 9). In contrast, 2000 North Polar stratospheric temperatures remained over 6°C below average throughout January–March (Lawrimore et al. 2001).

c. Global precipitation

As in 1999 and 2000, precipitation patterns throughout many areas of the globe continued to be influenced by La Niña in early 2001, but with the end of the cold phase of ENSO by June, traditional La Niña signatures became less evident during the latter half

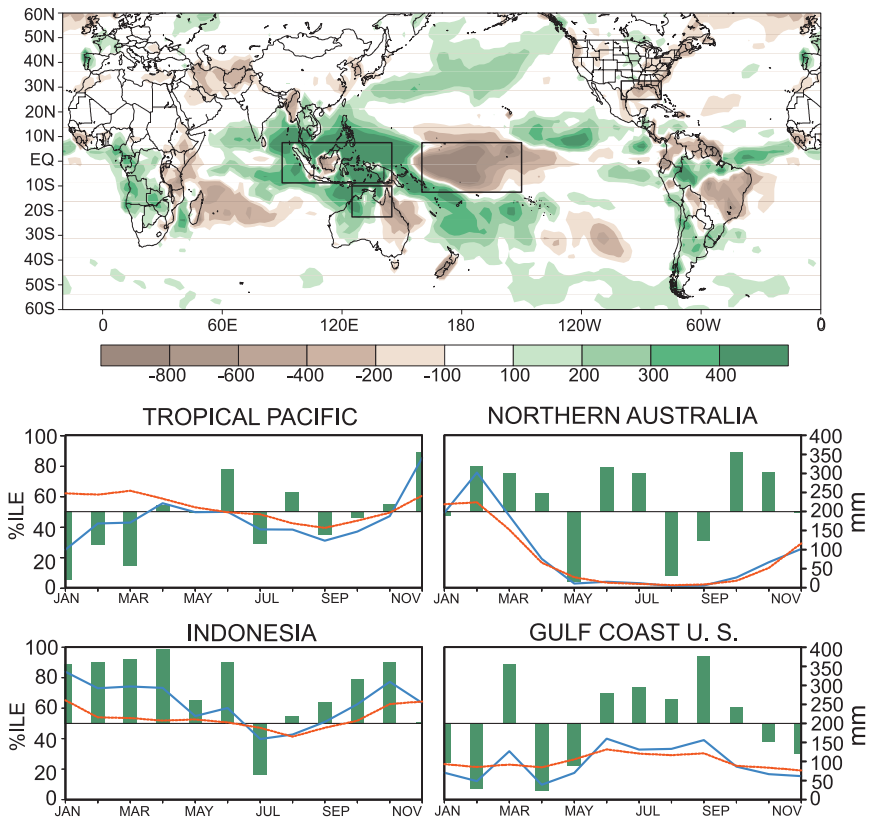

Fig. 10. Jan–May 2001 accumulated precipitation anomaly (top), and regional area-averaged estimates of monthly mean precipitation amounts (mm, blue lines) and precipitation percentiles (%, bars) during 2001 for the four boxed regions shown in (top). The monthly precipitation climatology (mm, dashed, red lines) is the 1979–95 base period monthly means. The percentiles are labeled on the left-hand vertical axis and totals are labeled on the right-hand vertical axis. Precipitation amounts are obtained by merging rain gauge observations and satellite-derived precipitation estimates (Janowiak and Xie 1999).

of the year. Precipitation anomalies consistent with past cold episodes (e.g., Ropelewski and Halpert 1989) were confined to regions in the Tropics and subtropics extending from the eastern Indian Ocean eastward to the central Pacific and along the Gulf Coast of the United States during January–May 2001 (Fig. 10). Positive precipitation anomalies were observed over Indonesia, the eastern half of the tropical Indian Ocean, Southeastern Asia, northern Australia, and the western and central subtropical South Pacific. This enhanced rainfall occurred during the rainy season in each of these areas, in association with a La Niña–related enhancement of the regional monsoon system. During the second half of the year, precipitation throughout the Tropics was highly variable, as a result of near-neutral ENSO and strong Madden–Julian oscillation (MJO) activity.

In contrast, significantly below-average rainfall was recorded over the central and west-central tropical Pacific throughout the early part of the year, in response to the La Niña–related suppression of tropical convection in that region. In the extratropics, the Gulf Coast of the United States also experienced below-average rainfall during the January–May period. Long-term dryness has affected this region since late 1998 (Lawrimore et al. 2001; Bell et al. 2000) in association with the persistent La Niña episode. However, rainfall was above normal during the June–October period.

The distribution and intensity of tropical convection represents a primary forcing on the atmospheric circulation via modulation of the wind and mass fields throughout the global Tropics and subtropics. During December–January–February (DJF) and March–April–May (MAM), the patterns of tropical convection typically associated with cold episodes prevailed, with enhanced convection [indicated by negative anomalies of outgoing longwave radiation (OLR)] observed across the climatologically convective regions of Indonesia and the western equatorial Pacific, and suppressed convection dominating the central Pacific (indicated by positive OLR anomalies shown; Figs. 11a,b). This pattern weakened during JJA (Fig. 11c) and SON (Fig. 11d), with near-normal convection found throughout most of the Tropics.

For the globe as a whole, precipitation over land areas was less than the 1961–1990 average (−1.9 %) for the first time since 1997. Globally averaged precipitation was more than 3% above normal in 1999 and 2000. Both the first and the last half of 2001 were drier than normal, −2.0% and −1.7% below normal, respectively. During the January–June period (Fig. 12a), the largest areas of drier-than-normal conditions occurred in the northern half of South America, across much of China through South-Cen-

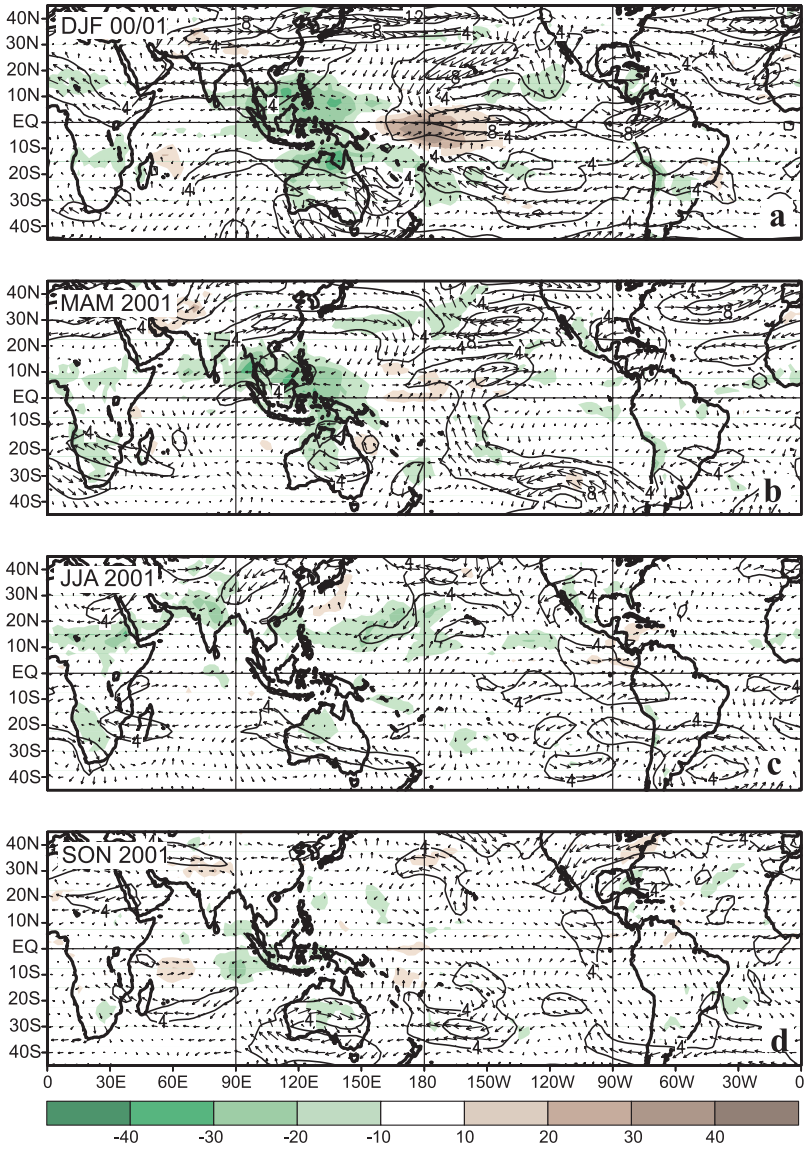

Fig. 11. OLR anomalies (shaded) and 200-hPa vector wind anomalies and isotachs for (a) DJF 2000/01, (b) MAM 2001, (c) JJA 2001, and (d) SON 2001. Contour interval for isotachs is 4 m s^{-1}. Shading interval for OLR anomalies is 10 W m^{-2}. Anomalies are departures from the 1979–95 base period monthly means.

tral Asia. A large part of the western United States and Canada were also drier than average as well as large parts of eastern and western Australia. In many of these regions, persistent negative precipitation anomalies contributed to developing or worsening drought conditions. Drought conditions continued for a third or fourth straight year in a large part of southern Asia (see section 6f). In Brazil an extremely dry austral summer and fall and heavy dependence on hydroelectric power led to severe energy shortages. Drought was also severe in the western United States and Canada as well as China in 2001 (see section 6a).

Wetter-than-normal conditions were most prevalent in the mid- to high latitudes of the Northern Hemisphere. Positive anomalies covered a large part of Europe through central Russia and the total within the region north of 55°N was 11.8% above normal.

Much of India was also wetter than normal during the first half of the year with the largest anomalies in the northwestern provinces. The premonsoon season (March–May) and first month of the Southwest monsoon season (June) were wetter than average for the country as a whole (104% and 133%, respectively). But drier-than-average conditions were predominant from July to September and precipitation during the monsoon season was 92% of normal (see section 6f). Precipitation totals during the last six months of the year (Fig. 12b) were below normal throughout almost all parts of India. In the northeastern United States, drought developed during the latter half of the year due to persistently drier-than-normal conditions (see section 6a). Six-month totals were more than 30% below the 1961–90 average throughout a large part of the region. The July–December period was predominantly wetter than average in the Southern Hemisphere and precipitation totals were generally above average north of the equator. Drier-than-normal conditions throughout a large part of North America, the Mediterranean, western Africa, and a large part of southern Asia contributed to a Northern Hemisphere July–December that was 2.6% drier than the 1961–90 average. The 6-month total in the Southern Hemisphere was 0.5% above normal as much of Argentina, southern Africa, and Australia received precipitation in excess of the 30-yr average.

During the past century, there has been an increase in precipitation within the mid- to high-latitude regions of the Northern Hemisphere. The in-

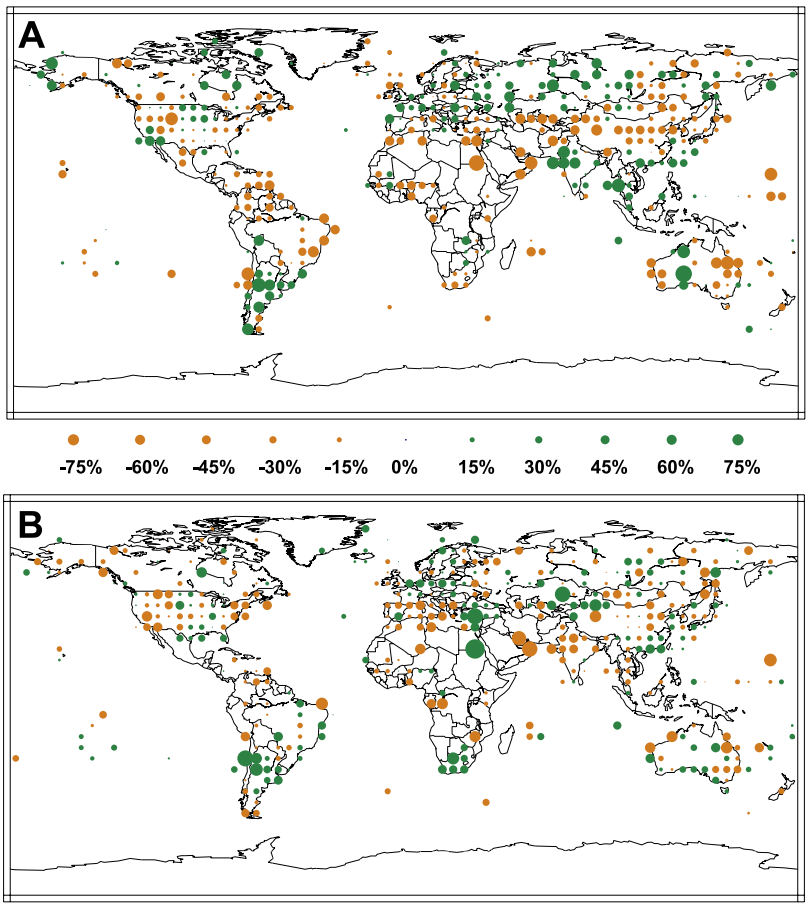

FIG. 12. Global precipitation anomalies for the period (a) Jan– Jun 2001 and (b) Jul–Dec. Anomalies are for 5° grid squares based on the 1961–90 base period and are expressed as percent departures from normal. The magnitude of the anomalies are depicted by the areas of the circles. Green indicates normal or above-normal, while brown indicates below-normal precipitation. Areas without circles reflect insufficient data for calculating anomalies. (Source NCDC's Global Historical Climatology Network.)

crease in temperature that has occurred over the past century (section 2a) also coincides with an increase in precipitation in many parts of these regions, although there are some areas with trends toward drier conditions (Lawrimore et al. 2001). The century-scale rate of increase is greater than 10% in the 55°–85°N latitude band and is near 5% in the region from 30° to 55°N. The trend in the 10°–30°N latitude band is negative (–3%), partly due to a multidecadal cycle of drought in the Sahel region of Africa from the 1960s to the early 1990s. Trends in the remaining latitude bands south of 10°N are positive and in the range of 2%–3% (Lawrimore et al. 2001).

d. Northern Hemisphere snow cover

Below-average Northern Hemisphere snow cover extent occurred for the fifth consecutive year in 2001, continuing a trend of reduced snow cover that began in the late 1980s. Snow cover was below average in all months except January, September, October, and December. Although December snow cover was the greatest since 1992, the positive anomaly was still moderate compared to the anomalies prior to the late 1980s (Fig. 13). Eurasian and North American snow cover extent were also below the 1966–2001 mean in 2001. For North America (including Greenland) all months except January, February, and March were below the average; and for Eurasia, all months except September, October, and December featured reduced snow cover extent relative to the mean.

On average, Northern Hemisphere (including Greenland) snow cover extent reaches a maximum in January (46.6 million km^2) and a minimum in August (3.7 million km^2). Approximately 33% of the land area north of the equator is covered by snow from November to April. Snow cover is approximately 50% in January. Eurasia contains the largest portion of snow-covered land area (60%) during midwinter and only Greenland (and some isolated mountainous areas) remain snow covered throughout the year.

Recent decreases in snow cover extent coincide with increasing temperatures in the Northern Hemisphere. A visible transition toward reduced snow cover occurred during the late 1980s (Fig. 13) on both the Eurasian and North American continents. The largest decreases in snow cover have occurred in late winter and early summer while the fall and early to mid-winter months show little or no trend (Fig. 14). The spring season decrease is consistent with a trend toward earlier dates of the last spring freeze as well as reductions in the number of frost days during March–May.

On regional scales, there is large interannual variability in the annual snow cycle. Some of this variability is related to the timing of snowmelt each spring. A detailed analysis of snowmelt variations on Alaska's

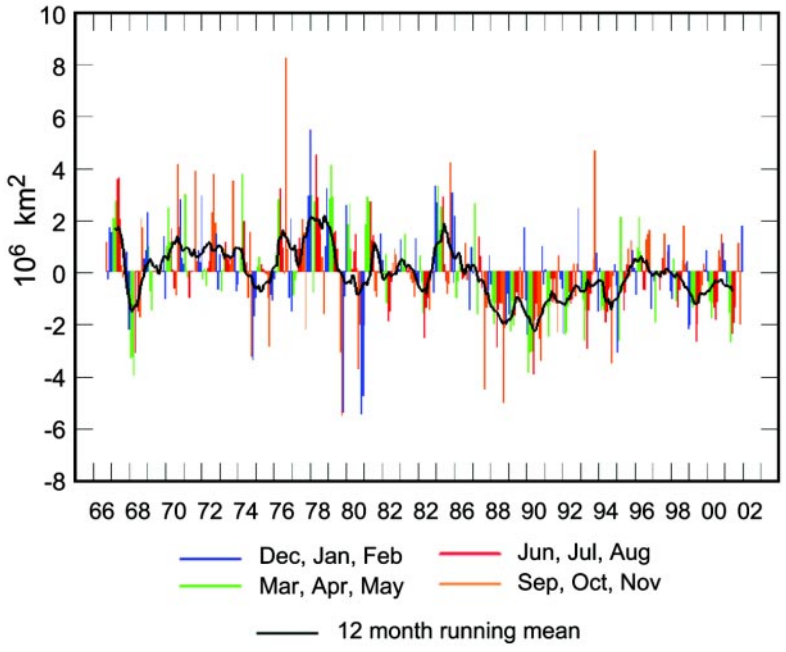

FIG. 13. Anomalies of monthly snow cover extent over Northern Hemisphere lands (including Greenland) between Nov 1966 and Dec 2001. Also shown are 12-month running anomalies of hemispheric snow extent, plotted on the seventh month of a given interval. Anomalies are calculated from NOAA/NESDIS snow maps. Mean hemispheric snow extent is 25.5 million km² for the full period of record. Monthly means for the period of record are used for 12 months in the late 1960s in order to create a continuous series of running means. Missing months fall between May and Oct, no winter months are missing.

North Slope is given in Stone et al. (2002). Independent records described below, generally indicate a long-term advance in the date of spring snowmelt over northern Alaska. An earlier spring melt has several consequences that include perturbations to biogeochemical cycles resulting from warmer temperatures and a longer growing season (e.g., Stone et al. 2002; and references therein).

Figure 15 shows a long time series of the date of snow disappearance at Barrow, Alaska, and a proxy record of melt dates derived from observations of seabird breeding initiation on Cooper Island, located about 40 km east of Barrow. The Barrow record is a composite of observations made at the National Weather Service in Barrow prior to 1962 and at or near NOAA's Barrow Observatory (BRW) from 1963 to the present. The time series from Cooper Island is based on the appearance of the first egg in a Black Guillemot colony. Black Guillemots need access to nest cavities that are at ground level. Thus, the onset of breeding and egg production is constrained by snow cover. Once females occupy their nests, the first eggs are laid about 14 days later. Therefore, breeding chronology tracks the snowmelt very closely. For the overlapping period, the Cooper Island and BRW records are reasonably well correlated (r = 0.66) suggesting that the sites are similarly affected by variation in climate. The advance in the date of snowmelt at the two sites is virtually identical as indicated by the linear regressions shown in Fig. 15.

Since the 1940s there has been an advance in the melt date in the vicinity of Barrow of about eight days (Fig. 15). The date of snow disappearance is highly variable, however. The anomalously early years of melt, 1990, 1996, and 1998, probably influence the regression analysis because these all occur near the end of the record. In contrast, 1999, 2000, and 2001 were all relatively late years of snowmelt, the timing being comparable to many years dating back to the late 1950s. The appearance of three consecutive seasons of relatively late snowmelt suggests that the long-term trend may be reversing, or has been temporarily interrupted. A preliminary analysis suggests that there has been another shift in synoptic patterns that affects northern Alaska's climate. In particular, extremely cold temperatures during May 2000 and May 2001 delayed the final phase of the melt season. At Barrow, May 2001 was the coldest since 1922, and May 2000 was the seventh coldest on record that began in 1921. There is corroborating evidence from Franklin Bluffs (69.9°N, 148.1°W), Sagwon (69.4°N, 148.8°W), and Imnavait Basin (68.62°N, 149.32°W), sites east and well south of Barrow, that the entire North Slope was much colder than normal in May 2000 and 2001. While many factors other than temperature affect the timing of snowmelt, especially winter snow accumulation, the rate at which snow melts at the end of the cycle is linked closely with air temperature. Winter snowfall amounts during 1999, 2000, and 2001 were high relative to 1990, 1996, and 1998 at BRW. Previous studies have linked variations in these factors to changes in large-scale circulation patterns, particularly the relative positions and intensities of the Aleutian low and Beaufort Sea high pressure systems (Stone et al. 2002). If and why these patterns may be shifting has not been determined but there may be a link to the changing mode of the Arctic Oscillation (AO;

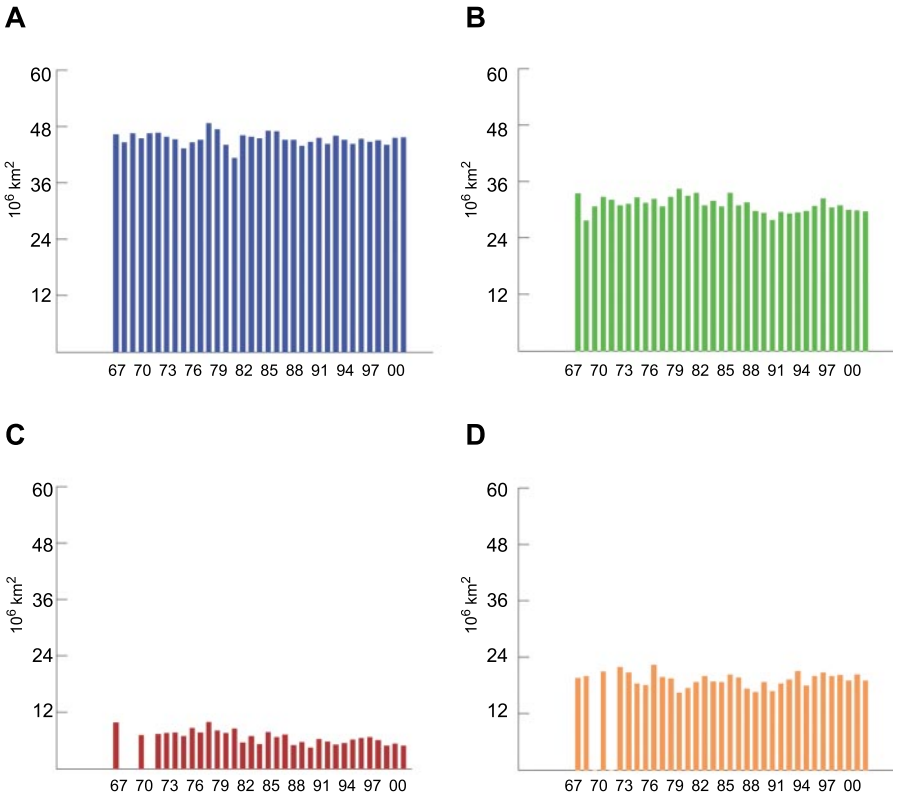

FIG. 14. Extent of seasonal snow cover over Northern Hemisphere lands (including Greenland) from the winter of 1966/67 through the autumn of 2001: (a) winter: Dec–Feb; (b) spring: Mar–May; (c) summer: Jun–Aug; (d) autumn: Sep–Nov).

proximately zero, with small decreases in some gases balancing increases of other gases (Hansen and Sato 2001). Methane decreased slightly in 2001, providing a small negative forcing increment estimated at 0.0004 W m^{-2} (Hansen and Sato 2001). This small negative change has been accounted for in Fig. 16, such that the total height of the bar for 2001 is somewhat reduced. If the present rate of growth of the greenhouse gas forcing continued the added forcing in the next 50 years would be about 1.3 W m^{-2}.

a. Carbon dioxide

Carbon dioxide (CO_2) directly affects climate by absorbing terrestrial infrared radiation. Its contribution to direct radiative forcing is 1.4 ±0.2 W m^{-2}

Thompson and Wallace 1998). In recent years the AO index has decreased, indicative of a weakening of the Arctic vortex that is expected to affect circum-Arctic weather patterns. On the basis of the periodicity that has characterized the AO historically, a shift toward a negative index appears to be a natural rather than an anthropogenic phenomenon. The apparent reversal in the timing in spring snowmelt on the North Slope of Alaska may be empirical evidence that the changing mode of the AO is beginning to influence synoptic patterns in the western Arctic.

3. TRACE GASES AND RADIATIVE FORCING

A summary of the annual growth rate of global climate forcing by well-mixed greenhouse gases is shown in Fig. 16. Although ozone and stratospheric water vapor are important greenhouse gases, they are neither well mixed nor well measured and are consequently not included in the figure. Historical perspective and more detailed descriptions of the major greenhouse gases are offered in sections 3a–d. The net chlorofluorobcarbon (CFC) change in 2001 was ap-

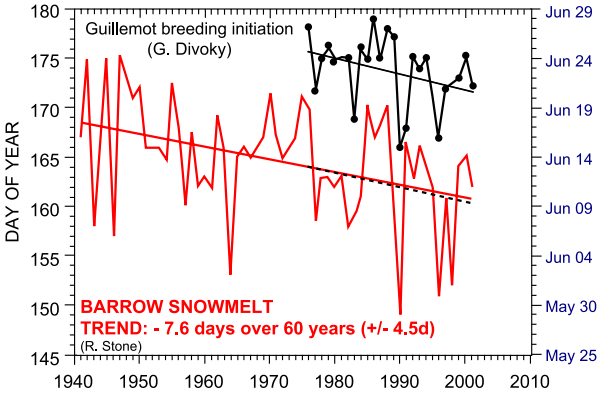

FIG. 15. Time series of the day of snow disappearance (melt date) during spring at Barrow, Alaska, and a record of breeding initiation of the Black Guillemots of Cooper Island. Breeding initiation relates to the appearance of the first eggs in nests that are cavities at ground level. Both time series are fitted linearly. At Barrow, melt dates have advanced by 7.6 days over the 60-yr period, significant at the 95% confidence level. Recent trends (dash-dot for Barrow) for overlapping periods of the records are almost identical (updated from Stone et al. 2002).

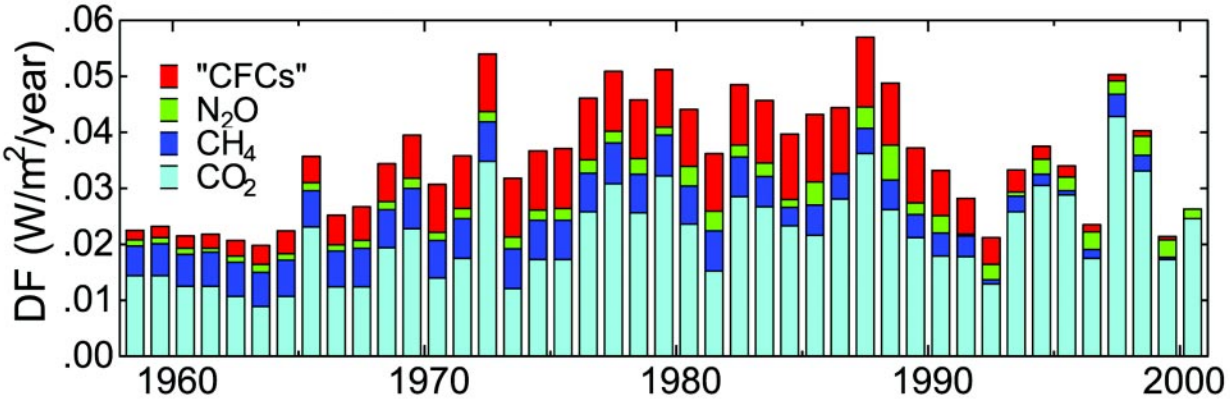

Fig. 16. Growth rate of direct climate forcing (DF) by well-mixed greenhouse gases. Ozone and stratospheric water vapor, which are neither well-mixed nor well-measured, are not included. (Data courtesy of J. Hansen.)

(Hansen and Sato 2001), or about 50% of the total. Between the end of the last glaciation and the industrial revolution, a period of 10 000 years, the global carbon cycle was at a steady state maintaining a nearly constant atmospheric abundance of CO_2 at ~280 ppm (ppm = parts in 106 by mole fraction). This abundance represented a balance among large seasonal fluxes (on the order of 100 Gt C yr^{-1}, where 1 Gt = 1015 g) between the atmosphere and biosphere (photosynthesis and respiration) and the atmosphere and the ocean (physical exchange of CO_2). Since the late-1800s, atmospheric CO_2 has increased by ~30%, due primarily to emissions from combustion of fossil fuels (currently about 7 Gt C yr^{-1}) and, to a lesser extent, deforestation (0–2 Gt C yr^{-1}). High-precision measurements of atmospheric CO_2 beginning in 1958 show that the average increase of CO_2 in the atmosphere corresponds to ~55% of the CO_2 emitted by fossil fuel combustion (Keeling et al. 1995), but this fraction varies from ~20% to ~90% (Conway et al. 1994; Ciais et al. 1995). The remaining fossil fuel CO_2 is removed from the atmosphere by the oceans and the terrestrial biosphere.

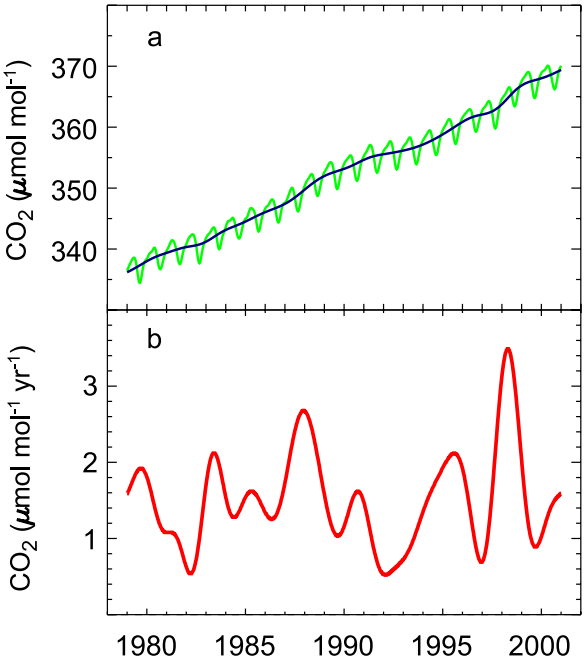

Fig. 17. (a) Globally averaged CO_2 mole fractions (green line) and deseasonalized trend (blue line) determined from NOAA/CMDL cooperative air sampling network measurements. (b) Instantaneous atmospheric CO_2 growth rate. (Courtesy T.J. Conway, NOAA/CMDL.)

Globally averaged CO_2 abundances (green line) and deseasonalized trend (blue line) are plotted for 1979–2001 in Fig. 17a. Seasonality in the global averages is driven by photosynthesis and respiration in the terrestrial biosphere, mostly in the midlatitudes of the Northern Hemisphere. The time derivative of the trend is plotted in Fig. 17b. Note the variability in the rate of atmospheric CO_2 increase during the 20-yr period, such as the rate decrease during the 1990s. Based on reported global emissions of carbon resulting from fossil fuel combustion (available from the Carbon Dioxide Information and Analysis Center, Oak Ridge, TN; online at http://cdiac.esd.ornl.gov/trends/emis/em_cont.htm), we know that these interannual variations in CO_2 growth rate are much larger than the variations in fossil fuel emissions. They arise from relatively small imbalances between the large one-way atmosphere–ocean and atmosphere–terrestrial biosphere fluxes. Most attempts to explain the interannual variability of the atmospheric CO_2 increase have focused on short-term climate fluctuations (e.g., ENSO and post-Pinatubo cooling) but the mechanisms, especially the role of the terrestrial biosphere, are not

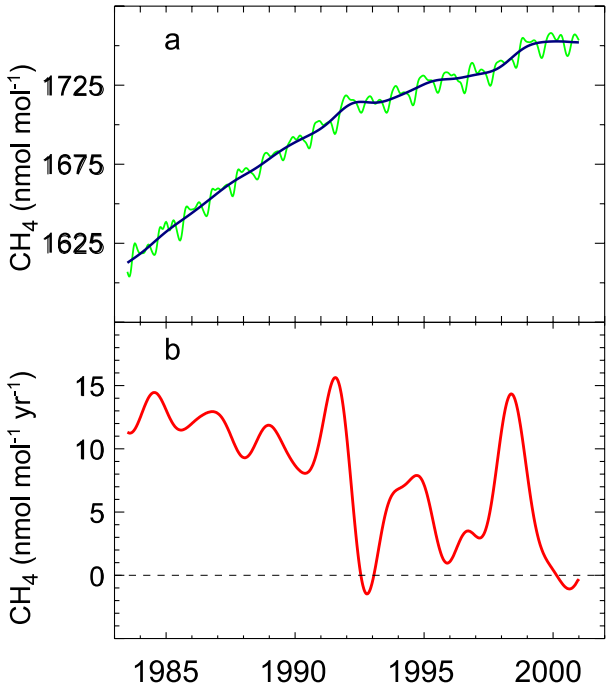

FIG. 18. (a) Globally averaged CH_4 mole fractions (green line) and deseasonalized trend (blue line) determined from NOAA/CMDL cooperative air sampling network measurements. (b) Instantaneous atmospheric CH_4 growth rate. (Courtesy E.J. Dlugokencky, NOAA/ CMDL.)

well understood. For example, it has been speculated that the high CO_2 growth rate in1998 was related to unusually warm temperatures that slightly increased respiration of CO_2 relative to photosynthetic uptake. This hypothesis is supported by measurements of the carbon-isotopic composition of CO_2.

b. Methane

Methane (CH_4) contributes to climate forcing directly by absorbing terrestrial IR radiation and indirectly by influencing greenhouse gases such as tropospheric ozone (O_3), stratospheric water (H_2O), and the concentration of hydroxy radicals (OH). Changes in OH concentration affect the lifetimes of other reduced greenhouse gases such as hydroflourocarbons (HFC) and hydrochloroflourocarbons (HCFC). Indirect radiative effects are estimated to add ~40% to the direct climate effect of methane (Lelieveld et al. 1993). Hansen and Sato (2001) estimate that radiative forcing for CH_4, including direct and indirect effects, is 0.7 ±0.2 W m^{-2}, one-half the contribution from CO_2.

High-precision measurements of atmospheric methane provide climate modelers with current and past rates of CH_4 increases, and the measurements are also useful as a top-down constraint on the global CH_4 budget. In Fig. 18a, smoothed, globally averaged CH_4 mole fractions from the NOAA/Climate Monitoring and Diagnostics Laboratory (CMDL) air sampling network are plotted as a function of time for the years 1983–2001. Instantaneous CH_4 growth rate, determined from the deseasonalized trend in Fig. 18a, is shown in Fig. 18b. This rate of increase is the net difference between total CH_4 emissions and CH_4 losses, and is equal to about 3% of total emissions during the 1990s. Over 20 years of measurements show CH_4 has increased, but the rate of increase has slowed, on average, over the past decade. Dlugokencky et al. (1998) have explained the decreasing growth rate as an "approach to steady state," meaning global emission rates and the CH_4 atmospheric lifetime are both nearly constant. The long-term trend can also be explained by increasing emission rates and decreasing CH_4 lifetime (Karlsdóttir and Isaksen 2000).

Superimposed upon the long-term decreasing CH_4 trend are significant interannual variations in the CH_4 growth rate; the largest were in 1991 and 1998. If these variations in the imbalance between sources and sinks can be associated with a particular event, then they can be used to test our knowledge

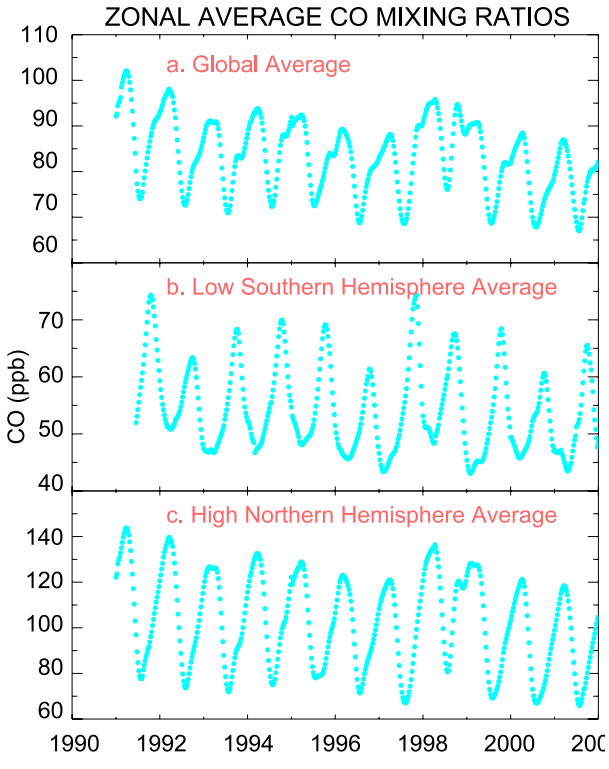

FIG. 19. Zonal average CO time series 1991-2001. (a) Global average, (b) low Southern Hemisphere average, and (c) high Northern Hemisphere average. (Courtesy P.C. Novelli, NOAA/ CMDL.)

of specific terms in the methane budget. For example, the increase in CH_4 growth rate during 1991 occurred immediately after the eruption of Mt. Pinatubo. Dlugokencky et al. (1996) attributed this to the effects of SO_2 and ash injected during the eruption on CH_4 chemical loss rates. During 1998, the imbalance between larger CH_4 sources and smaller sinks more than doubled relative to the previous three years; 1998 was also the warmest year on record for the period of the CH_4 measurements. Dlugokencky et al. (2001) found that the warm conditions during 1998 likely resulted in more CH_4 emissions from natural wetlands, a CH_4 source that is strongly temperature dependent. While the measurements of CH_4 in the contemporary atmosphere cannot be used to predict the future atmospheric abundance of this important greenhouse gas, a warmer climate in the future may contribute to an increase in atmospheric methane.

c. Carbon monoxide

Carbon monoxide (CO) plays an important role in atmospheric chemistry. In many parts of the troposphere, the reaction of CO and the hydroxyl radical (OH) controls the ability of the atmosphere to cleanse itself of reduced compounds, many of which are greenhouse gases. Under conditions commonly found in areas of fossil fuel or biomass burning, the destruction of CO can also lead to the production of tropospheric ozone, a key contributor to poor urban air quality. While CO does not strongly absorb in the infrared wavelengths (and therefore is not considered a direct greenhouse gas), carbon monoxide has an indirect effect on the earth's radiation budget equal to that of nitrous oxide (Daniel and Solomon 1998).

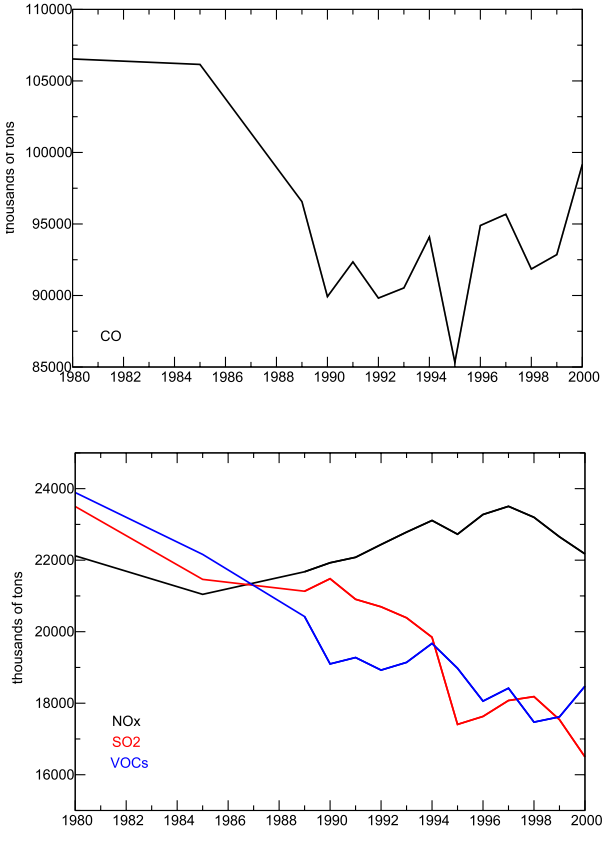

FIG. 20. Total emissions from the United States of (a) CO and (b) NOx (black line), SO2 (red line), and VOCs (blue line) in thousands of tons. Data courtesy of the EPA.

In the background troposphere (areas well removed from local sources), CO mixing ratios show large year-to-year variation as shown in Fig. 19 and discussed by Novelli et al. (1998). A notable feature of the recent global CO time series is the strong global CO enhancements observed in 1997–98. Beginning in mid-1997 and through late 1998, CO mixing ratios are well above previous years. Perhaps most striking is the very shallow drawdown of CO measured in June–September 1998. This feature has been attributed to extensive burning of forests in both the Tropics and in boreal regions. Levine (1999) estimated that 77 Tg of CO were emitted from fires burning in Kalimantan and Sumatra from mid-1997 to mid-1998. These estimates could easily double if all of Indonesia and surrounding countries were included. The strong enhancement of CO due to emissions from these fires can also be seen in the low Southern Hemisphere (equator–30°S) zonal time series (Fig. 19b).

The 1998 fire season was quite active, due in part to drought conditions that are believed to have resulted from the ENSO event that year. CO levels in the high latitudes of the Northern Hemisphere (Fig. 19c) exhibit a very weak summer minimum, followed by peak mixing ratios in fall 1998. These high CO concentrations occurred six months before the typical seasonal maximum. The 1998 boreal forest fires, particularly those that burned across Siberia, were estimated to have emitted 105–144 Tg of CO (Kasischke and Bruhwiler 2002). Average CO emissions from biomass burning have been estimated at between ~450 and 750 Tg yr^{-1} (Holloway et al. 2000). For the high Northern Hemisphere (latitudes greater than 30°N), Wotawa et al. (2001) show that about 75% of the interannual CO variation observed over the past eight years can be explained by year-to-year variations in boreal biomass burning.

In the United States, annual carbon monoxide emissions decreased markedly from 1980 to 1995 (Fig. 20a). This decreasing trend is partly due to a re-

duction in on-road vehicular emissions, which showed a particularly sharp decline from 1994 to 1995. However, emissions from nonroad vehicles were increasing over the same period. Some of the increase in 1996 and thereafter can be attributed to a large jump in recreational vehicle emissions, although larger increases over the period 1995–2000 were due to wildfire activity. The CO emissions in 2000 were high primarily due to the intense wildfire season (Lawrimore et al. 2001). On-road vehicle emissions have continued to decrease over the entire period (P. Lorang 2002, personal communication).

d. NOx, VOCs, SO_2

Nitrogen oxide (NOx) affects tropospheric ozone production, through a sequence of reactions, leading to the production of O_3 and CO_2, and contributing to a reduction in the atmospheric burden of CO, CH_4, and HFCs. There is significant variability (temporally and spatially) in the measured abundance of NOx, and it is not possible to derive a global burden for this reactive gas. Generally, NOx is more abundant in urban areas than in remote parts of the globe, and though NOx is more quickly removed from the atmosphere in polluted regions, emissions directly into the free troposphere have a much larger impact on global greenhouse gases (Houghton et al. 2001). In the United States (Fig. 20b), NOx emissions have remained relatively stable since 1980 with slight increases up to 1997, followed by a decline in emissions. A primary source of NOx in the United States is fossil fuel burning from industry and automobiles. Emissions from on-road vehicles have remained fairly constant since 1980, while recreational and off-road vehicle emissions have shown moderate increases over the same time period. Emissions from fuel combustion in the production of electricity and other utilities have decreased slightly, with some interannual fluctuations since 1980, though emissions from combustion in industrial processes have changed very little (P. Lorang 2002, personal communication).

As with NOx, it is not possible to derive a global burden for volatile organic compounds (VOCs) but unlike NOx, they have a small direct impact on radiative forcing, though their primary impact on the climate is through the production of organic aerosols leading to ozone production. The primary emissions source is also natural vegetation rather than anthropogenic. However, natural emissions are concentrated in the Tropics and are measured in much smaller amounts in the northern midlatitudes, with the highest abundances occurring primarily in

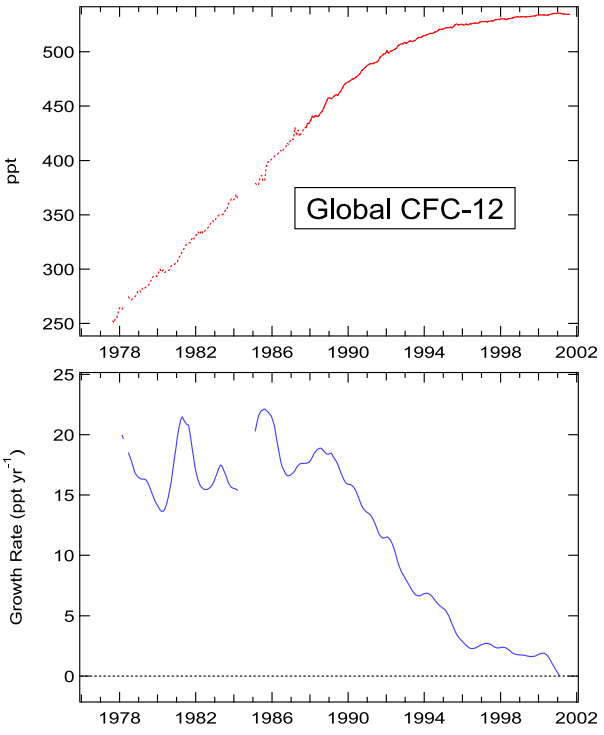

Fig. 21. Global tropospheric CFC-12 (CCl_2F_2) mixing ratios (dry molar) in ppt (1×10^{-12}) from flasks (top panel, dashed line) and in situ instruments (top panel, solid line) from the NOAA/CMDL network for 1977–2001. Growth rates (bottom panel) were ~18 ppt yr^{-1} prior to 1989, and have reached zero in 2002. Growth rates for Figs. 21–23 are calculated using a loess nonparametric fitting technique described in Elkins et al. (1993). All halocarbon and nitrous oxide data are available online at ftp://ftp.cmdl.noaa.gov/hats. (Courtesy J. Elkins, T. Thompson, G. Dutton, and B. Hall, NOAA/CMDL.)

boreal summer. VOCs are generally concentrated near their source and therefore anthropogenic emissions tend to significantly alter local and regional atmospheric chemistry even though global anthropogenic emissions compose a small fraction of total emissions (Houghton et al. 2001). Therefore, in the United States, emissions from anthropogenic sources are of significance, the most important of which is from motor vehicles, primarily from the incomplete combustion and/or evaporation of fuel. Biomass burning also contributes substantially to VOC emissions. The general decline of U.S. VOC emissions observable in Fig. 20, is due in part to a reduction in motor vehicle, chemical manufacturing, and petroleum production emissions. The decline in wildfire activity in the United States also contributed to the reduction in emissions until the intense wildfire season of 2000, which led to a small increase in VOCs (P. Lorang 2002, personal communication).

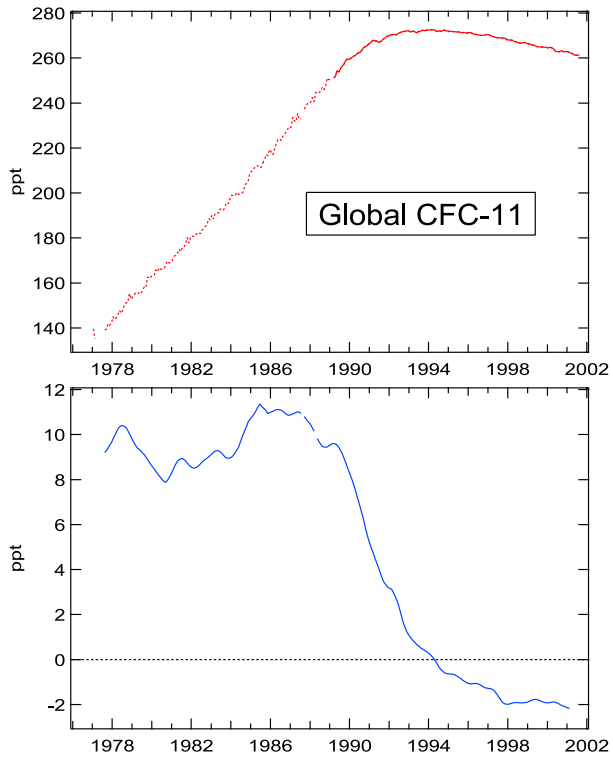

FIG. 22. Global tropospheric CFC-11 (CCl3F) mixing ratios (dry molar) from flasks (top panel, dashed line) and in situ instruments (top panel, solid line) from the NOAA/CMDL network for 1977–2002. Growth rates (bottom panel) were about 10 ppt yr^{-1} prior to 1989, and are currently averaging about –2 ppt yr^{-1}. (Courtesy J. Elkins, T. Thompson, G. Dutton, and B. Hall, NOAA/CMDL.)

Sulfur dioxide (SO_2) emissions have also shown a decrease since 1980 in the United States. SO_2 is produced mainly by anthropogenic activity and volcanoes. Up to half of SO_2 emissions do not have an opportunity to be converted to sulfate aerosols, existing in the atmosphere for only 0.6–2.6 days. However, once SO_2 has been chemically transformed into a sulfate, wet deposition (precipitation) will likely account for its removal from the atmosphere in less than a week. Despite its short atmospheric lifetime, it is an important negative radiative forcing agent since most sulfate aerosols are efficient light scatterers and will therefore reflect incoming solar radiation (Houghton et al. 2001). The effects of anthropogenically produced SO_2 tends to be local because deposition usually occurs within a few days, though the effects of volcanoes can be long lasting (several years), due to the transport of SO_2 to the stratosphere and the resulting slower deposition. Most of the decrease in U.S. anthropogenic emissions of SO_2 shown in Fig. 20 is a result of a sharp decline in emissions associated with electricity production. Emissions from coal-generated electricity production alone have been reduced by 30% since 1989 (P. Lorang 2002, personal communication).

e. *Halocarbons and nitrous oxide*

Measurement of chlorofluorocarbon-12 or CFC-12 (CCl2F2), CFC-11 (CCl3F), and nitrous oxide (N_2O) from the four NOAA/CMDL baseline observatories (Pt. Barrow, Alaska; Niwot Ridge, Colorado; Mauna Loa, Hawaii; Cape Matatula, American Samoa, and the South Pole) and one cooperative station (Niwot Ridge, Colorado) have been made since 1977. All three of these gases are significant ozone-depleting gases and greenhouse gases. All CFCs directly contribute 0.35 W m^{-2} and indirectly contribute –0.1 W m^{-2} because they decrease stratospheric ozone, a greenhouse gas. This is a net contribution of 0.25 W m^{-2}, or 9% of the climate forcing from all at-

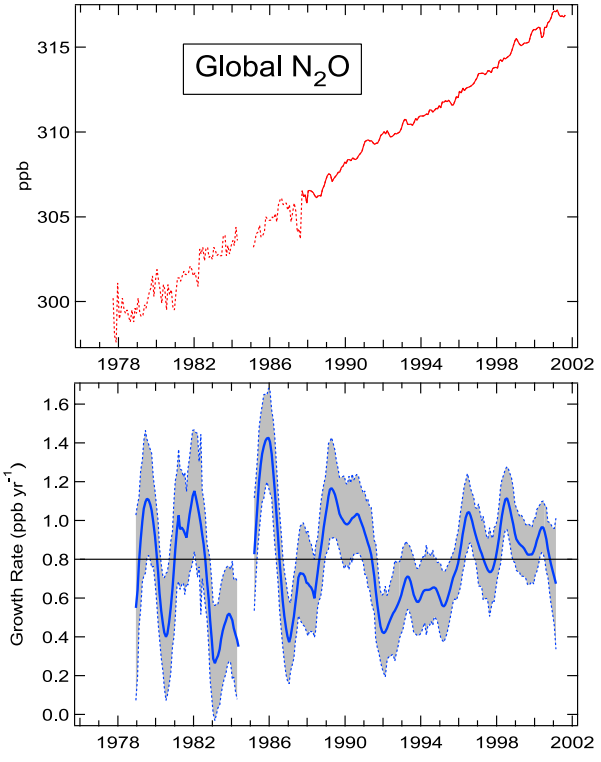

FIG. 23. Global tropospheric nitrous oxide (N_2O) mixing ratios (dry molar) in ppb (1×10^{-9}) from flasks (top panel, dashed line) and in situ instruments (top panel, solid line) from the NOAA/CMDL network for 1977–2002. Growth rates (bottom panel) and 1 std dev (shaded areas) show year to year variability with a mean global growth rate over the period of 0.8 ppb yr^{-1}. The std devs are calculated using a bootstrap technique described in Elkins et al. (1993). (Courtesy J. Elkins, J. Butler, T. Thompson, G. Dutton, and B. Hall, NOAA/CMDL.)

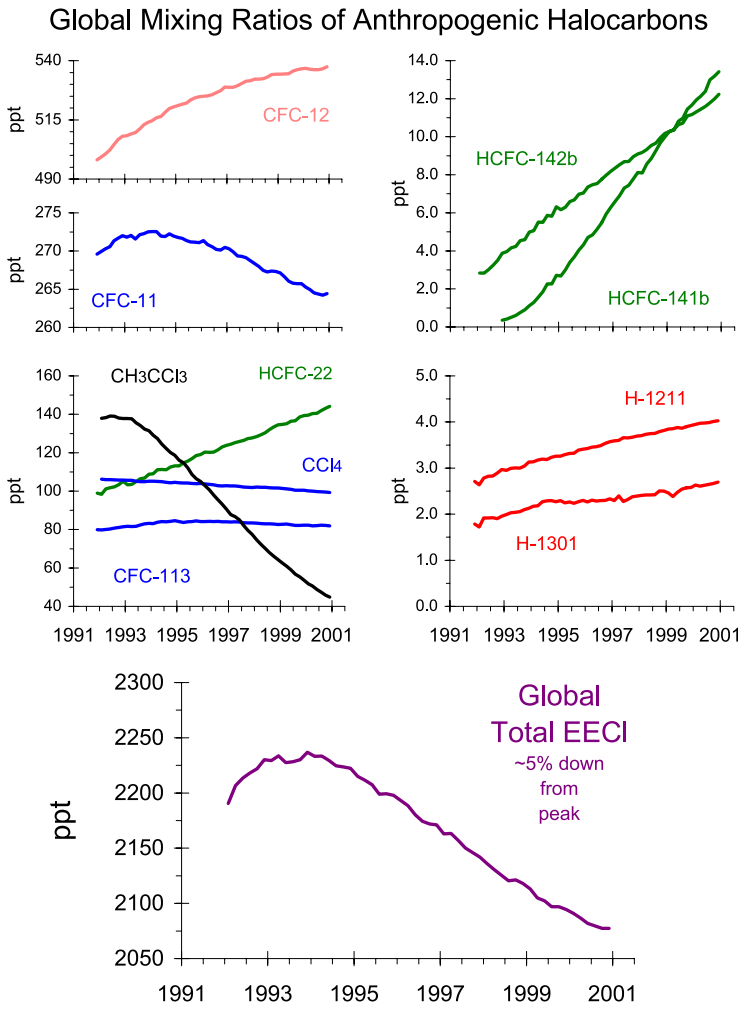

FIG. 24. Trends of global tropospheric mixing ratios of CFC-12(CCl2F2), CFC-11(CCl3F), methyl chloroform (CH3CCl3), carbon tetrachloride (CCl4) from in situ EC-GC, and CFC-113 (CCl2FCClF2), HCFC-22 (CHClF2), -141b (CH3CCl2F), -142b (CH3CClF2), halons (H-1211, CBrClF2 and H-1301, CBrF3) from flask analyses of samples collected from the NOAA/CMDL network. The total EECl includes the individual compound's efficiency of releasing reactive chlorine and bromine (50 times more effective than chlorine in destroying ozone) in the stratosphere. [Courtesy S. Montzka, J. Butler, T. Thompson, D. Mondeel, and J. Elkins; updated from Montzka et al. (1996, 1999).]

mospheric increases of greenhouse gases between 1850 and 2000 (Hansen and Sato 2000). Nitrous oxide was included as one of the six major groups of greenhouse gases to be regulated by many nations under the Kyoto Protocol. Atmospheric nitrous oxide has contributed 0.15 W m^{-2}, or about 5.5% of the total climate forcing caused by all greenhouse gases between 1850 and 2000 (Hansen and Sato 2000). The CFCs, HCFCs, and certain chlorinated solvents are already scheduled for emission reduction by the Montreal Protocol to Reduce Emissions of Substances that Destroy the Ozone Layer.

The most noteworthy event for 2001 is that CFC-12 appears to have leveled off, reaching a global atmospheric growth rate of zero in early 2001 (Fig. 21). The global growth rate of CFC-12 in the late 1970s and 1980s averaged about 18 parts per trillion (ppt) yr^{-1} or 3%–7% yr^{-1} (Elkins et al. 1993). The primary uses of CFC-12 area agents are in aerosol propellants, automobile air conditioners, and smaller refrigerators.

The atmospheric growth rate of CFC-11 (Fig. 22) reached zero quickly in 1994 from global means of about 10 ppt yr^{-1} (3%–7% yr^{-1}) in the late 1970s and early 1980s. This fast reduction is the result of its relatively short atmospheric lifetime of ~45 yr compared to the atmospheric lifetime of CFC-12 that is relatively long at about 100 yr (Elkins et al. 1993). CFC-11 is used primarily in large air conditioning and refrigeration units. Mandated and voluntary reductions before 1995 caused the global atmospheric growth rates for both CFC-12 and CFC-11 to decline. Developing countries (e.g., China and India) can still produce CFC-12 and CFC-11 until 2010, and developed countries can produce small amounts of both for exempted uses (like medical inhalers). Global concentrations of CFC-12 and CFC-11 will take between 50 and 100 yr to reach levels observed in the atmosphere prior to the beginning of the Antarctic ozone hole.

Global mean nitrous oxide concentrations averaged about 317 parts per billion (ppb) in 2001 (Fig. 23, top). Land sources of N_2O emissions from bacteria are considered the dominant source with a significant ocean source (20%–40% of the total). Sources are about 30% higher than the only known stratospheric sinks through photolysis and reaction with excited oxygen atoms. There are numerous man-made sources of N_2O including fertilizer, formation in combustion gas in catalytic converters, nylon processing, nitric acid production,

human and animal waste, and through reactions of oxides of nitrogen and sulfur dioxide in the troposphere. The exact magnitude of each source is somewhat uncertain. The mean growth rate since 1977 has averaged about 0.80 ppb yr^{-1} (0.25% yr^{-1}) with significant oscillations over the 24-yr-old record (Fig. 23, bottom). Between 1991 and 1996, the growth rate dropped to a low of about 0.4 ppb yr^{-1} for a number of possible reasons including decreased fertilizer consumption by the former Soviet Union, enhanced stratospheric loss from volcanic-induced circulation changes, and a long ENSO event reducing transport of a deep oceanic source into the atmosphere.

Total effective equivalent chlorine (EECl), including both chlorine and bromine-containing compounds, continued to decrease in the atmosphere in 2001 (Fig. 24). Since 1994, the total equivalent chlorine has decreased by 5% as a result of mandated and voluntary reductions from the Montreal Protocol in emissions of ozone-depleting compounds. The main reason for the decrease is the dramatic drop in the emissions of methyl chloroform (CH3CCl3). The global mixing ratio of CH3CCl3 was 140 ppt in 1991; and at the beginning of 2002, it was 45 ppt, a decrease of 68%. This rapid drop is a direct result of reducing a significant amount of emissions after 1989 and its relatively short atmospheric lifetime of 5.2 yr (Montzka et al. 2000). Developing countries may still produce CH3CCl3 until 2015. The halons, H-1211 and H-1301, continue to increase in the atmosphere because of their long atmospheric lifetimes (11 and 65 yr, respectively) and the large unused bank of chemicals in existing fire extinguishing systems (Butler et al. 1998). Developing countries may continue to produce halons until 2010. The continued growth of halons after CH3CCl3 is exhausted in the atmosphere may introduce a "kink" in the almost linear decrease of total equivalent chlorine since 1994 (Montzka et al. 1999).

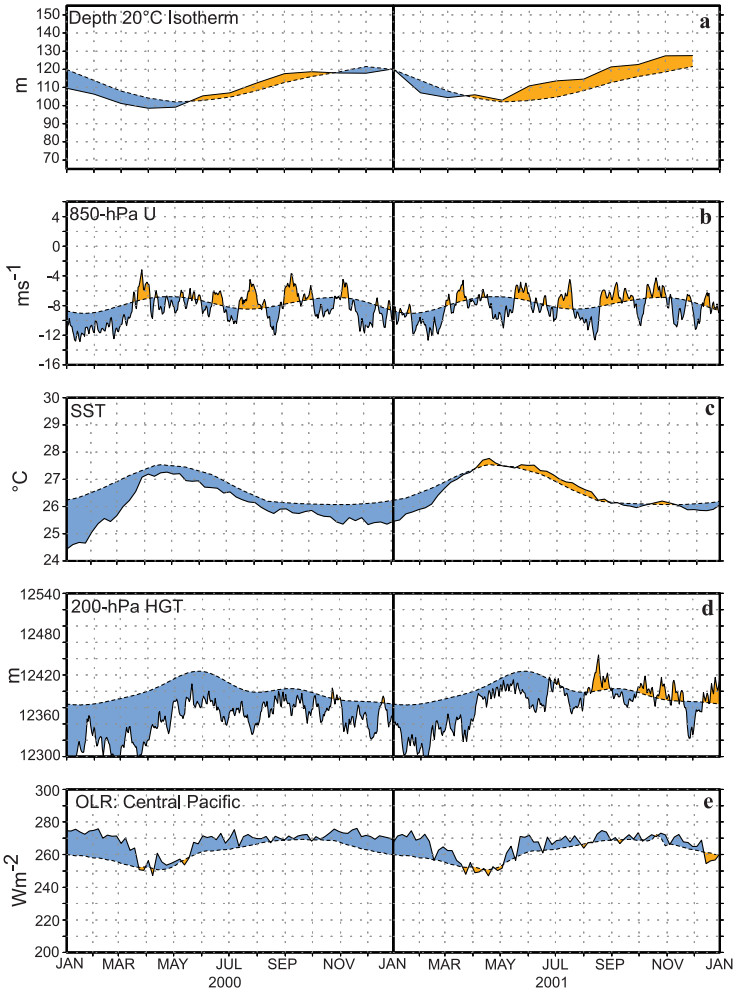

FIG. 25. Monthly time series of (a) the depth of the 20°C isotherm (m), (b) 850-hPa zonal wind speed (m s^{-1}), (c) SST (°C), (d) 200-hPa height (m), and (e) OLR (W m^{-2}) over the central Pacific. Values are determined by averaging over the region bounded by 5°N–5°S and 180°–100°W in (a)–(d), and 20°N–20°S and 180°–100°W in (e). The solid curve in all panels shows the monthly mean values and the dashed curved shows the climatological mean. The anomalies are shown shaded, with orange (blue) shading indicating positive (negative) anomalies, except for in (e) where the shading convention is reversed. The climatology and anomalies are computed with respect to the 1979–95 base period.

4. THE TROPICS

a. ENSO and the tropical Pacific (including MJO)

1) OVERVIEW

Weak cold episode (La Niña) conditions that persisted in the tropical Pacific during January–May 2001 ended during the Northern Hemisphere (NH) summer. This marked the end of a long-running cold episode that began in mid-1998, immediately following the very strong 1997/98 warm episode. During this 3-yr period there was considerable seasonal variability in the strength and extent of the accompanying oceanic and atmospheric anomalies. Cold episode conditions were strongest during the 1998/99, 1999–2000, and 2000/01 NH

winter seasons, followed by a weakening of the cold episode during the NH spring seasons.

The periods of mature cold episode conditions (January–March) during both 2000 and 2001 are indicated by the persistence of an anomalously shallow 20°C isotherm depth across the eastern equatorial Pacific (Fig. 25a), and below-average sea surface temperatures (SSTs) over the central equatorial Pacific (Fig. 25c). Characteristic atmospheric features which accompanied these oceanic conditions throughout this period included the following: 1) enhanced low-level equatorial easterly winds across the central and west-central equatorial Pacific (Fig. 25b), 2) below-normal 200-hPa heights throughout the region associated with a reduction in atmospheric heating (Fig. 25d), and 3) suppressed tropical convection [indicated by positive anomalies of OLR across the central and eastern equatorial Pacific (Fig. 25e)].

A return to near-normal SSTs and a significant deepening of the thermocline and appearance of positive depth anomalies across the central Pacific occurred during June–December 2001. The low-level wind (Fig. 25b;c also see Fig. 28) and tropical convection anomalies (Fig. 25e) also weakened considerably during this period and were strongly modulated by MJO activity (see section 4d). This MJO activity contributed to periodic reversals in the sign of the low-level wind and tropical convection anomalies (especially during June–December 2001).

2) Equatorial Pacific Ocean sea surface and subsurface temperatures

The typical La Niña–related pattern of seasonal SSTs was observed during (December–February) DJF 2000/01 and to a lesser extent during (March–May) MAM 2001. This pattern is reflected by an enhanced cold tongue extending westward from the west coast of South America to the vicinity of the date line (Fig. 26a). Accompanying this cold tongue was a westward retreat of the 28°C isotherm to near 160°E during DJF, which is 30° west of its climatological mean position near 170°W. The 28°C temperature represents the approximate threshold for deep tropical convection over the central equatorial Pacific (Gadgil et al. 1984), and the decrease in SSTs to below this level was consistent with the persistent pattern of suppressed convective activity during this season.

This anomalous westward extension and strengthening of the equatorial cold tongue is further highlighted by a persistent pattern of below-average SSTs

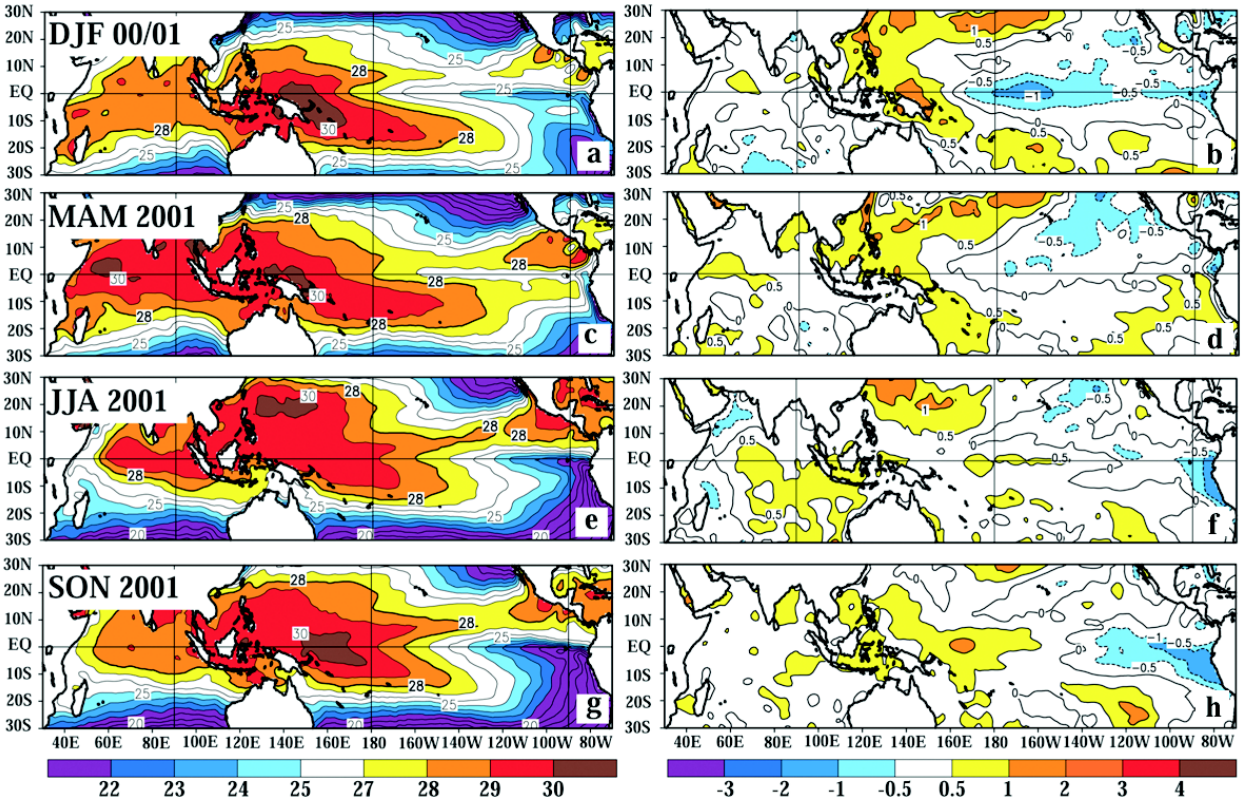

Fig. 26. Seasonal SST (left) and anomaly (right) for (a), (b) DJF 2000/01, (c), (d) MAM 2001, (e), (f) JJA 2001, and (g), (h) SON 2001. Contour interval is 1°C, with the 0.5°C anomaly contour included. Anomalies are departures from the 1971–2000 adjusted OI climatology (Smith and Reynolds 1998).

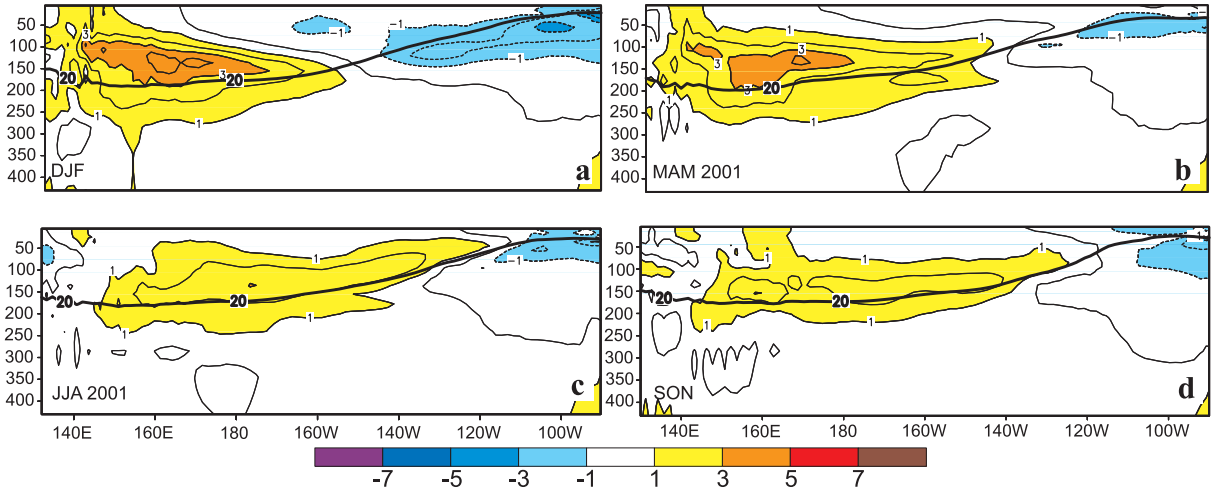

Fig. 27. Equatorial depth–longitude section of ocean temperature anomalies for (a) DJF 2000/01, (b) MAM 2001, (c) JJA 2001, and (d) SON 2001. Contour interval is 1°C. The dark line is the 20°C isotherm. Data are derived from an analysis system that assimilates oceanic observations into an oceanic GCM (Behringer et al. 1998). Anomalies are departures from the 1981–2000 base period means.

(more than 1.0°C below normal) across the central and eastern Pacific during DJF (Fig. 26b). The negative SST anomalies across the central and eastern Pacific diminished during MAM, and SSTs remained near normal during JJA (Figs. 26d,f). Negative SST anomalies reappeared in the eastern Pacific during SON (Fig. 26h). Farther west, the cold episode conditions during DJF were accompanied by anomalously warm SSTs (averaging 0.5°–1.0°C above normal) throughout the western tropical Pacific. During the remainder of the year, SSTs in the western and central Pacific slowly evolved toward a warm episode, with above-normal SSTs observed over much of the western and central equatorial Pacific by SON (Fig. 26h).

The subsurface temperature structure is a fundamental component of La Niña (and El Niño) episodes. An examination of the subsurface thermal structure during DJF indicates that the anomalously cold ocean temperatures extended down to a depth of approximately 150 m across the central and eastern equatorial Pacific (Figs. 27a), while anomalously warm ocean temperatures were evident over the western Pacific between approximately 50 and 300 m. These subsurface temperature anomalies reflected an increased slope of the oceanic thermocline, and resulted from the characteristic La Niña–related pattern of strong oceanic upwelling over the eastern half of the Pacific and increased downwelling over the western Pacific.

During the remainder of the year, there was a gradual expansion of the area of positive equatorial subsurface temperature anomalies into the central Pacific and a gradual decrease in the strength and areal extent of the negative subsurface temperature anomalies in the eastern Pacific (Figs. 27b–d). This evolution is consistent with a slow decay of the subsurface thermal structure that characterizes the mature phase of cold episodes and the development of conditions usually found just prior to warm episodes.

3) Tropical circulation

(i) Pacific basin

Many of the prominent atmospheric circulation features typical of past Pacific cold episodes were again observed during DJF and MAM, as they had been during much of the period from mid-1998 to 2000. In the Tropics, the La Niña–related anomaly features included the following: 1) upper-level westerly wind anomalies across the central and eastern Pacific (Figs. 11a,b), 2) lower-level easterly wind anomalies across the central and western Pacific (Fig. 28a,b), 3) enhanced ascending motion and convective activity over the western Pacific and Indonesia, and 4) anomalous descending motion and suppressed convective activity over the central Pacific. These conditions reflected an enhanced equatorial Walker circulation across the Pacific basin, a well-known feature of Pacific cold episodes.

In the meridional direction the circulation during DJF and MAM featured anomalous equatorward flow in the upper troposphere over the central tropical Pacific (Fig. 11), as well as anomalous upper-tropospheric convergence and anomalous lower-level di-

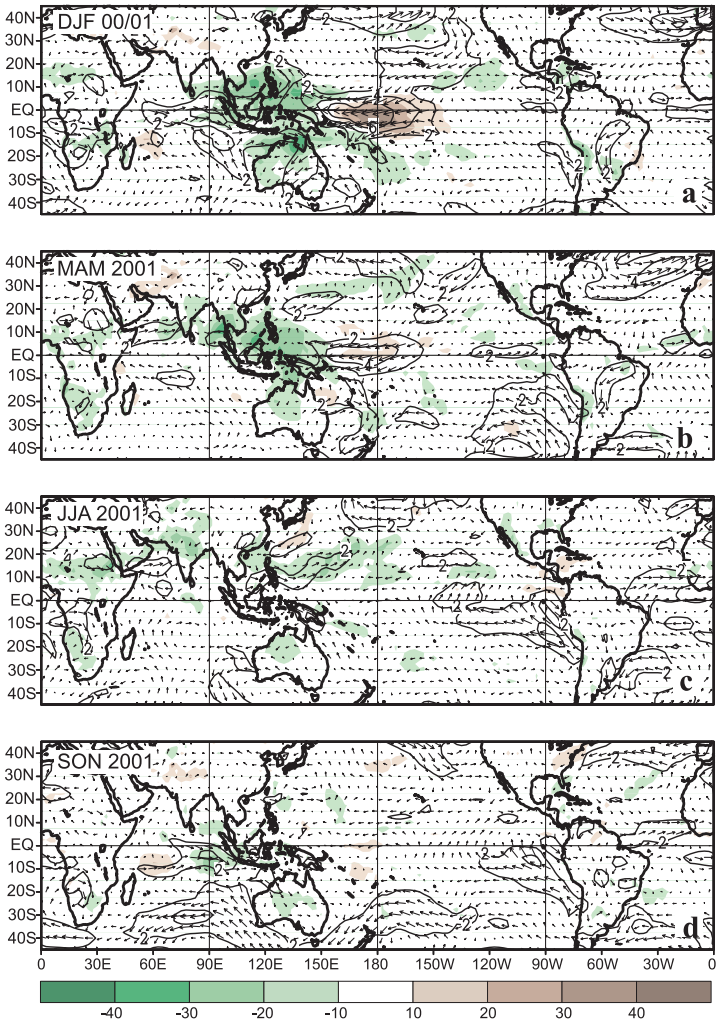

FIG. 28. OLR anomalies (shaded) and 850-hPa vector wind anomalies and isotachs for (a) DJF 2000/01, (b) MAM 2001, (c) JJA 2001, and (d) SON 2001. Contour interval for isotachs is 2 m s^{-1}. Shading interval for OLR anomalies is 10 W m^{-2}. Anomalies are departures from the 1979–95 base period monthly means.

vergence (implied by the anomalous OLR pattern in Fig. 11). These conditions reflected a suppressed Hadley circulation, which is another well-known feature of Pacific cold episodes.

The above wind patterns were also consistent with cyclonic streamfunction anomalies [indicated by negative (positive) anomalies in the Northern (Southern) Hemisphere] in the subtropics of both hemispheres (Figs. 29a,b), which flanked the region of suppressed tropical convection over the central and east-central Pacific. These cyclonic anomalies reflected an amplification of the mid-Pacific troughs in both hemispheres and a confinement of the low-latitude ridges to the heavy-convection region of the western Pacific and Australasia (Fig. 29b).

(ii) Upper-tropospheric anticyclonic anomaly pattern in the subtropics

Outside of the Pacific sector, upper-tropospheric anticyclonic circulation anomalies [indicated by positive (negative) streamfunction anomalies in the Northern (Southern) Hemisphere] were also evident in the lower- and midlatitudes of both hemispheres during December 2000–May 2001 (Figs. 29a,b). This global-scale anomaly pattern is the leading mode of atmospheric variability, and explains approximately 43% of the total interannual and interdecadal variance between 40°N and 40°S (Mo and Kousky 1993). It also explains approximately 60% of the local interannual and interdecadal variance in the vicinity of the subtropical ridges outside of the Pacific basin. This mode is strongly controlled by the ENSO cycle, with the pattern of tropical convection typical of La Niña conditions favoring the anticyclonic streamfunction anomalies shown in Figs. 29a,b. Similar anomaly patterns were also prominent during the mid-1998–2000 period of cold episode conditions (Bell et al. 2000; Lawrimore et al. 2001).

4) The Madden–Julian oscillation

Low-frequency variability in the Tropics is strongly influenced by the MJO (e.g., Madden and Julian 1971, 1972, 1994). The MJO is an atmospheric disturbance that modulates the patterns of tropical precipitation and atmospheric circulation with a typical period in the range of 30–60 days. It tends to be most active during ENSO-neutral years (Kousky and Kayano 1994), especially just prior to El Niño (Higgins et al. 2000). The MJO also modulates the occurrence of some extreme weather events, such as floods (Higgins et al. 2000) and hurricane activity in each of the ocean basins (Maloney and Hartmann 2000a,b; Higgins and Shi 2001). While the MJO does not cause El Niño, it can contribute to the speed of development, and possibly the intensity of El Niño episodes via the generation of oceanic Kelvin waves (Zhang et al. 2001).

There was substantial seasonal-to-interannual variability in MJO activity during 2000 and 2001, with periods of increased activity (e.g., June–November 2000 and June–December 2001) followed by periods in

which the oscillation was weak or absent (e.g., December 2000–May 2001; Fig. 30). Many tropical Pacific atmospheric and oceanic variables were influenced by MJO activity during the second half of 2001. Alternating periods of low-level easterly and westerly wind anomalies over the western and central Pacific were consistent with this activity during the period (Fig. 25b). Upper-level velocity potential anomalies showed continuous propagation of this activity around the global Tropics (Fig. 30).

The period from late November to December 2001 featured low-level westerly wind anomalies that expanded eastward from the western equatorial Pacific to the international date line (180°W). The weakening of the easterlies (actual reversal to westerlies for a brief period) generated a strong eastward-propagating oceanic Kelvin wave that contributed to a deepening of the oceanic thermocline and warming of the sea surface temperatures in the vicinity of the date line by the end of the year. Kelvin waves are oceanic gravity waves that feature downwelling at their leading edge and upwelling behind. A typical eastward propagation rate for these waves is roughly 10 degrees of longitude per week. Successive waves, combined with an overall weakening of the equatorial low-level easterlies, can maintain the thermocline at a deeper-than-normal level, even after initial waves have passed.

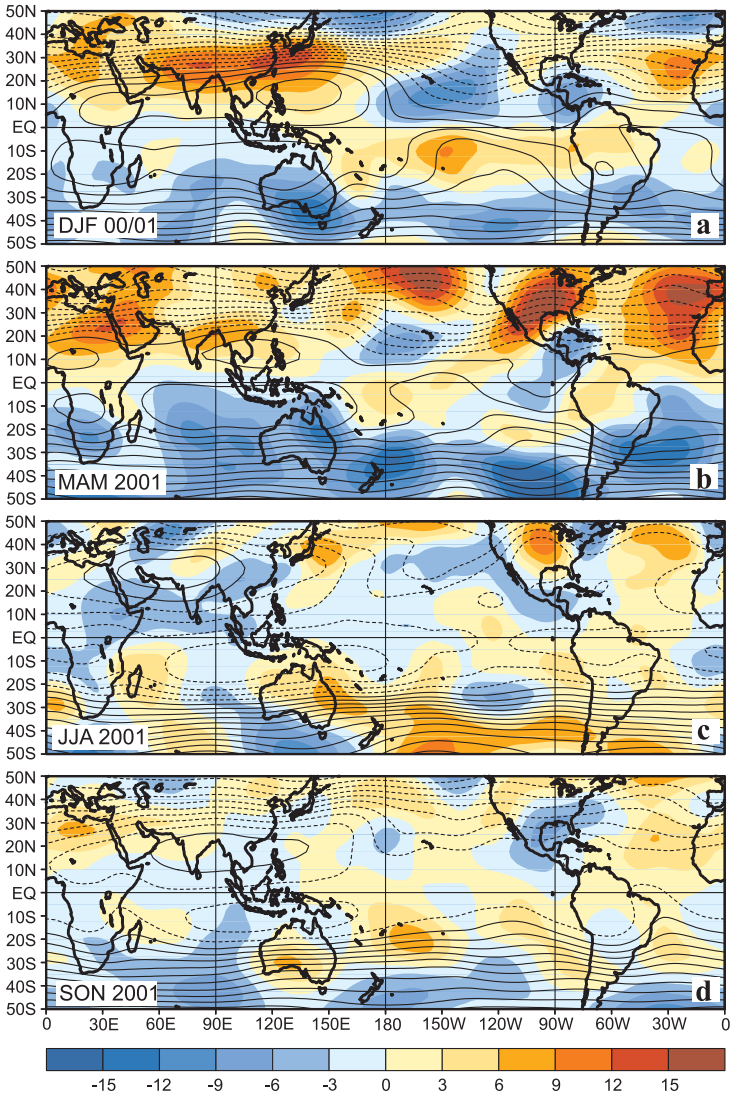

Fig. 29. Seasonal 200-hPa streamfunction (contours) and anomalies (shaded) during (a) DJF 2000/01, (b) MAM 2001, (c) JJA 2001, and (d) SON 2001. Units are 1.0×10^{-6} m^2 s^{-1}. Contour interval is 10. In the Northern Hemisphere, positive (negative) values indicate an anticyclonic (cyclonic) circulation. In the Southern Hemisphere, negative (positive) values indicate a cyclonic (anticyclonic) circulation. Anomalies are departures from the 1979–95 base period means.

As a consequence of the large-scale changes in convection accompanying the MJO, the jet streams over both the North Pacific and South Pacific are often influenced during the cold season (Higgins and Mo 1997). For example, the jets often exhibit a westward retraction during periods of enhanced convection over Indonesia, and an eastward extension as the enhanced convection moves toward the central equatorial Pacific. In the Northern Hemisphere these east–west modulations of the Pacific jet stream can contribute to transitions in the large-scale circulation pattern, with recurrent blocking activity over the high latitudes of the eastern North Pacific and a negative phase of the PNA pattern prior to the transition, and a positive phase of the PNA pattern following the transition (Higgins and Mo 1997). Two such transitions were observed in the Pacific-North American region late in the year, the first during early November 2001 and the second during mid-December 2001. In each case the period prior to the transition featured cooler-than-normal (warmer than normal) conditions in the western (eastern) United States with warmer-than-normal (cooler than normal) conditions after the transition.

b. Atlantic hurricane season

1) Overview

During the North Atlantic hurricane season (June–November). An average of 9–10 tropical

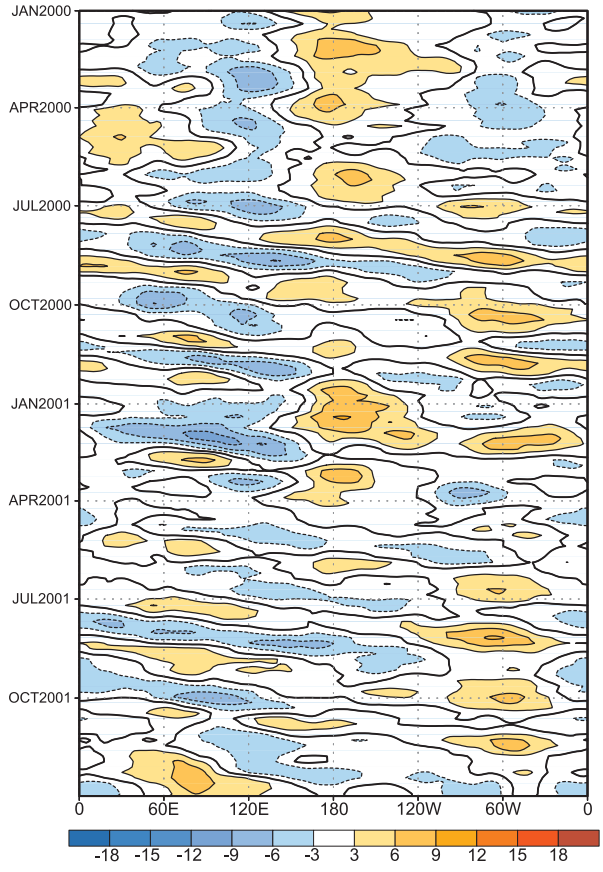

FIG. 30. Time–longitude section (5°N–5°S) of anomalous 200-hPa velocity potential (10^6 m^2 s^{-1}). Contour interval is 3×10^6 m^{2}s^{-1}. Anomalies are departures from the 1979–95 base period pentad means. The data are smoothed temporally by using a 3-point running average.

storms are observed, 5–6 hurricanes, and 2 major hurricanes [measured by a category 3, 4, or 5 on the Saffir–Simpson scale (Simpson 1974)]. The 2001 Atlantic hurricane season featured an above-average number of named storms (15), hurricanes (9), and major hurricanes (4), the third largest number of named storms since the beginning of aircraft reconnaissance flights in 1945. Seventeen named storms formed in 1969, and 19 in 1995. The above-average number of storms in 2001 is consistent with an increase in activity that began in 1995 (Goldenberg et al. 2001).

The climatological peak in hurricane activity is from mid-August to mid-October. A majority of the named storms during this two-month period typically originate from African easterly waves (Reed et al. 1977) over the main development region (MDR) of the tropical Atlantic and Caribbean Sea (Landsea 1993; Goldenberg and Shapiro 1996). The MDR refers to the combined regions of the tropical Atlantic south of 20°N and Caribbean Sea. During 2001 nine of the 15 named storms, including six of the nine hurricanes and three of the four major hurricanes, formed during the mid-August–mid-October period. Seven of the 15 named storms, four of the nine hurricanes, and all four major hurricanes, formed in the MDR.

Three named storms also formed over the Gulf of Mexico, and five formed in the extratropics (defined as the portion of the North Atlantic north of 20°N, excluding the Gulf of Mexico and the northern Caribbean Sea). Two of the first three named storms of the season formed over the Gulf, while three of the last four named storms formed in the extratropics after 26 October.

2) Comparing overall activity with past seasons

Overall activity in a given hurricane season is characterized by the combined strength, duration, and number of named storms. Gray (1999, personal communication) developed two measures of overall seasonal activity referred to as the hurricane destruction potential (HDP) index and the net tropical cyclone activity (NTC) index. A third measure of overall seasonal activity is the accumulated cyclone energy (ACE) index (Bell et al. 2000; Fig. 31a). All three indices are highly correlated (greater than 0.9), and all are useful for making quantitative comparisons in seasonal activity on both interannual and interdecadal timescales.

The ACE index is calculated by summing the squares of the estimated 6-hourly maximum sustained wind speed in knots^2 ($V_{max}{}^2$) for all periods while the system is either a tropical storm or hurricane. This index has been chosen due to its inclusion of systems while at tropical storm strength, and its ability to easily quantify activity occurring in specific parts of the Atlantic basin such as the MDR.

The ACE index (Fig. 31a) indicates that while the 2001 hurricane season reflected a continuation of the above-average activity that began in 1995, the activity was considerably less than has been observed in several of the more recent active seasons. Nonetheless, the 1995–2001 period is the most active since reliable records began in 1945, contrasting sharply with the substantially reduced activity during the preceding 25-yr period (Gray 1990; Landsea 1993; Landsea et al. 1999).

Regional ACE indices were computed similar to the total ACE index, except that each regional index is based only on systems that first become named storms within the specified region. The MDR-based ACE index (Fig. 31b) is strongly correlated (+0.96) with the total ACE index, and accounts for 71% of the

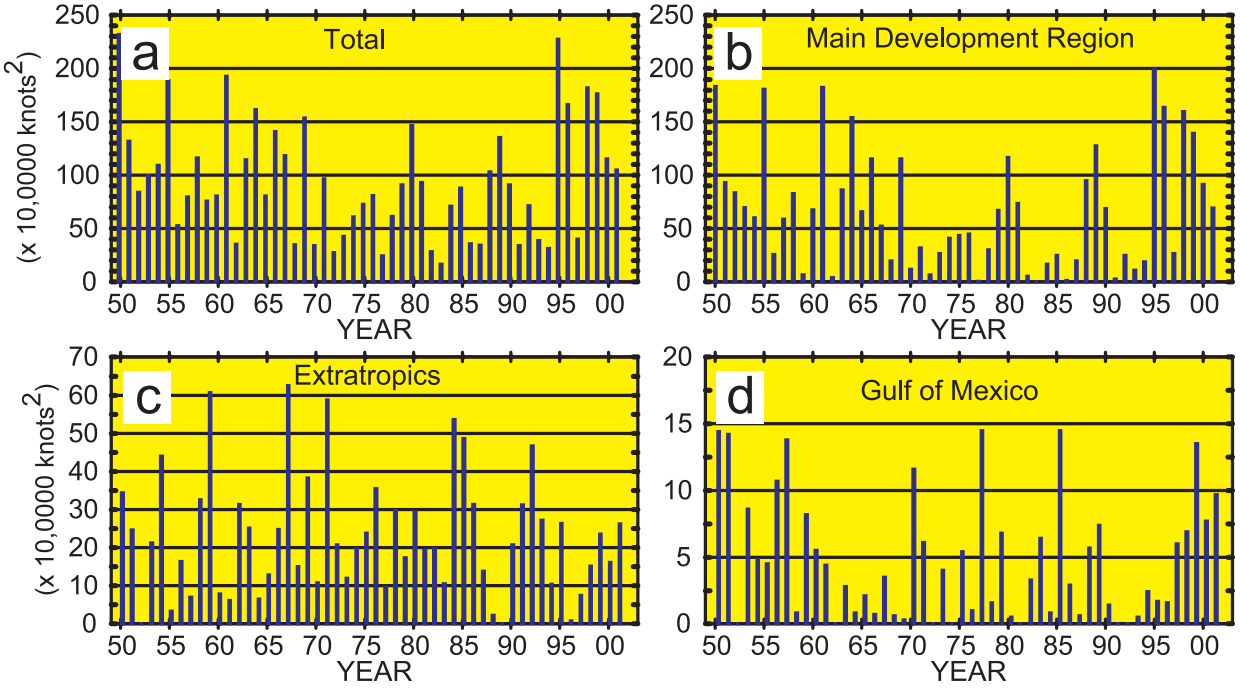

FIG. 31. Seasonal ACE index for (a) the entire Atlantic basin, (b) the MDR of the tropical Atlantic between 10° and 20°N including the Caribbean Sea, (c) the extratropics (located north of 20°N, excluding the Gulf of Mexico and Caribbean Sea), and (d) the Gulf of Mexico. The total ACE index (a) is defined as the sum of the squares of the estimated 6-hourly maximum sustained wind speed (kts^2) for all named Atlantic systems while they have at least tropical storm strength. The regional ACE indices (b)–(d) are similarly calculated, except that they are based only on systems that first become named storms within the specified region. Note the change in scale on the vertical axis in (c) and (d).

total basin-wide activity during the 1950–2000 base period. The strong multidecadal variations in total activity during this 51-yr period are accounted for primarily by storms first named in the MDR, with significantly below-average MDR activity during 1970–94 followed by a dramatic increase in activity beginning in 1995. This result is consistent with Landsea et al. (1999), who note that the multidecadal variations in seasonal Atlantic basin activity are related primarily to multidecadal variations in hurricane and major hurricane activity originating in the MDR.

For the 2001 season the activity associated with storms first named in the MDR accounted for 66% of the total. However, the MDR activity was less than during the past several seasons, and resulted in the relative drop in total activity noted above. The activity associated with storms first named in the extratropics accounted for 25% of the 2001 season total, and was comparable to levels seen during 1999 and in the early 1990s (Fig. 31c). Climatologically, 24% of the total activity in a given season is associated with storms first named in the extratropics. The activity associated with systems first named in the Gulf of Mexico accounted for approximately 9% of the 2001 season total, and was also higher than many of the past recent seasons (Fig. 31d). Climatologically, the Gulf of Mexico systems contribute approximately 5% to the total seasonal activity.

3) LANDFALLING TROPICAL STORMS

Three tropical storms, all forming over the Gulf of Mexico, made landfall in the United States during the 2001 hurricane season. Tropical Storm Allison was an extremely slow-moving system that formed on 5 June and caused extensive flooding across southeastern Texas and portions of the southeastern United States (see section 6a). Tropical Storm Barry formed on 2 August and caused heavy rainfall in Arkansas and Louisiana. Tropical Storm Gabrielle caused localized flooding in Florida on 14–15 September prior to becoming a hurricane over the western Atlantic.

Two named storms made landfall in Central America. The first was Tropical Storm Chantal, which crossed the central Yucatan Peninsula on 21 August and dissipated rapidly thereafter. The second was major Hurricane Iris, which hit Placentia, Belize, as a category-4 storm on 8–9 October and caused numerous deaths. Later in the season major Hurricane

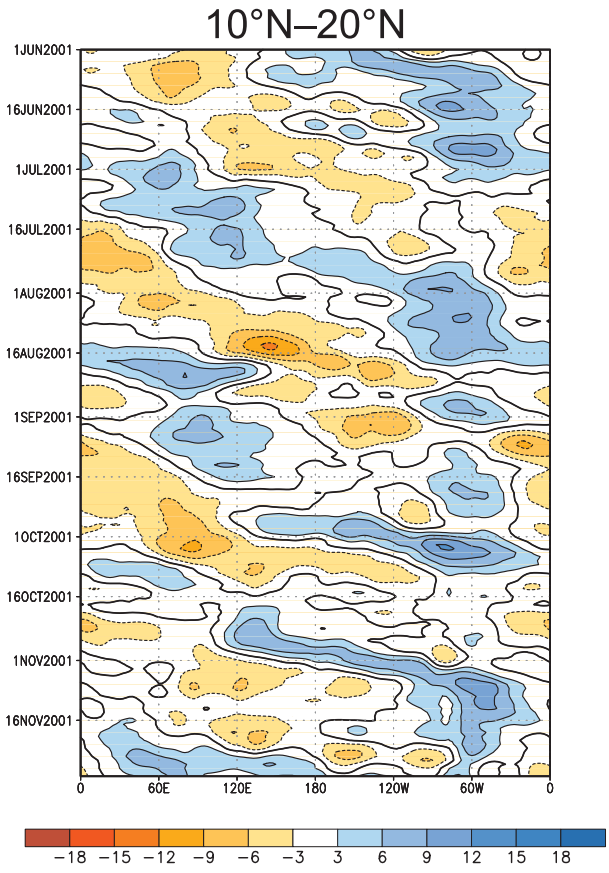

FIG. 32. Time–longitude sections of 5-day running mean 200-hPa velocity potential anomalies averaged over the latitude band 10°–20°N. Contour interval is 3 × 10^6 m^2 s^{-1}, and the thick contour represents the zero value. Anomalies are departures from the 1979–95 base daily means.

Michelle formed over the southern Caribbean Sea, and moved rapidly across central Cuba on 4 November. As a category-4 storm, it was the strongest hurricane to make landfall in Cuba since 1952

4) Strong intraseasonal variability during the 2001 Atlantic hurricane season

Mo (2000) and Maloney and Hartmann (2000) showed that the MJO significantly impacts the large-scale atmospheric circulation across the western half of the MDR, thereby affecting tropical cyclone and hurricane formation in the MDR. The easterly and westerly phases of the MJO derive their names from the sign of the low-level zonal wind anomalies over the eastern tropical Pacific. Mo (2000) notes that the easterly phase is associated with enhanced convection over the central tropical Pacific and suppressed convection over the Indian Ocean. This anomalous convection produces cyclonic 200-hPa streamfunction anomalies over the eastern Pacific and tropical Atlantic, and reduced upper-level easterlies and enhanced low-level easterlies in the MDR. The resulting increase in vertical wind shear directly inhibits Atlantic hurricane formation. Opposite patterns of anomalous convection during the westerly phase of the MJO produce anticyclonic circulation anomalies at 200 hPa in the subtropics of both hemispheres over the eastern Pacific and tropical Atlantic, along with an increased strength and increased poleward extent of the tropical easterly jet across the tropical Atlantic. The resulting reduction in vertical wind shear is conducive to increased hurricane activity in the MDR. Maloney and Hartmann (2000) suggest a nearly four-fold increase in hurricane activity in the MDR during the westerly phase of the MJO.

The large-scale atmospheric circulation during the 2001 hurricane season exhibited considerable intraseasonal variability, with much of the hurricane activity occurring during westerly MJO periods. A time–longitude section of 200-hPa velocity potential anomalies averaged between 10° and 20°N (Fig. 32) indicates transitions between phases of the MJO at nearly 1-month intervals across the Indian Ocean and tropical North Pacific from the beginning of July to the end of November, with higher-frequency transitions evident over the central Pacific in October.

Focusing on the climatological peak in activity, negative velocity potential anomalies (indicative of anomalous rising motion) were observed over the tropical Pacific during August 2001 in association with the easterly phase of the MJO. Consistent with Mo (2000) this easterly phase resulted in cyclonic streamfunction anomalies at 200 hPa in both hemispheres across the subtropical eastern Pacific and western Atlantic (Fig. 33a), and above-average vertical wind shear across the western Caribbean Sea and the Gulf of Mexico (Fig. 34a). These conditions were not conducive to hurricane development, and are consistent with the failure of two tropical storms to reach hurricane strength in the MDR during the second half of August.

In contrast, the active 1 September–7 October 2001 period featured six named storms, of which five became hurricanes and three became major hurricanes. During this period positive 200-hPa velocity potential anomalies (indicative of anomalous sinking motion) were observed over the tropical Pacific in association with the westerly phase of the MJO. Consistent with the study of Mo (2000) this westerly MJO phase produced anticyclonic 200-hPa streamfunction anomalies in subtropics of both hemispheres from the central Pacific to eastern Africa (Fig. 33b),

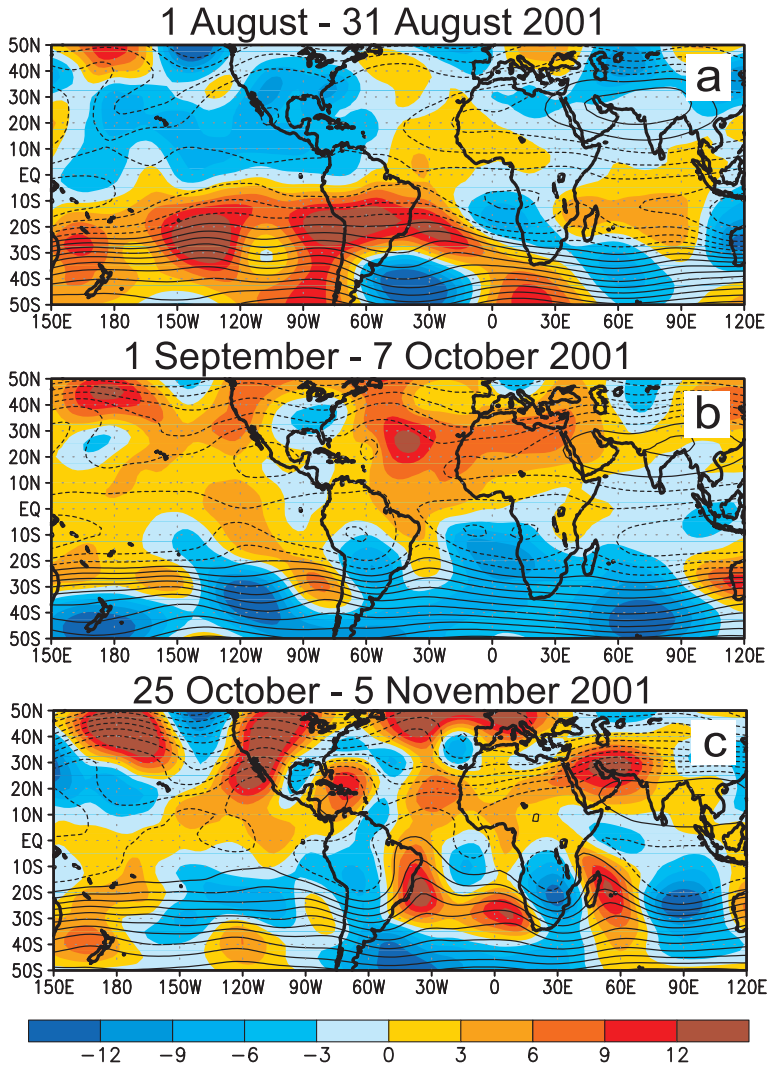

FIG. 33. 200-hPa streamfunction (contours) and anomalies (shading) for (a) 1–31 Aug 2001, (b) 1 Sep–7 Oct 2001, and (c) 25 Oct–5 Nov 2001. In the Northern (Southern) Hemisphere, positive (negative) anomalies indicate an anomalous anticyclonic circulation. Contour interval for the streamfunction is 10×10^6 m^2 s^{-1}, and shading interval for anomalies is 3×10^6 m^2 s^{-1}. Anomalies are departures from the 1979–95 base period daily means.

During the 2001 season the periods of activity and inactivity in both October and November also exhibited a strong relationship to the MJO. For example, a second period of increased hurricane activity during late October and early November 2001 coincided with the return of positive velocity potential anomalies across the central and eastern North Pacific in association with the westerly phase of the MJO (Fig. 32). The resulting anticyclonic streamfunction anomalies (Fig. 33c) and anomalously low vertical wind shear (Fig. 34c) over the MDR and southern Caribbean Sea contributed to the development of category-4 Hurricane Michele on 29 October.

No tropical storm activity was subsequently noted during 7–22 November as the easterly phase of the MJO returned to the tropical North Pacific. However, the return during late November to the westerly phase of the MJO was associated with the development of the ninth and final hurricane (Olga) of the season on 24 November. Although Olga developed in the extratropics it persisted over the low latitudes of the central North Atlantic and MDR in an area of low MJO-related vertical wind shear for 11 days before dissipating on 4 December. Olga accounted for 10% of the seasonal ACE index value (Fig. 31a) and 40% of the seasonal extratropical ACE index value (Fig. 31c).

and anomalously low vertical wind shear across the central MDR and the subtropical North Atlantic (Fig. 34b). Lawrimore et al. (2001) described a similar relationship during the 2000 hurricane season between opposing phases of the MJO, the associated patterns of anomalous 200-hPa streamfunction and 200–850-hPa vertical wind shear, and the primary periods of peak-season hurricane activity and inactivity (see their Figs. 37, 38). During 11 September–4 October 2000, for example, they showed that the westerly phase of the MJO was associated with the development of five hurricanes and two major hurricanes in the MDR.

5) Comparison of MDR activity during 2001 versus past seasons

Two important factors seem to distinguish the modest activity in the MDR during 2001 (Fig. 31b) from the higher levels of activity of the past several seasons. First, anomalously high vertical wind shear covered the Caribbean Sea and Gulf of Mexico during both August and September 2001(Figs. 34a,b), in association with an amplified upper-level trough that extended southward from the eastern United States (Figs. 33a,b). As a result the anomalously low shear that developed during September 2001 in association with the westerly phase of the MJO was confined to

the central MDR, and did not extend across the entire western tropical Atlantic and Caribbean Sea as is typical of more active hurricane seasons (Goldenberg and Shapiro 1986; Shapiro and Goldenberg 1998; Landsea et al. 1998; Bell et al. 1999, 2000). Note that while this amplified trough was detrimental to tropical cyclogenesis, it also helped to steer tropical systems that formed in the MDR out to sea prior to reaching the United States.

Second, the location of the 600-hPa African easterly jet (AEJ) during September was centered near 13°N (Fig. 35a), approximately 2 degrees south of its climatological mean position. As a result, large areas of cyclonic relative vorticity along the equatorward flank of the AEJ were confined to the extreme south-central and southeastern portions of the MDR (Fig. 35a), thereby only modestly overspreading the region of anomalous low vertical wind shear in the central MDR (cf. Fig. 34b). While these conditions are notably distinct from the inactive hurricane seasons (Bell and Chelliah 1999), they were not as conducive to hurricane development in the MDR as has been observed during the past several active seasons. For example, during both September 2000 and September 1998 the mean AEJ was centered near 17.5°N (Figs. 35b,c), and considerable cyclonic relative vorticity was present between 10° and 15°N over the central MDR. Developing disturbances migrating westward across the tropical Atlantic were able to strengthen in the extended region of strong cyclonic vorticity prior to and during their movement through the low-shear region that extended across the central and western MDR (Bell et al. 1999; Lawrimore et al. 2001).

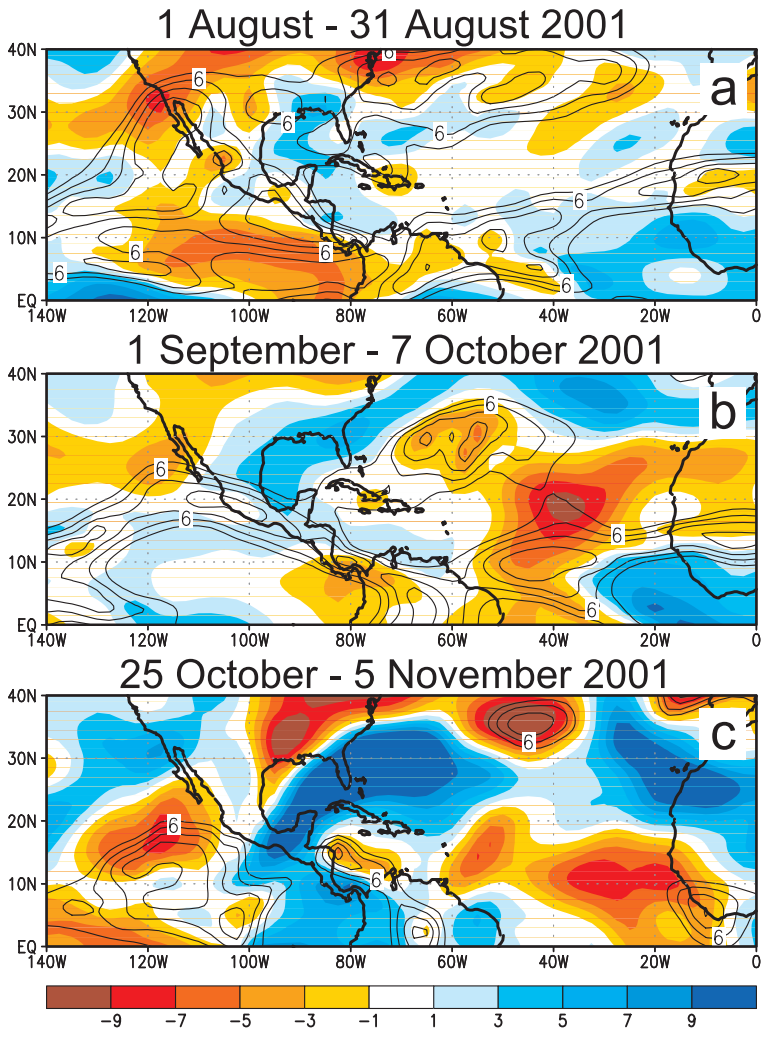

FIG. 34. Mean (contours) and anomalous (shading) vertical wind shear for (a) 1–31 Aug 2001, (b) 1 Sep–7 Oct 2001, and (c) 25 Oct–5 Nov 2001. Wind shear is calculated as the difference in vector wind speeds between 200 and 850 hPa. The contour interval for mean shear is 2 m s^{-1}, with values less than 8 m s^{-1} shown contoured. Shading interval for anomalies is 2 m s^{-1}. Below-average wind shear are shaded red and above-average wind shear shaded blue. Anomalies are calculated with respect to the 1979–95 base period daily means.

6) Increased activity in the extratropics

Five named storms developed in the extratropics during the 2001 hurricane season. The first was Hurricane Humberto in late September, and the last was Hurricane Olga in late November. The combination of Humberto and Olga accounted for 20% of the total seasonal ACE index value (Fig. 31a), and 80% of the seasonal extratropical ACE index value (Fig. 31c).

Three late-season storms formed in the lower extratropics after 26 October. All formed in regions of vigorous upper-level divergence ahead of large-amplitude troughs (Fig. 36). All three also formed during the westerly phase of the MJO (Fig. 32). The first of these systems (Tropical Storm Lorenzo) formed on 27 October over the eastern Atlantic near 27.5°N, 30°W (denoted by a closed circle in Fig. 36a). Hurricane Noel formed on 4 November over the cen-

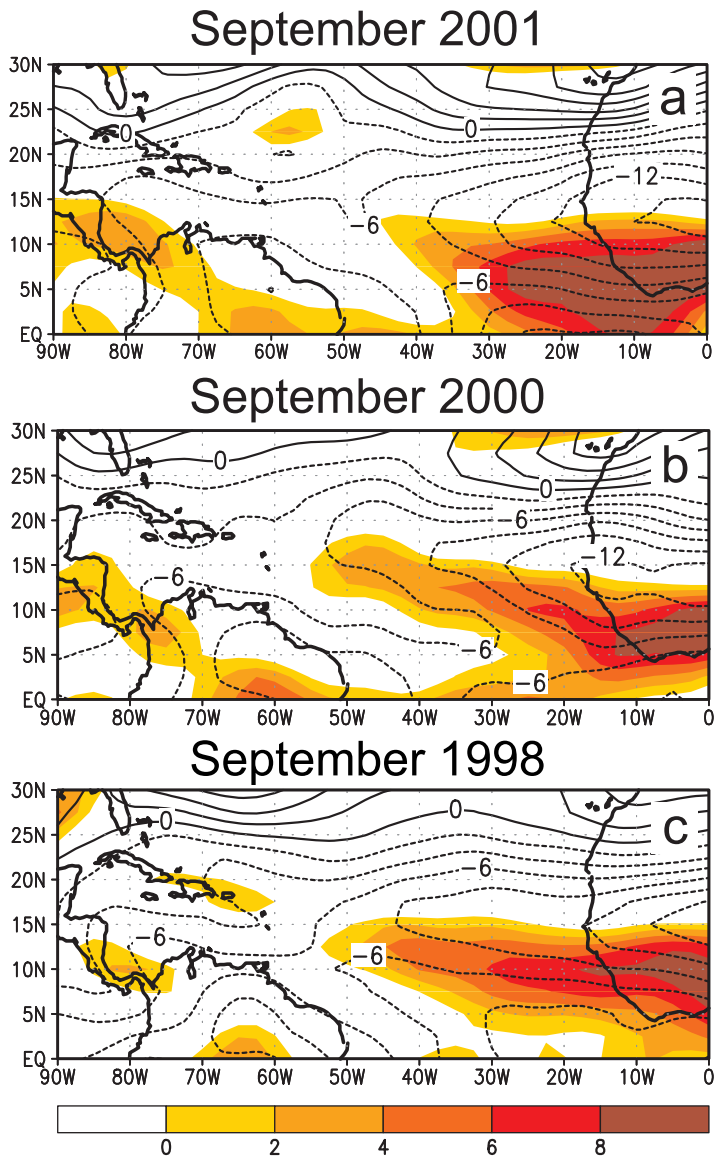

Fig. 35. Monthly mean 600-hPa zonal wind (contours) and cyclonic relative vorticity (shading) for (a) Sep 2001, (b) Sep 2000, and (c) September 1998. Contour interval for zonal wind is 2 m s^{-1}. Shading interval for cyclonic relative vorticity is 2 × 10^{-6} s^{-1}.

tical wind shear beneath an amplified upper-level ridge (not shown). It is likely that these conditions, and hence the longevity of Hurricane Olga, were again related to the return of the westerly phase of the QBO in late November.

c. Pacific tropical storms

1) Eastern tropical Pacific

The hurricane season in the eastern tropical Pacific occurs from May to November. On average, 16 named storms form including nine hurricanes, of which four are "major" (category 3 or higher on the Saffir–Simpson scale). In 2001, there were a total of 17 tropical cyclones, of which 15 became named storms and 8 hurricanes. Two hurricanes were classified as major storms.

No storm impacted land while at hurricane strength during 2001, though Hurricane Juliette, was just below minimal hurricane strength when it came ashore in Baja California on 30 September. For several days prior to landfall, Hurricane Juliette, a category-4 hurricane at its peak insensity, remained off the coast of the southern Baja California peninsula bringing hurricane-force winds, heavy rain, and battering waves to the region. Juliette produced the second lowest pressure ever recorded for a hurricane in the eastern Pacific at 923 hPa on 25 September. Despite the proximity to land and the strength of the storm, only two deaths were reported as a direct result of Juliette.

Another notable hurricane in the eastern Pacific basin in 2001 was Hurricane Adolph, the first named storm of the season. Forming on 25 May, it achieved hurricane status on the 27 May and maximum sustained winds of 125 kt were recorded on 29 May. It became the strongest and only category-4 May hurricane on record in the basin with a minimum central pressure of 940 hPa.

tral Atlantic near 33°N, 50°W (Fig. 36b). Both of these systems were short lived, and their association with the MJO-related distribution of below-average vertical wind shear over the tropical Atlantic (recall Fig. 34c), if any, is unclear. However, Hurricane Michelle formed during this period on 29 October over the southern Caribbean Sea within this region of below-average vertical wind shear (Fig. 34c).

The third system, Hurricane Olga, formed on 24 November near 29.5°N, 50°W ahead of a large-amplitude trough (Fig. 36c). Olga subsequently drifted for 11 days over the central subtropical Atlantic near 27.5°N, 65°W, in a region of well below-average ver-

2) Western North Pacific

Typhoon activity in the Western North Pacific occurs throughout the year although the peak activity is generally between July and November. In 2001 there were 33 tropical cyclones (including typhoons, tropical storms, and tropical depressions), close to the

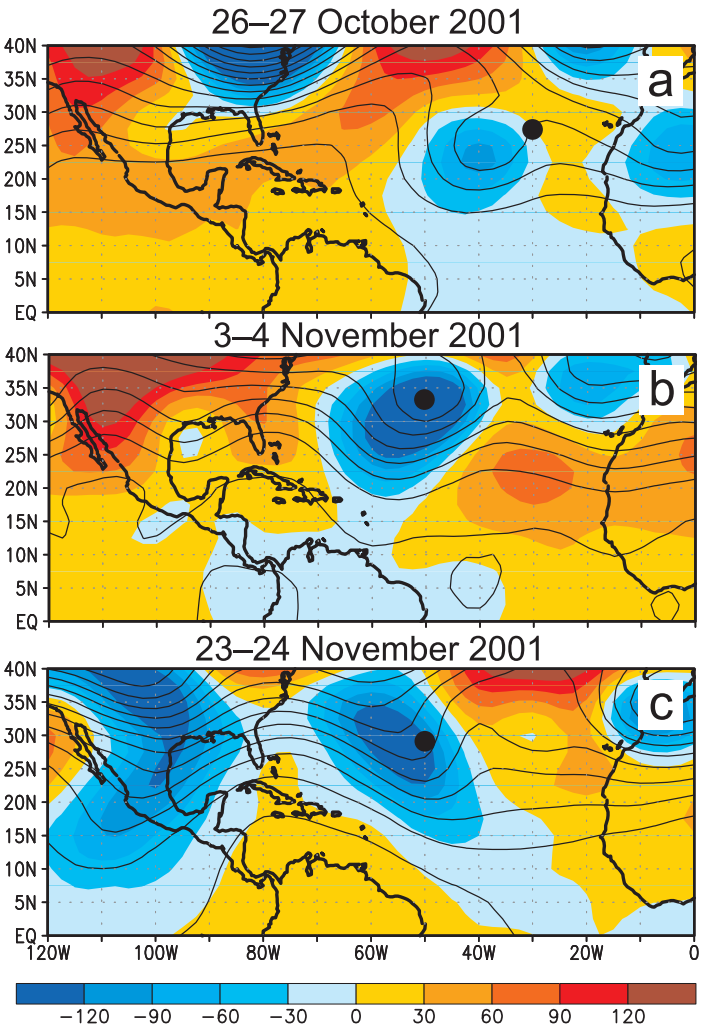

FIG. 36. 200-hPa height (contours) and anomalies (shading) for (a) 26–27 Oct 2001, (b) 3–4 Nov 2001, and (c) 23–24 Nov 2001. The solid circle in each panel represents the location at which (a) Tropical Storm Lorenzo formed, (b) Hurricane Noel formed, and (c) Hurricane Olga formed, respectively. Contour interval for heights is 60 m. Shading interval for height anomalies is 30 m. Anomalies are calculated with respect to the 1979–95 base period daily means.

1959–2001 average of 31.8 (Joint Typhoon Warning Center). Of these 33 tropical cyclones, 20 reached typhoon intensity, compared to an average of 17.6. Three typhoons, Wutip, Podul and Faxai, reached supertyphoon intensity.

Typhoon frequency during the 2001 season closely resembled the monthly climatology, with the number of storms increasing in June, peaking in August, and diminishing from September on. A notable feature of the 2001 season, was the development of two typhoons and a supertyphoon (Faxai) in December. The last occurrence of a supertyphoon in December was in 1964 (Supertyphoon Opal).

The ACE index (Bell 2000) for the western North Pacific is shown in Fig. 37. The ACE is the sum of the squares of the estimated 6-hourly maximum sustained wind speed in knots for all periods in which the tropical cyclones in the western North Pacific have either tropical storm or typhoon intensity during the June–November season. The 2001 ACE index value confirms this season's activity as being near normal, as does the number of tropical cyclones in 2001.

The 2001 typhoon season had a significant impact on Taiwan as the tracks of the three typhoons, Toraji, Nari, and Lekima, crossed the country as shown in Fig. 38. The average number of typhoons that pass through the Taiwan region is 3.6 (Sui et al. 2001, manuscript submitted to *Eos*). Because the country is densely populated these storms caused great economic damage and more than 100 fatalities. Typhoon Nari was especially damaging as it moved slowly over Taiwan during a 3-day period, bringing torrential rains to the island. Especially hard-hit was the northern part of the country with severe flooding, blackouts, and 92 associated deaths (Sui et al. 2001, manuscript submitted to *Eos*). Taipei received 1490 mm of rainfall in September 2001, more than four times the September climatological mean of 325 mm, primarily due to Typhoon Nari.

Japan was also heavily affected by typhoons in 2001. Two typhoons made landfall; Typhoon Pabuk and Typhoon Danas. Pabuk was the first typhoon to directly hit the Tokyo metropolitan area in three years. Typhoon Danas made landfall near Kamakura, about 45 km southwest of Tokyo, causing flooding and landslides and shutting down Japan's bullet trains.

In the Philippines, another strong typhoon—Utor—killed more than 70 people. The storm then made landfall in China, damaging hundreds of homes and flooding farmlands.

5. THE POLES

a. The Antarctic

1) STRATOSPHERIC OZONE

Since 1986, the NOAA/CMDL has flown ozonesondes at the South Pole station to provide a detailed

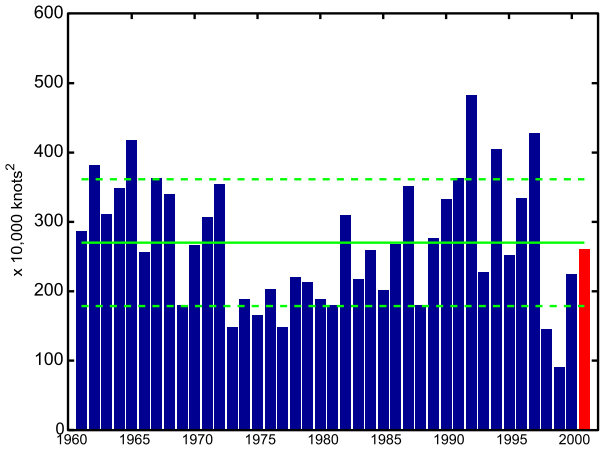

FIG. 37. ACE index for the western North Pacific for the years 1961–2001. The solid green line indicates the average for 1961–2000 and the dashed green lines show the average plus/minus 1 std dev. Data for 1960–2001 obtained from the Joint Typhoon Warning Center (JTWC). Units are knots^2.

look at the yearly ozone hole development. Balloon-borne ozonesondes are launched once per week throughout the year, but the frequency is increased to two or more per week as the first signs of ozone depletion appear in late August and then to every other day as the annual minimum approaches.

Figure 39a shows the summary of data obtained from 71 ozonesondes flown at the South Pole station in 2001. The blue line gives the total integrated ozone in Dobson Units (DU), while the red line shows the average temperature in the 20–24-km layer. Colder stratospheric temperatures precede severe ozone depletion, creating a more favorable environment for the formation of polar stratospheric clouds (PSCs). PSCs greatly enhance the reactions that process chlorine into compounds that are then easily photolyzed. At sunrise, free chlorine is produced in the stratosphere and begins destroying ozone in a catalytic cycle.

Three individual ozone profiles of altitude versus ozone partial pressure from the 2001 data are also presented in Fig. 39. Figure 39b shows the ozone profile before the ozone hole period began. As shown in Fig. 39c, ozone concentrations in the 14–22-km layer started dropping quickly after 1 September 2001 and reached a minimum by 28 September 2001 when nearly all the ozone in that region was destroyed. The ozone hole period (< 220 DU) ends when the polar vortex breaks up and midlatitude ozone-rich air moves over the Antarctic continent (Fig. 39d). The dashed lines in Fig. 39a show the data from 2000 when the polar vortex breakup occurred and, thus, also the end of the ozone hole, several weeks earlier than in 2001.

2) Temperature and sea ice

The climate of Antarctica is a crucial component in the global climate system. One important process in this region, which is ultimately controlled by temperature, is the formation of dense seawater at the coastal margin of the continent, which sinks and gradually moves northward contributing to the global ocean circulation. If temperature is warmer than average in these areas, the seawater does not cool down (one requirement for increasing density), nor is sea ice present, which, when formed, effectively increases salinity in the remaining unfrozen water (another requirement for creating water dense enough to sink). Failure for "deep water" to be formed in this region can have far-reaching climatic consequences both temporally and spatially. Temperature and precipitation across Antarctica also affects the extent of snow cover and sea ice, both of

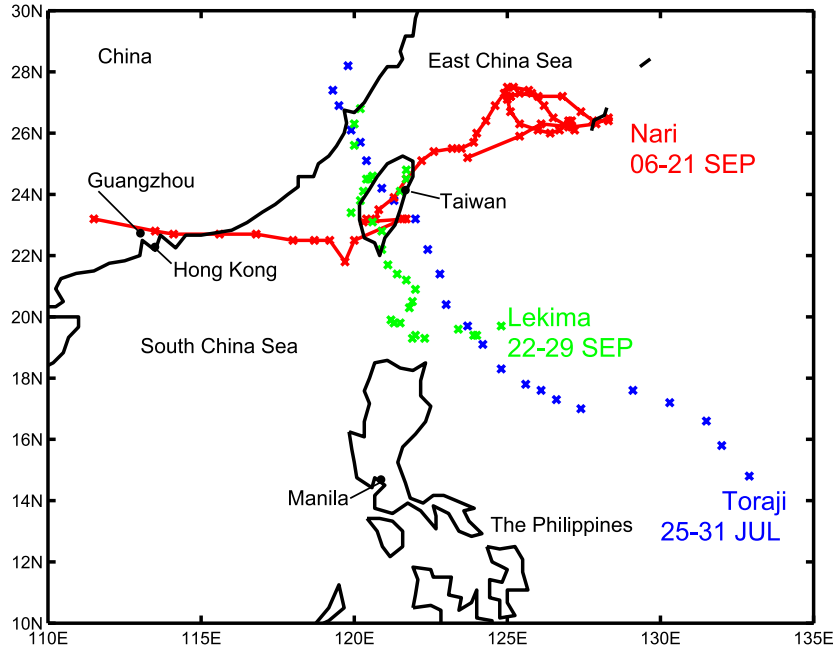

FIG. 38. Tracks of the three typhoons that hit Taiwan in 2001. Data obtained from the RSMC Tokyo-Typhoon Center.

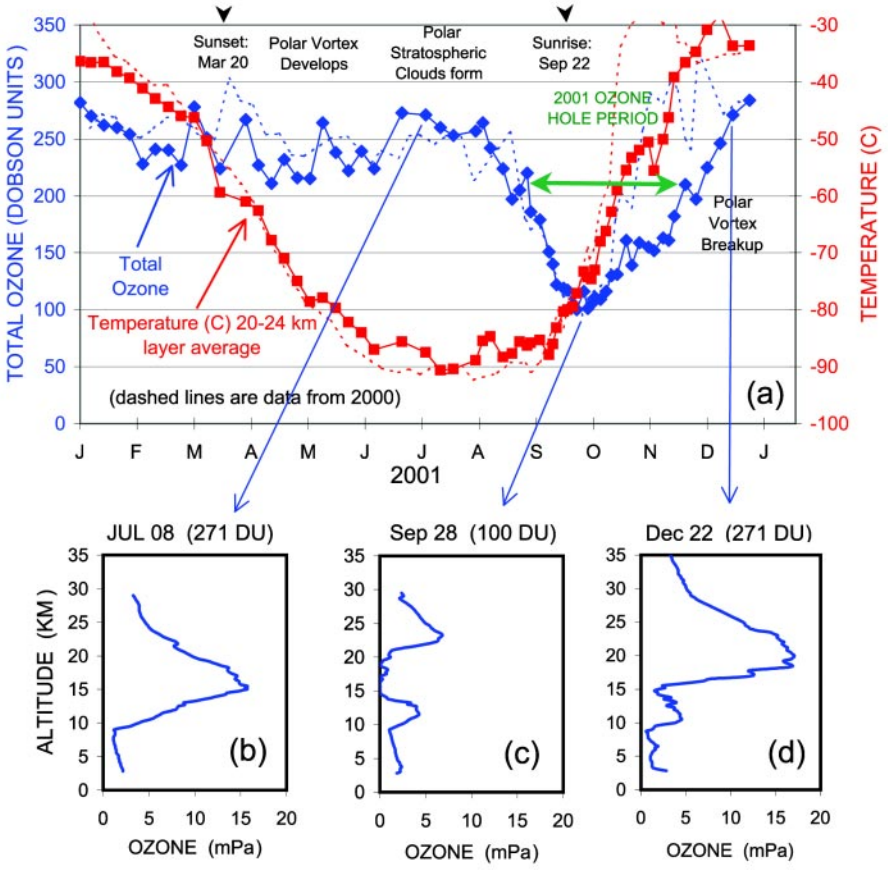

Fig. 39. (a) Summary of South Pole total ozone, DU and stratospheric temperatures measured by ozonesondes during 2001. Three selected profiles of altitude vs ozone partial pressure (millipascals) are also shown for (b) prior to the 2001 ozone hole, (c) at the peak of the hole, and (d) in the recovery phase. (Courtesy B. Johnson and S. Oltmans, NOAA/CMDL.)

which lead to changes in surface albedo. Reflectivity of the large Antarctic continent is an important component in the global radiation budget.

The annual temperature anomaly averaged over the continent of Antarctica for 2001 is shown in Fig. 40. Temperature was slightly below the 1971–2000 mean and was similar to 2000. The last eight out of nine years have remained below average temperature, in contrast to the general increasing temperature trend from 1959 to the early 1990s. In 1991, the Mount Pinatubo (Philippines) and Mount Hudson (Chile) volcanoes erupted, and it is possible (Jacka and Budd 1998) that these eruptions had a significant influence on the general lowering of temperatures after that year. Global temperatures have increased at a rate approximately 0.6°C century^{-1} since 1900, but since 1976 the global average has risen at a rate approximately 3 times faster than the century-scale trend. However, temperature records from surface observing stations in Antarctica do not reflect a similar rise. The cause of these differing trends may be, in part, due to the lack of available surface station data on the continent, especially since 1992. Depending on the dataset and analysis technique used in calculating average temperatures, the 1976–2001 trend in annually averaged temperature on the Antarctic continent is near zero in one type of analysis technique and nearly –0.4°C decade^{-1} using another technique. The large negative temperature anomalies during the years 1992 and 1993, may be partly due to the number of observing stations dropping significantly in addition to or instead of the effects of the aforementioned volcanic eruptions. During this same time period the Antarctic sea ice extent has remained relatively stable, or even slightly increased.

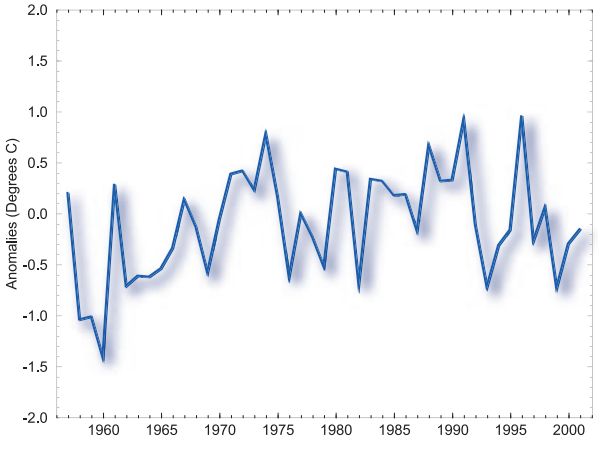

Fig. 40. Annual mean temperature anomalies (from a 1971–2000 base period) averaged across the Antarctic continent. (Global Historical Climate Network data and UKMO data.)

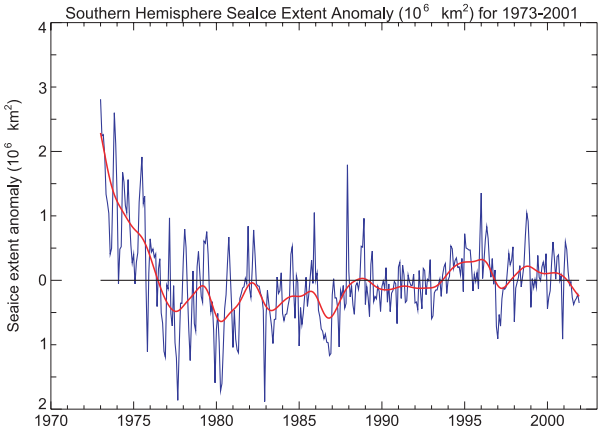

Fig. 41. Sea ice extent anomalies for the Southern Hemisphere. (Source: Hadley Centre, Met Office. Updated with help from NOAA/NCEP.)

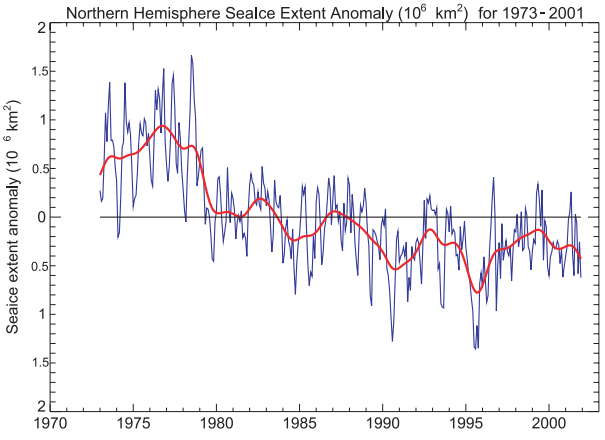

Fig. 42. Sea ice extent anomalies for the Southern Hemisphere. (Source: Hadley Centre, Met Office. Updated with help from NOAA/NCEP.)

In 2001, from the maps in section 7, it is clear that the Southern Ocean transitioned from generally below-average SSTs in the early part of the year, to mostly warmer-than-average SSTs toward the end of 2001. This is reflected in the Southern Hemisphere sea ice extent anomalies shown in Fig. 41. Sea ice extent was greater than average in the first 6 months of 2001, reaching a peak positive anomaly of approximately 1 million km^2 in the first 3 months.

b. The Arctic

Snow cover in the Northern Hemisphere, including Greenland and land regions extending into the Arctic is described in section 2d.

Annual sea ice extent was less than average in 2001 (Fig. 42), reaching a minimum anomaly of approximately –0.6 million km^2 in the middle of the year, continuing a general trend toward reduced sea ice since the early 1980s. However, there was not the sustained reduction of sea ice that was seen in 2000. Slighter greater-than-average sea ice extent existed for the first half of the year, before falling below average during the latter half of the year. Due to the land configuration north of the Arctic Circle, sea ice is highly variable between separate basins with different areas sometimes displaying opposite sea ice extent anomalies at the same time. In Fig. 43, sea ice extent is shown for the Arctic Basin over (Fig. 43a) the last 10 years and (Fig. 43b) over the last six months. This is the region covering the North Pole, and extending south to the coasts of Greenland and Iceland. It is clear from this figure that in 2001, the Arctic Basin experienced much-reduced sea ice compared to the last 10 years (Fig. 43a), and that the largest anomalies occurred in mid-September, with a significant, though short-lived reduction in sea ice in November (Fig. 43b). The largest anomalies in Sep-

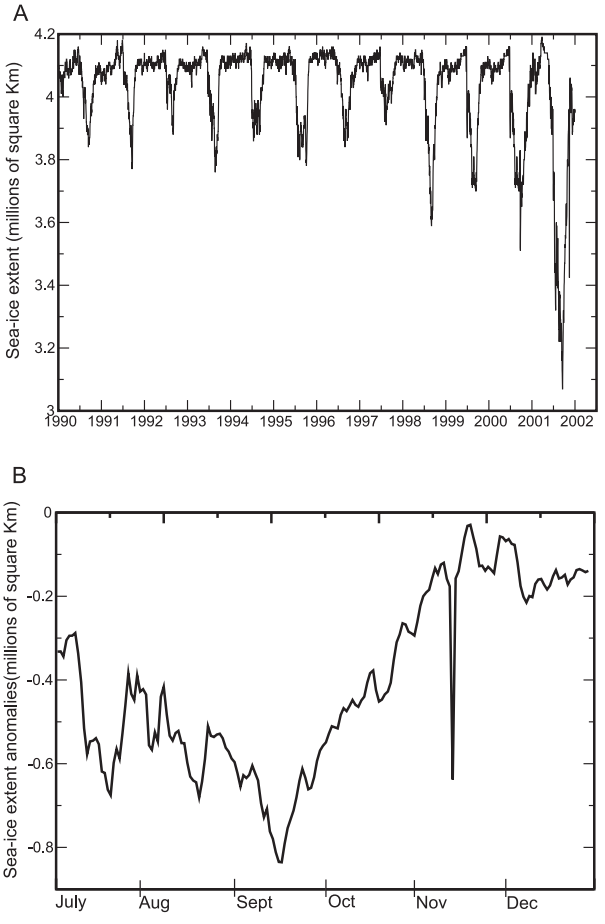

Fig. 43. (a) Sea ice extent for the Arctic Basin from Jan 1990 to Dec 2001, and (b) sea ice extent anomalies for the Arctic Basin in Jul–Dec 2001. (Data courtesy of B. Chapman, UIUC.)

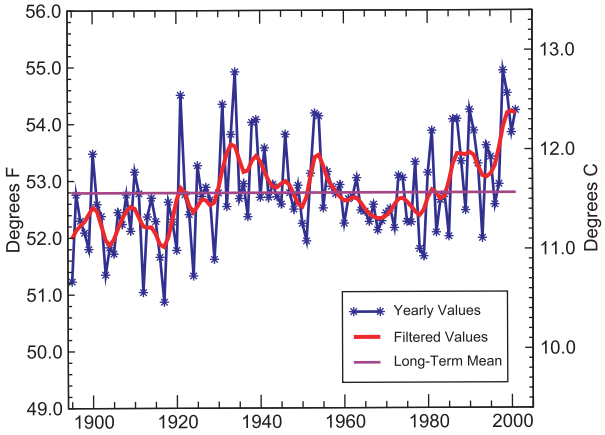

Fig. 44. Annual temperature for the contiguous United States over the period 1895–2001.

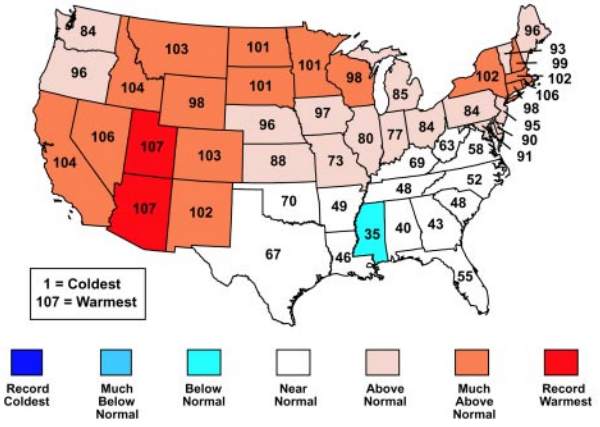

Fig. 46. Statewide rankings of temperature averages for Sep–Nov. See Fig. 45 caption for further details on how the states are ranked.

tember correspond to large positive 500-hPa height anomalies over much of the Arctic region during this month (not shown), along with pervasive Northern Hemisphere warmth throughout the boreal autumn.

6. REGIONAL CLIMATE

a. North America

1) United States temperature

The 2001 annual average temperature for the contiguous United States was 0.8°C above the long-term mean (1895–2001). This corresponds with a ranking of seventh warmest on record (Fig. 44). For the year, much above-normal temperatures (those within the top 10% of the historical distribution) existed across most of the Southwestern and Great Lakes states (Fig. 45), while above-normal temperatures occurred over the rest of the country except the Southeast where near-normal conditions prevailed.

Warmer-than-average temperatures dominated much of the western half of the United States during the spring, summer, and most notably in the fall in association with above-normal 500-hPa heights (Figs. 82, 84, and 86). Parts of the Southeast experienced cooler-than-normal conditions during January, March, June, and July, and especially September. During November, two-thirds of the country experienced much warmer than normal temperatures, which contrasts sharply with November and December of 2000, where more than half of the country was unusually cold.

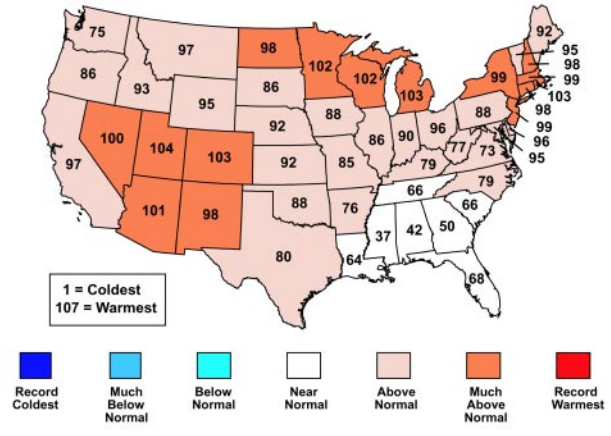

Fig. 45. Statewide temperature ranks for 2001. A rank of 107 represents the warmest year since 1895. Much above normal temperature is defined as occurring in the top 10 of recorded years which corresponds to a rank of 98-107. Above-normal temperature is defined as occurring in the warmest third of recorded years (or ranks 72–97). Much below normal temperature is likewise the 10 coolest years since 1895 and below normal is defined as the remaining cool third of the distribution.

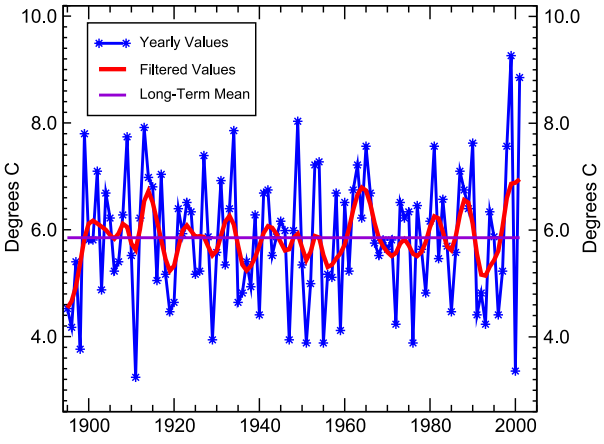

Fig. 47. Nov temperature for the contiguous United States over the period 1895–2001.

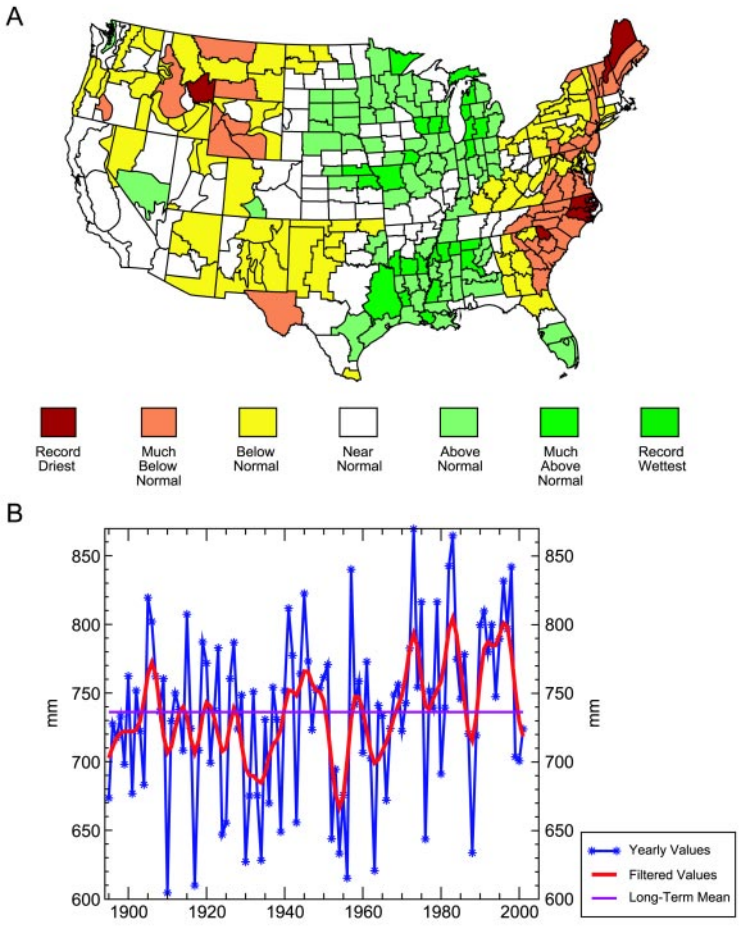

FIG. 48. (a) The 2001 annual precipitation distribution by climate division. Period of record for each division is 1896–present. The above- and below-normal ratings are calculated in the same way as for temperature, described in the caption for Fig. 45. (b) Annual precipitation totals averaged over the contiguous United States over the period 1896–2001.

A number of temperature records were broken during 2001. Most notably in Nevada, where the May, August, September, and fall season temperatures exceeded previous records. New Mexico and Arizona also broke records for the warmest fall, with temperatures in an additional 16 states in the West, northern Plains and the Northeast ranking in the top 10 warmest falls on record (Fig. 46). Alaska had its warmest winter (December 2000/February 2001) on record, 6.7°C above the long-term (1918–2000) mean. Five states (Minnesota, Iowa, Wisconsin, Michigan, and Illinois) set new temperature records in November, as all states in the contiguous United States experienced above-normal warm temperatures for the month. The large positive height anomalies observed across the United States during November reflected a persistent large-scale ridge over North America that corresponded to the displacement of the mean Hudson Bay low from its climatological position over eastern Canada and the eastern United States [Climate Prediction Center (CPC) 2001c]. Over the past three years, considerable variability in the November temperature record is apparent. November 2001, was the second warmest November on record for the contiguous United States. This followed the second coldest November on record in 2000 and the warmest in 1999 (Fig. 47).

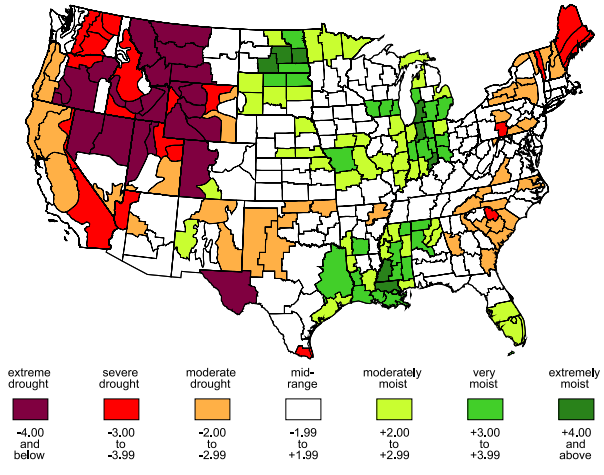

FIG. 49. The Palmer Drought Hydrological Index for October 2001 over the contiguous United States. This illustrates long-term hydrological drought conditions.

2) U.S. PRECIPITATION, DROUGHT, AND WILDFIRES

The wildfire season in the United States began later than usual, but escalated rapidly. Nationally, wildfire activity for the season was similar to the 10-yr average (1990–99), although Florida, Nevada, Washington, and Oregon had more active seasons than is typical. The combination of hot, dry, and windy conditions in addition to dry thunderstorms contributed to intense wildfire activity in many western states. Nearly 3.6 million acres burned during the 2001 season compared to 7.4 in 2000, one of the worst fire seasons in 50 years (Lawrimore et al. 2001).

Precipitation was slightly below average for the conterminous United States in 2001 with wetter-than-average conditions across much of the midsection of the country and dry conditions along the East Coast and parts of the Southwest and Northwest (Fig. 48a).

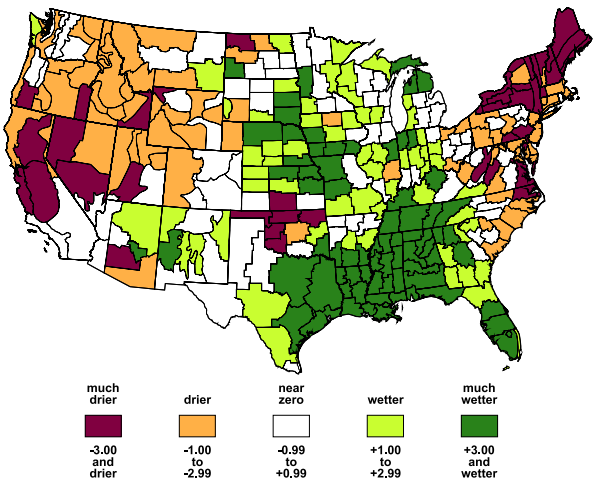

FIG. 50. The difference in the Palmer Hydrological Drought Index between 31 Dec 2000 and 31 Dec 2001, by climate division.

The preliminary annual average precipitation was 726 mm, which was 13 mm below the long-term (1895–2001) mean. This year marked the third consecutive year of below-average precipitation following nine years of precipitation surpluses (Fig. 48b).

Drought conditions across the United States in 2001 were not as widespread as in 2000. As the long-running La Niña faded to neutral conditions in the middle of the year, parts of the southern United States recovered from the nearly three-and-a-half-year drought, with the most notable improvement in Florida. Drought relief also occurred in the western United States with the onset of the climatological wet season late in the year. Severe to extreme drought (as measured by the Palmer Drought Hydrological Index) gradually expanded from about 15% of the country in January to a peak of about 20% in October 2001 (Fig. 49). This is considerably less than in August 2000 when nearly 36% of the country experienced severe to extreme drought conditions. A series of Pacific storms brought rain and snow to much of the western drought areas beginning in late autumn, contributing to a decrease in the drought area to about 15% by the end of December. The duration of the current drought period exceeds that of the late 1970s, but is less than that of the late 1980s, and the dust bowl droughts of the 1930s and 1950s. The most significant drought conditions in 2001 occurred in three broad regions: (i) across much of the western United States and Hawaii; (ii) in Florida and the Southeast; and (iii) along the Mid-Atlantic and New England states (see sections below). Figure 50 shows the change in drought conditions from the end of 2000 to December 2001 indicating that the East Coast and much of the West became drier during the year, while all of the Gulf States

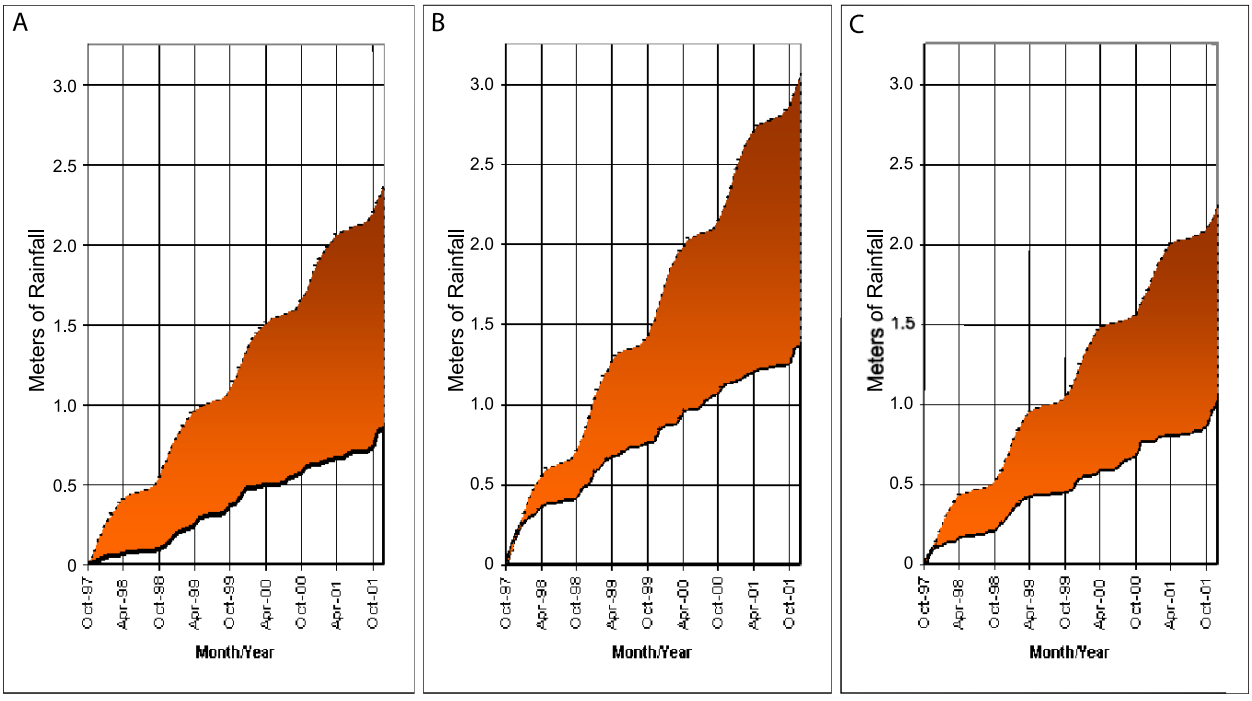

FIG. 51. Oct 1997–Oct 2001 accumulated observed precipitation (solid line) and accumulated 1961–90 mean precipitation (dashed line) for (a) Honolulu, (b) Molokai, and (c) Kahalui, Hawaii. Shading depicts the extent of the precipitation deficits.

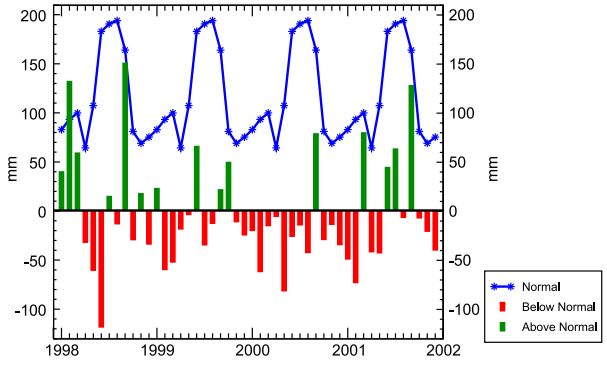

Fig. 52. Precipitation averaged over Florida for the period Jan 1998–Dec 2001. Normal and departures from normal.

and most of the central United States generally experienced wetter or much wetter conditions by year's end.

(i) The West Coast, Rocky Mountains, and Hawaii

Drought conditions, amplified by an atmospheric circulation pattern that deflected storm systems away from the West during the winter of 2000/01, affected many of the western states during 2001. Extremely dry conditions from November 2000 to March 2001 resulted in the second driest rainy season in the last 107 years in the Pacific Northwest, second only to 1976–77. Many rivers reached record low streamflow levels and reservoirs were depleted to meet water demands. Washington, Oregon, and Idaho each declared drought emergencies as the year progressed. The 2000–01 water year (1 October–30 September) was the driest on record for a number of locations in the western United States, Astoria, Portland, and Eugene, Oregon, broke previous low water year records by 20.5, 21.3, and 84.3 mm, respectively. Observations at these locations began in 1953 (Astoria), 1871 (Portland), and 1891 (Eugene). Reno, Nevada, also had its driest water year on record with a total of 54.1 mm, which is 28% of normal. Riverton, Wyoming, had its driest year (January–December) on record in 2001 with only 46% of the normal (1961–90) precipitation.

Wildfire potential in the western United States was exacerbated by much below normal precipitation during the winter of 2000/01. Dry, parched timber and grasslands were susceptible to ignition from lightning during dry thunderstorms and by late July through early August, the fire season escalated rapidly. Low relative humidity and strong winds helped spread the fires. During the first 20 days of August, 1.23 million acres were blackened in the Great Basin, Pacific Northwest, and northern California. Even though the western fire season began later than usual, it quickly reached proportions similar to the 10-yr average. Nevada, Washington, and Oregon had a more active fire season than usual, while acreage burned in the remainder of the West was less than average.

Beginning in October 2001, the northern branch of a pronounced split-flow configuration of the east Asian jet stream brought a series of Pacific storms across the Gulf of Alaska and into the Pacific Northwest, resulting in beneficial rains to the coast and snow to the western mountains (CPC 2001b). Much of Washington, Oregon, California, Nevada, and Idaho saw measurable improvement in drought conditions during the last three months of 2001, as an active storm track continued to bring much needed precipitation to the region.

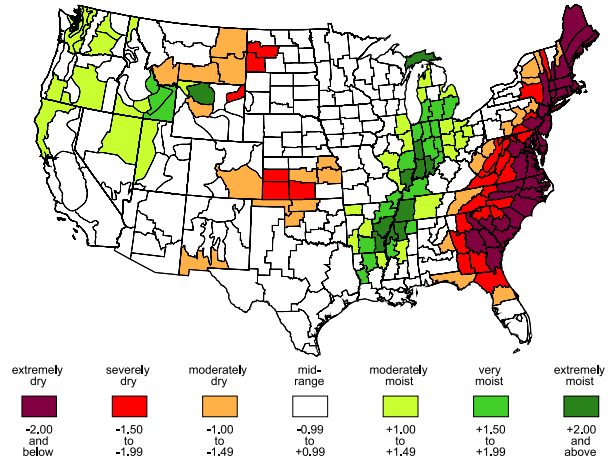

Fig. 53. The standardized precipitation index (showing short-term meteorological drought) for the 3-month period Oct–Dec 2001.

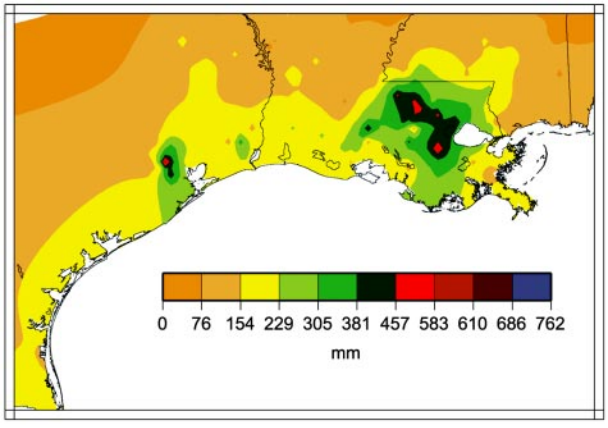

Fig. 54. Map of the Gulf States showing precipitation totals between 4 and 10 June, as a result of Tropical Storm Allison.

In Hawaii, drought conditions have persisted across a number of the islands since October 1997. Precipitation departures throughout the year in Honolulu, Molokai, and Kahului (Fig. 51) continued to increase until a more active precipitation pattern developed in October, associated with a well-defined subtropical jet stream, and rainfall amounts reflected near-average conditions through the end of 2001. As a result, drought conditions improved late in the year, but impacts associated with the drought persisted into the beginning of 2002.

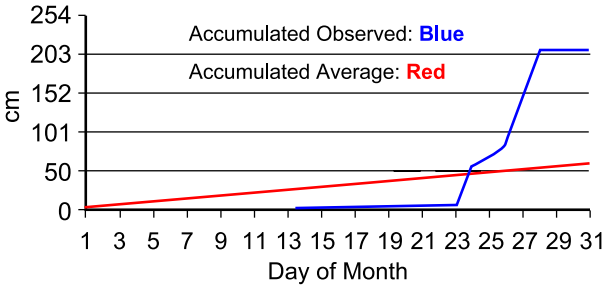

Fig. 55. Average and Dec 2001 snow accumulation for Buffalo, NY.

(ii) Florida and the Southeast

The drought in Florida began in mid-1998, with the onset of La Niña conditions in the eastern equatorial Pacific. The atmospheric circulation pattern that ensued inhibited the flow of Gulf moisture from Florida and the eastern states and resulted in a prolonged period of dry and warm conditions (Fig. 52). At the beginning of 2001, the drought and wildfire potential across much of Florida continued to be high. With ongoing warm and dry conditions, wildfires ignited throughout much of the northern and central portions of the state from February to May. Over 3100 wildfires burned more than 335,300 acres during the first five months of the year. By early March, Lake Okeechobee, the back-up reservoir for the east coast of Florida, dropped to just 2.7 m above sea level, the lowest level on record. In response to the worst drought conditions since the 1930s, emergency water-use restrictions were mandated across many Florida communities. Some relief, in the form of frontal activity, came in March, but it was not until Tropical Storms Allison and Barry in June and August, respectively, produced large rainfall totals, that much of the state began to recover. In September, Tropical Storm Gabrielle brought additional rainfall to the peninsula and finally broke the drought that had lasted for more than three years. By the end of the year, short-term dryness crept back into Northeastern Florida as drought conditions throughout much of the Southeast intensified.

Drought conditions throughout much of the Southeast also began in mid-1998. As with Florida, parts of the Southeast received some relief with frontal precipitation during March and summertime temperatures were generally cooler than normal across the region. Most of the Southeast appeared to be recovering from the long-term drought conditions until October, when the subtropical jet stream became entrenched across much of the Mississippi River and Tennessee Valleys, effectively shielding the Southeast from normal precipitation totals. As a result of the dry and unseasonably warm fall temperatures, drought conditions worsened across much of South Carolina, Georgia, and North Carolina during the last three months of the year. Charlotte, North Carolina experienced its driest year on record with only 61% of normal (1961–90) precipitation. Drought was blamed for one of the worst shrimping seasons on record in Georgia, and water restrictions were implemented in some Georgia cities by September. South Carolina forestry officials reported that January 2001 had more wildfire activity than any January in the last 15 years. South Carolina also had its second driest year on record (1954 was the driest). By mid-November, the worst wildfire season in a decade spread across parts of the southern and central Appalachians as warm, dry weather and an abundance of fallen leaves created near-ideal wildfire conditions. Nearly 1 million acres were consumed in the southern United States during the 2001 fire season.

(iii) The Mid-Atlantic and New England

Much of the eastern seaboard, from Georgia to Maine, experienced very dry conditions during 2001.

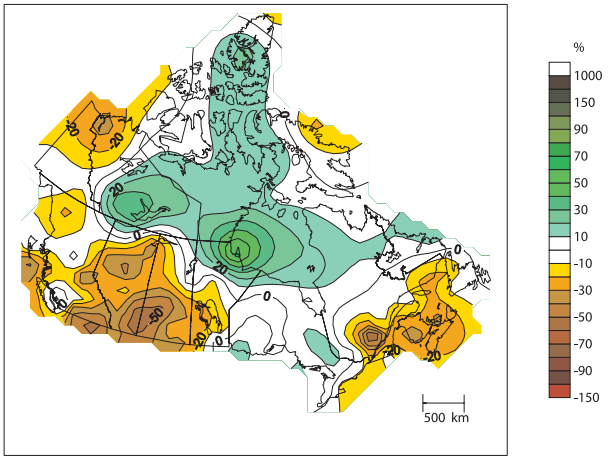

Fig. 56. Annual precipitation anomalies for Canada in 2001. Departures are from the 1951–80 base period.

Although the Southeast had been suffering from a drought for several years, a region of emerging drought in 2001 extended from Virginia northward into Maine. April 2001 was the driest April on record for both New York and Maine and during the last three months of the year drought conditions intensified (Fig. 53) along the entire eastern seaboard as a result of upper-level convergence and a large-scale sinking motion, which effectively reduced storminess and increased temperatures (CPC 2001c).

By early November, the upper Delaware Basin reservoir storage declined to drought warning levels, triggering emergency reductions in Delaware River flow targets and water diversions to New York City and New Jersey. November streamflow into the Chesapeake Bay was the lowest since records began in 1937. Both Delaware and Virginia experienced their driest fall (September–November) on record. Maine had its driest year on record (1895–2001) receiving only 738.5 mm of precipitation. This broke the previous record set in 1965 by 51.05 mm. As a result of the exceptionally dry conditions throughout the year, the Palmer Drought Index for December in Maine was the most severe in the last 100 years.

3) U.S. HEAVY PRECIPITATION EVENTS

Even though drought conditions prevailed across much of the western and eastern United States, a number of notable heavy precipitation events occurred in 2001. The most notable event was flooding along the Gulf and East Coasts from 4 to 18 June associated with Tropical Storm Allison. The storm itself was small in areal coverage, but remained close enough to the Gulf of Mexico and Atlantic Ocean to feed off the warm ocean waters. This allowed the system to survive over land for a long period, resulting in copious amounts of rainfall. On 5 June, an area of thunderstorms in the western Gulf of Mexico became increasingly organized and moved northward as Tropical Storm Allison, making landfall on Galveston Island. The strongest sustained winds were reported in southeast Texas, reaching 21.5 m s^{-1} with gusts up to 27.3 m s^{-1}. On 6 June, the storm weakened to a depression and continued to move inland reaching Lufkin, Texas, before turning southwest and heading back toward the Gulf of Mexico. After reentering the Gulf, Allison traveled eastward and made landfall along the coast of Louisiana. Although rainfall amounts associated with Allison were most notable in Texas and Louisiana (Fig. 54), Allison continued to move slowly across the Southeast and up the eastern seaboard resulting in very heavy rainfall. Storm totals across parts of Texas and Louisiana exceeded 500 mm with more than 200 mm along portions of the East Coast. Allison was the costliest tropical storm in U.S. history with $5 billion in damage.

In the northeast United States, a series of late-winter snow storms kept significant snowpack in place well into spring. An early February snowstorm brought more than 60 cm of snow from New Jersey to Maine with lesser amounts falling inland. Strong winds, which led to considerable drifting of snow, increased the impact of the storm. In early March, an-

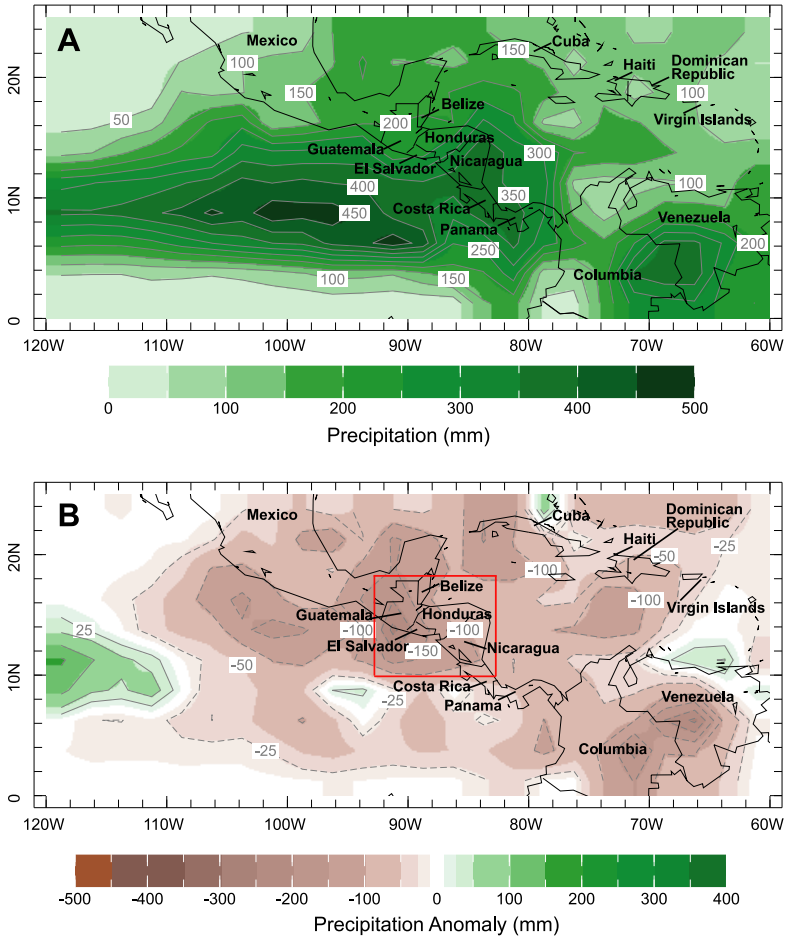

FIG. 57. (a) Climatological precipitation (mm) for June. Data from NOAA/Climate Prediction Center, CAMS_OPI. (b) Precipitation anomaly (mm) for Jun 2001. Data from NOAA, Climate Prediction Center, CAMS_OPI.

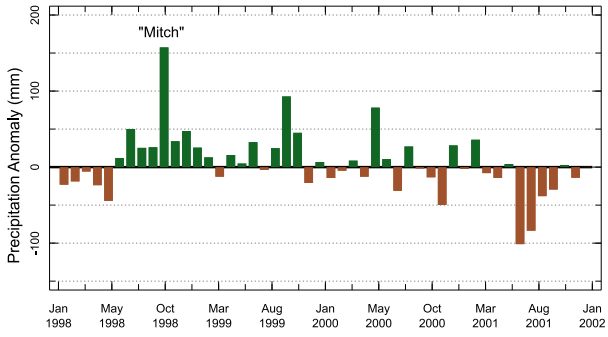

FIG. 58. Monthly precipitation anomaly (mm) for boxed region in Fig. 57b for the period Jan 1998–Dec 2001. Data from NOAA, Climate Prediction Center, CAMS_OPI.

other strong storm system moved up the East Coast. The heaviest snows occurred across interior sections of Pennsylvania, New York, and New England with 60 cm–1 m of snow reported at a number of locations. Winds associated with this storm gusted to over 27 m s^{-1}. Near the end of March, yet another storm moved up the East Coast bringing additional accumulations across portions of the mid-Atlantic and New England states. The snow lasted well into April with over 60 cm of snow still on the ground across much of Maine, Vermont, New Hampshire, New York, and Massachusetts.

Rapidly melting snowpack and heavy rainfall in portions of the Midwest led to flooding along the upper Mississippi River Basin. In places, flooding exceeded the levels of the great flood of summer 1993. Thirty to 60 cm of snow melted in early April across parts of northern Minnesota and Wisconsin and rainfall totals exceeded 200 mm in Saint Cloud and Duluth, Minnesota, and 175 mm in Rochester and Minneapolis, Minnesota. By midmonth, a low pressure system entered the Midwest and brought additional heavy rain to parts of Iowa, Minnesota, and Wisconsin. Both the Red and Mississippi Rivers exceeded flood stage by considerable margins in many places including Fargo, North Dakota; La Crosse, Wisconsin; and Winona, Minnesota. Flood levels at Davenport, Iowa, were just below levels reached during the 1993 flood. More than 300 miles of the Mississippi River were flooded with levels more than 1.5 m above flood stage by the end of the month. A second flood crest came in early May from St. Paul, Minnesota, to Hannibal, Missouri, when further heavy rains occurred in Iowa, Minnesota, and Wisconsin. River levels began to subside and conditions across the region gradually improved later in the month.

In December 2001, Buffalo, New York, broke a record for the most snowfall received during any month of the year with 210 cm, nearly all of which fell from 24 to 28 December (Fig. 55). The previous maximum monthly snowfall record of 173 cm occurred in December 1985. Downwind of Lake Ontario, Montague, New York, received 322 cm of snow during the same period. Unseasonably warm temperatures during the fall and early winter in the Northeast kept the Great Lakes water temperatures warmer than normal. By the last week of December, a strong polar low pressure system over Hudson Bay became cut off from the upper-air pattern and remained in place for several days. This system advected strong and cold Canadian air across Lake Erie, which led to the unprecedented snowfall amounts observed in and around the Buffalo area. Prior to Christmas Eve, only 3 cm of snow had fallen the entire season.

4) CANADA

Canada experienced one of its most serious and extensive droughts on record in 2001 (Fig. 56) The worst affected areas were in the Canadian Prairies where the 2001 drought follows two to three years of below-average rainfall. Saskatoon, Saskatchewan, was 30% drier than in any other year in the last 110, and the government of Alberta declared a drought before the summer season began. Yet, despite the exceptionally dry conditions, the wildfire season in Canada was the least active in the last 11 years of monitoring in terms of hectares burned. A combination of high humidity, few lightning strikes, and good fire management ensured that the enormous fire potential in much of Canada was not realized.

Canada had its third warmest year in over 50 years

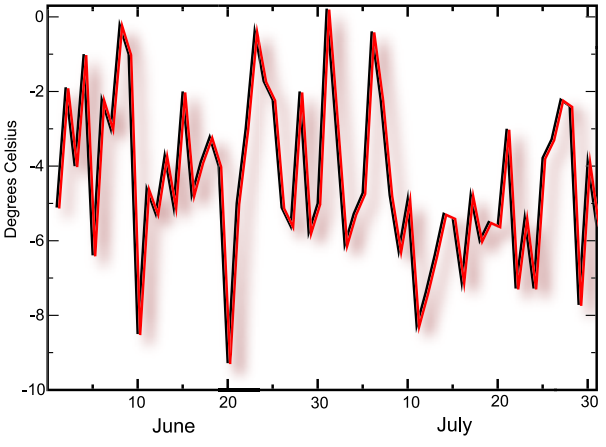

FIG. 59. Daily minimum temperatures (°C) for Jun and Jul in La Paz, Bolivia. (Source: National Climatic Data Center, DATSAV3 database.)

of reliable records. As with many other countries, 1998 remained the warmest year on record and in Canada, 1981 holds second place. Through the end of 2001, Canada had experienced 18 consecutive seasons with above-average temperatures, starting in the summer of 1997. During the summer season, many cities far exceeded previous records for the number of "hot days" (temperatures above 30°C). Montreal had 23 hot days in 2001 compared to an average of 9, and Ottawa had 26 compared to the average of 14. An exceptional heat wave also occurred across southern Canada, due, primarily, to an amplified summertime ridge extending from Texas north to Hudson Bay, and then moving westward throughout the second half of August. In Winnipeg, high humidity in addition to warm temperatures led to a heat index of 46°C in early August, and resulted in many heat-related illnesses.

In contrast, the 2000/01 winter in eastern Canada was one of the snowiest in 20 years. In Toronto, there were 104 consecutive days of snow on the ground—the longest stretch in 130 years of records. In Newfoundland, the largest seasonal snowfall accumulation in over a century fell in the capital, St. John's, with a final total of 648.4 cm. St. John's was in the path of almost every winter storm that crossed North America in 2000/01. In contrast, the 2001/02 winter season started very late with temperatures barely dipping below freezing in Toronto by the middle of December, a reflection of ridging over eastern Canada and the eastern United States.

b. Central America

The climate of Central America can generally be described as tropical wet or dry in the western areas of the isthmus, and tropical wet in the eastern areas. Locally, precipitation can be highly dependent on topography and its relative orientation to the prevailing easterlies. In general, the annual pattern of rainfall is bimodal with relative maxima in early boreal summer and autumn with greatest total annual precipitation amounts along coastal areas of the Caribbean. In 2001, following near-average rainfall in May, an abrupt and widespread failure of wet season precipitation during the month of June (Fig. 57) marked the onset of severe drought conditions across much of Central America as deficient rainfall persisted in many areas through July and August (Fig. 58). Most affected were the countries of Honduras, Nicaragua, Guatemala, and El Salvador, although unusually dry conditions were also observed in sections of Costa Rica and Panama. Over one million people were directly affected by the drought, considered to be the worst natural disaster to impact the region since the devastating effects of Hurricane Mitch in October of 1998.

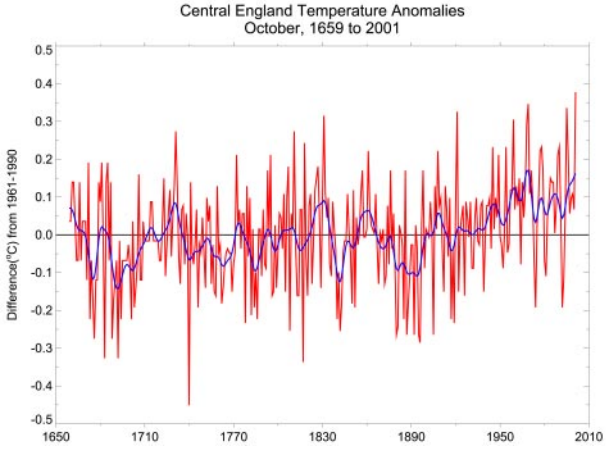

FIG. 60. Central England mean temperature anomalies for Oct, 1659 to 2001. The time series is fitted with a smoothed 21-term binomial filter [Source: Parker et al. 1992).]

With much of the region dependent on subsistence farming, the drought had dire consequences. In many agricultural areas the onset of the drought occurred during early stages of the first crop cycle with crop failures becoming numerous by the end of June as adequate rainfall failed to materialize. In Nicaragua, the World Food Program reported maize crop losses exceeding 90% in some areas with bean crop failures as high as 70%. Significant crop losses also occurred in Honduras and in Guatemala where June rainfall in some locations was only 40% of the long-term average. Due to the drought, many subsistence farmers were forced to consume seeds intended for planting of second-season crops. All of the affected countries are net importers of maize and beans and the implications of drought on the economy and food security led the governments of Honduras and Guatemala to declare states of emergency in July.

Rainfall in July and August, though generally more widespread than in June, remained well below average in many locations. A return to more abundant rainfall occurred over much of the region during September, when many second-season crops are planted. Hurricane Iris struck Belize and northern Guatemala in early October with Tropical Storm Michelle bringing very heavy rains and flooding to east coastal areas of Nicaragua and Honduras later in the month.

c. South America

The climate of South America for 2001 was characterized by significant variability. As for many other countries, the annual mean temperature over the whole continent was generally above average. Regions

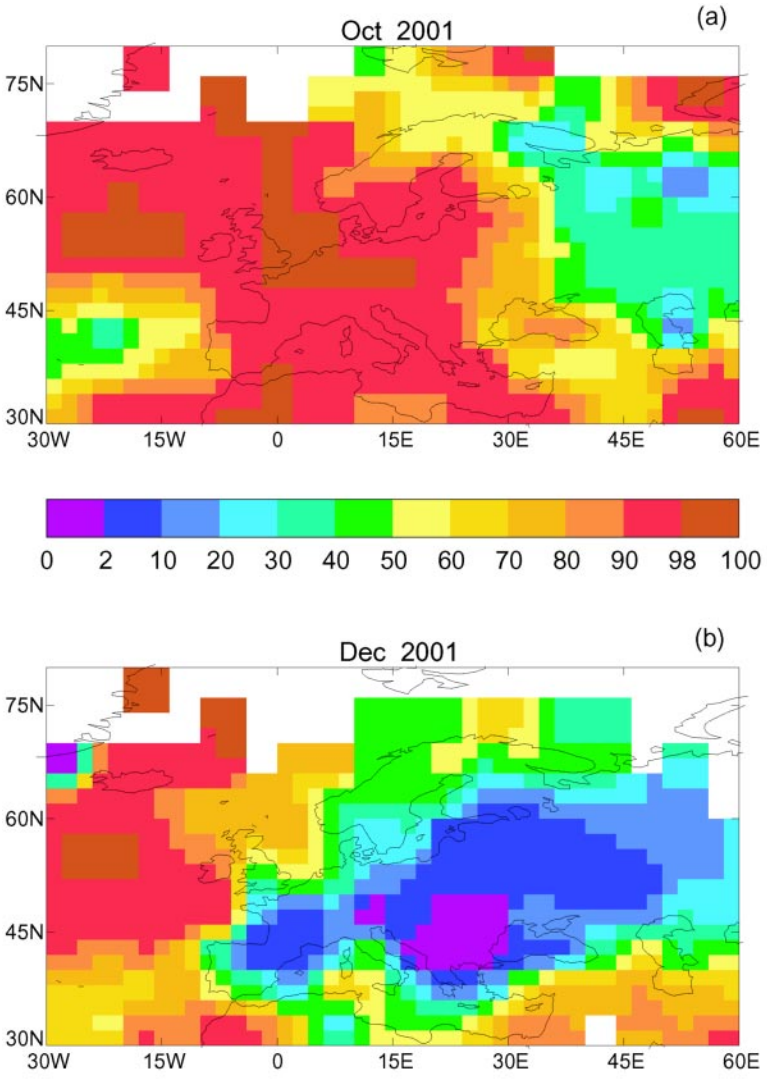

Fig. 61. European surface temperature expressed as percentiles of 1961–90 modified 2-parameter gamma distributions for (a) Oct 2001 and (b) Dec 2001 [Source: Jones et al. (2001), Horton et al. (2001).]

that experienced especially warm temperatures included much of Brazil, portions of Argentina, and the northwestern portion of the continent (far western Amazon Basin and Colombia) while cool anomalies were limited to areas of Bolivia (Fig. 3).

Most of Brazil suffered from drought throughout the austral summer (December 2000 to February 2001) and autumn (March–May; Fig. 10). The summer dryness resulted primarily from a lack of convective activity usually associated with the South American Convergence zone (SACZ). The summer is generally the rainy season for southeastern and central Brazil so the lack of rain caused a critical energy shortage, since most of the power in this populated region is generated from hydroelectricity. Dryness continued into the autumn with some areas in western and northwestern Brazil experiencing rainfall deficits of greater than 400 mm. Despite some torrential rainfall in April in western Brazil, which killed at least 13 people, rainfall deficits persisted into the winter (dry) season. Although beneficial rains led to improved conditions by November, considerable time will be required for water recharge.

In contrast to the drought in Brazil, the year began with heavy rainfall and flooding in parts of Peru and Bolivia. The rainfall from January to March led to the declaration of a state of emergency by the Bolivian government in February and over 40 people died as a result of the flooding. The La Paz area experienced the worst conditions with over 20 000 families being affected. Flooding in east-central Argentina also occurred in March, with between 200–300 mm falling in portions of the Cordoba and Buenos Aires provinces.

Heavy rains and winds occurred in Chile and Uruguay in June. The rains caused 5000 people to lose their homes in the northern Uruguayan city of Artigas. Winds from the strong midlatitude storm gusted up to 41 m s^{-1} in the southern portion of Uruguay and caused millions of dollars of damage and lead to the death of at least three people. Also in June and July, Bolivia experienced unusually cold conditions

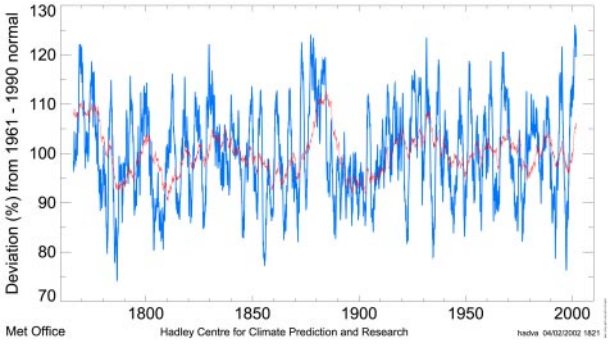

Fig. 62. 24-month running England and Wales precipitation totals, 1766–2001 (blue), based on Jones and Conway (1997) and Alexander and Jones (2001). The low-pass time series (red) has been passed through a 121-term binomial filter to highlight interdecadal variations.

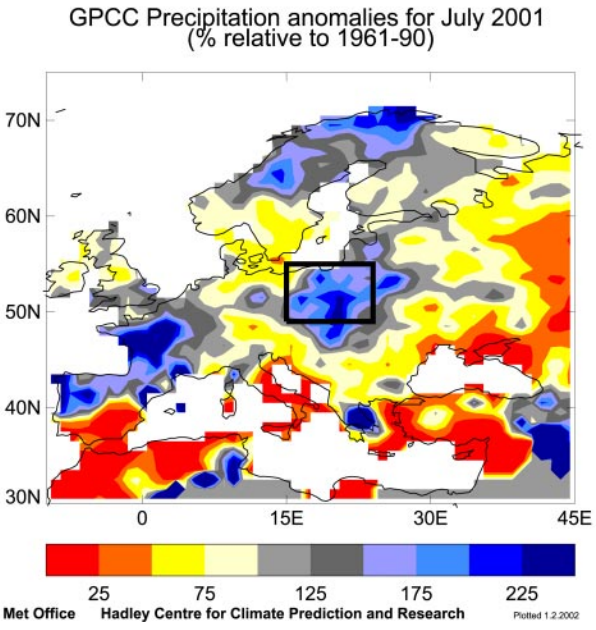

Fig. 63. Percentage precipitation anomalies with respect to 1961–90 in Jul 2001 for the European region. The black rectangle indicates the position of Poland. [Source: GPCC (1998), Rudolf et al. (1994).]

(Fig. 59), with La Paz, El Alto, and Tarija reporting several deaths from the low temperatures and accompanying snow. Snow accumulated in El Alto to a depth of 10 cm.

During the late winter and spring (August–October) in Argentina and adjacent Uruguay, above-average precipitation led to severe flooding in the Pampas region. More than 3.2 million hectares of agricultural land were inundated and thousands of people were forced to evacuate the area. October rainfall amounts were twice the average in Buenos Aires.

d. Europe

1) Temperature

Annual temperatures in 2001 were above average across Europe. Western Europe experienced annual anomalies (with reference to a 1961–90 base period) of 0.5°–1°C above average while eastern Europe was generally warmer, with average departures of more than 1°C. (Fig. 3) The only area of cooler-than-normal temperatures occurred in parts of Scandinavia where temperatures averaged as much as 0.5°C below the mean, with the most anomalous conditions in the spring (March–May) season.

Anomalous warmth was widespread in all four seasons, though there was much regional variability. Most of Europe had above-average temperatures during the 2000/01 winter season (December 2000/February 2001; Fig. 80) with the largest positive anomalies occurring over the eastern Mediterranean region. Cooler-than-average conditions were limited to Ireland and parts of Norway. Record cold temperatures also occurred over portions of Sweden, although the winter season was warmer than average for the country as a whole. March was notably warm across most of southern Europe. Record high temperatures occurred in Bulgaria, Cyprus, and eastern Spain, while the spring season was notably warm in the eastern Mediterranean but cool in a large part of Scandinavia. A heat wave developed in western Europe during June, but was broken by a series of thunderstorms in July. Warmer temperatures returned in August when parts of eastern Europe experienced record high temperatures in the middle of the month. This was consistent with the 500-hPa circulation anomalies that featured above-average heights from the central North Atlantic to southwestern Russia for the month of August (CPC 2001a).

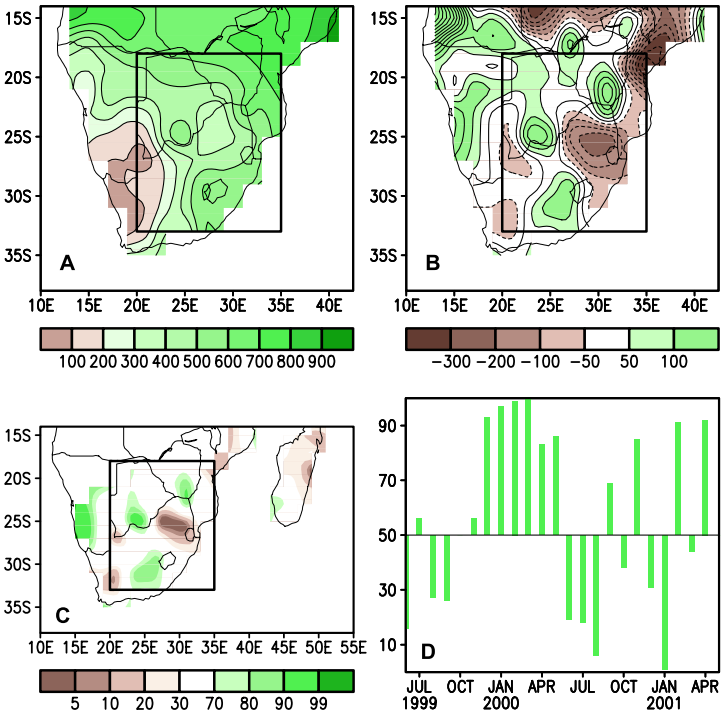

Fig. 64. Oct 2000–Apr 2001 (a) total precipitation (mm), (b) precipitation anomalies (mm), (c) precipitation percentiles based on a gamma distribution fit to the 1961–90 base period. (d) A monthly time series of precipitation percentiles, based on precipitation totals averaged over the boxed region depicted in (a)–(c).

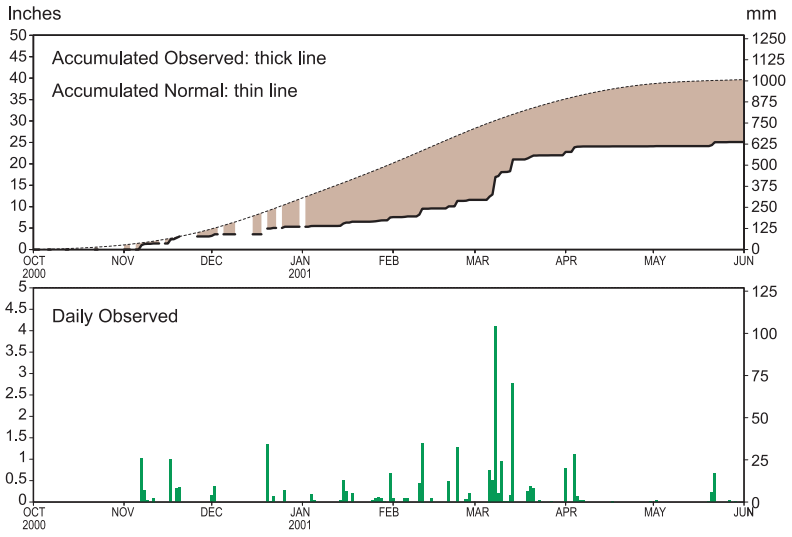

Fig. 65. Daily and accumulated precipitation (mm) at Nampula, Mozambique, during Oct 2000–Jun 2001. Accumulation of climatological precipitation also shown. Base period 1971–2000.

In the 343-yr central England temperature time series, October 2001 was the warmest October on record (Fig. 60). Every day in October was warmer than the long-term average for central England and several days were above the 95th percentile of the 1961–90 temperature distribution. The anomalous warmth was also reflected in Denmark and Germany as they experienced their warmest October since records began in the late nineteenth century. Temperatures in Germany were as much as 4°C above average. Most of Europe recorded temperatures in the top 10th percentile, with some areas exceeding the 98th percentile (Fig. 61a). The year ended (Fig. 61b) with severe winter weather resulting from a strong depression that tracked south from Russia and settled over Greece and much of southern Europe. A state of emergency was declared in parts of Greece and main roads into Greece and Turkey were closed as temperatures fell to as much as 23°C below average and snowstorms made travel hazardous or impossible. The northeastern region of Catalonia in Spain also experienced extreme cold and snow and was virtually cut off from the rest of the country. [See also section 6d(ii).] Scandinavia and the United Kingdom were much less affected by this severe weather and the United Kingdom experienced its sunniest December in nearly a 100-yr record.

2) Precipitation

Much of the Mediterranean region and southern Europe experienced below-average precipitation in 2001, as did the northwestern United Kingdom. Wetter-than-average conditions prevailed over central and northern Europe and Scandinavia.

After a dry start across much of Europe in January and February, many regions experienced more than twice their average monthly precipitation in March. Most notably, northwestern Iberia was affected by persistent heavy rainfall throughout most of the month with the Portuguese town of Porto receiving nearly 4 times its normal amount of precipitation. However, eastern parts of Spain experienced well below average precipitation during the same period. The Bretagne region of France had exceptional precipitation in the 6-

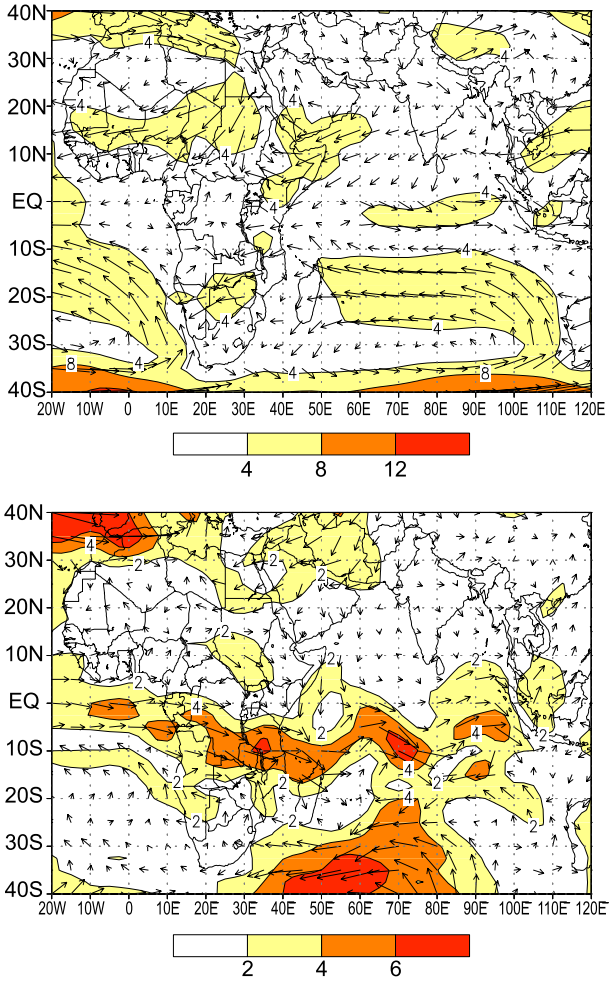

Fig. 66. 850-hPa total wind for (a) Oct 2000–Apr 2001 and (b) Jan 2001 wind anomalies. Anomalies are departures from the 1979–95 base period means.

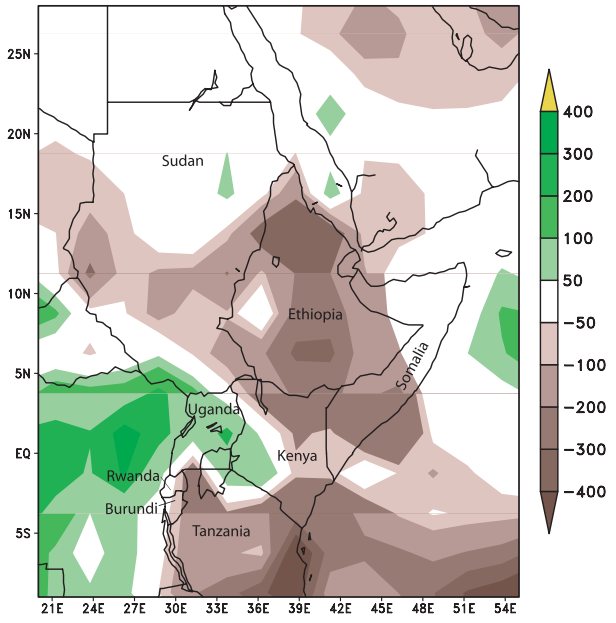

Fig. 67. Annual precipitation anomalies for 2001 from (CAMS) combined satellite and rain gauge–derived precipitation estimates. The anomaly base period is 1979–95.

month period ending in March with numerous cities setting 6-month rainfall records. The 24-month period ending in March was the wettest in the 236-yr England and Wales precipitation series (Fig. 62). Also in March for a third consecutive year there was severe flooding in parts of eastern Europe. The Tisza River rose to 7.6 m at Zahony in Hungary, its highest level since 1888. Poland experienced more wet weather in April and although most of Europe was very dry in May and June, a series of July storms produced the worst flooding to affect Poland since 1997 along the Wisla River (Fig. 63). These floodwaters killed at least 52 people in Poland and 39 in the Czech Republic and displaced 140 000 people from towns and villages in southern and southwest Poland. The principal cause of the extreme precipitation was a nearly stationary upper-level low pressure center over southeast Europe. Figure 63 also shows that at this time there was well above average rainfall in much of France and the northwest of Spain and Portugal. Although Europe was generally drier than average in August, some regions received extreme daily rainfall amounts such as the town of Pozega, Yugoslavia where more than the average monthly rainfall fell in just 6 h. The year ended in Europe with an upper-level trough of low pressure bringing snow, floods, and high winds across much of the southern part of the continent. Two ships sank in the Black Sea off the coast of Turkey due to strong storms on 8 and 9 December. Snows also cut off hundreds of villages in northeastern Turkey.

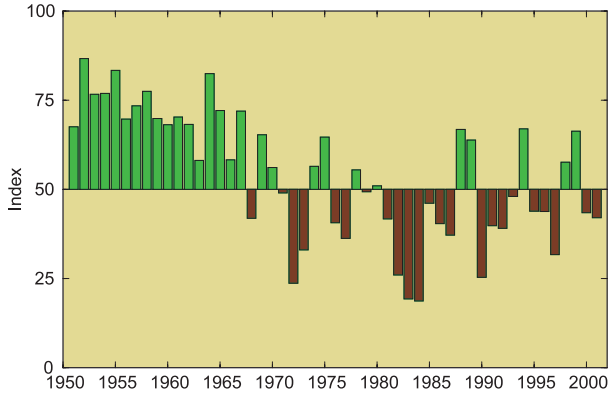

Fig. 68. Jun–Sep 2000 precipitation anomalies (mm) for the Sahel.

e. *Africa*

1) The southern Africa rainy season

The rainy season in southern Africa extends from October to April, with the largest rainfall totals typically observed between December and March. In general, southern Africa rainfall tends to be below aver-

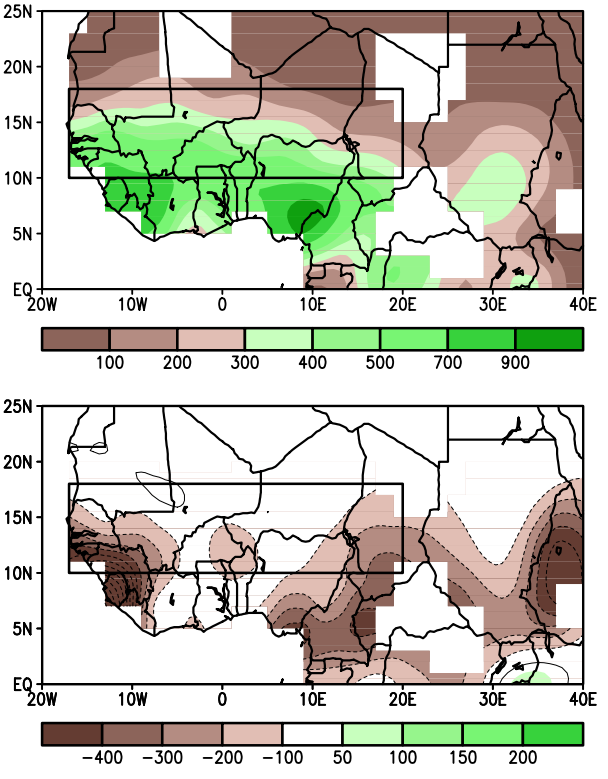

Fig. 69. Percentile index (average gamma percentiles of station precipitation within region) for the Sahel during Jun–Sep. Percentiles are computed for the 1961–90 base period.

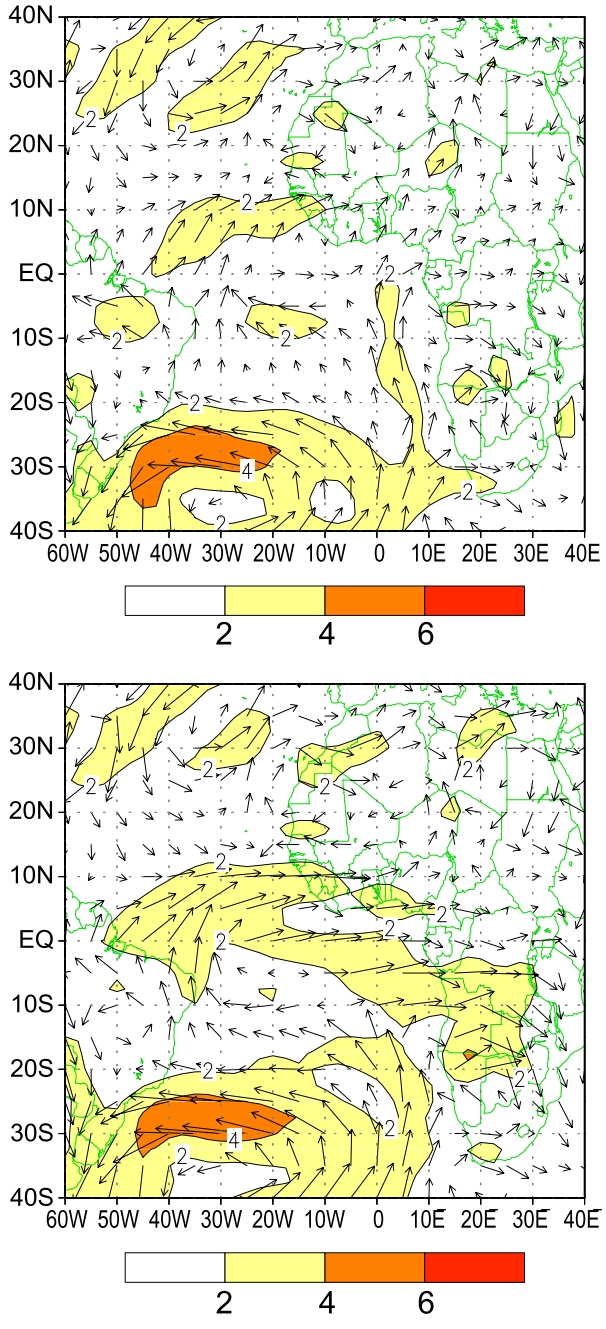

Fig. 70. (a) 925-hPa wind speed (m s^{-1}) and vector wind during Aug–Sep 2001. (b) 850-hPa wind speed anomalies and vectors for Aug–Sep 2001. Anomalies are departures from the 1979–95 base period.

age during El Niño episodes, and wetter than average during La Niña (Ropelewski and Halpert 1987, 1989, 1996; Hastenrath 1995; Dai et al. 1997; Thiaw et al. 1999). However, the overall rainfall pattern in 2000–01 was more the result of internal variability in the atmosphere, and less consistent with the prolonged cold ENSO episode that lingered from the fall of 1998 into the fall of 2001, and which resulted in above-normal rainfall across much of southern Africa during the 1998–99 and 1999–2000 seasons.

The 2000–01 southern Africa rainy season was characterized by significant rainfall deficits along the east coast from northeastern South Africa northward into Mozambique (Figs. 64a,b). Rainfall amounts in this region averaged only between 300 and 800 mm, and only in the 5th–20th percentile locally in northeastern South Africa (Fig. 64c). Overall, the rainy season was marked by large intraseasonal variability, with a delay in the onset of the rains in October 2000, a late withdrawal of the rains in April 2001, and alternate periods of dry and wet spells in between (Fig. 64d). A time series of cumulative and daily precipitation for Nampula in northeastern Mozambique, shown in Fig. 65, is typical of the dryness along the east coast of southern Africa. Rainfall was well below normal in December and January, followed by a gradual recovery in February and March 2001. The exception to the dryness in the east coast of southern Africa was southern Zimbabwe, which received rainfall totals in the 70th–90th percentile. Near- to above-normal rainfall was also observed over much of central and western southern Africa, which is climatologically drier than the east coast. Rainfall totals in central South Africa, Botswana, and Namibia, ranged between 200 and 600 mm and were in the 70th–90th percentile in some areas.

The low-level atmospheric circulation for the 2000–01 rainy season featured easterly winds that averaged about 4 m s^{-1} from the east-central Indian Ocean westward into Madagascar and portions of interior southern Africa. This easterly flow was found along the equatorward flank of the Mascarene high pressure system and was very close to the climatological mean wind in this region for the period October–April (Fig. 66a). The significant rains observed early in November 2000 were associated with an amplification of the Mascarene high pressure system indicated by 2–6 m s^{-1} easterly wind anomalies across much of the southern and central Indian Ocean and the presence of a cyclonic circulation centered over southern Angola. This cyclonic–nticyclonic pattern resulted in strong low-level convergence and enhanced convection across much of northeastern southern Africa. In contrast, the dry spell observed in December 2000 and January 2001, when the season was at its strongest was associated with a weakening of the Mascarene high pressure system, indicated by 2–4 m s^{-1} westerly wind anomalies across much of the central Indian Ocean and eastern southern Africa. This anomalous circulation was even more enhanced in January, with broad westerly wind

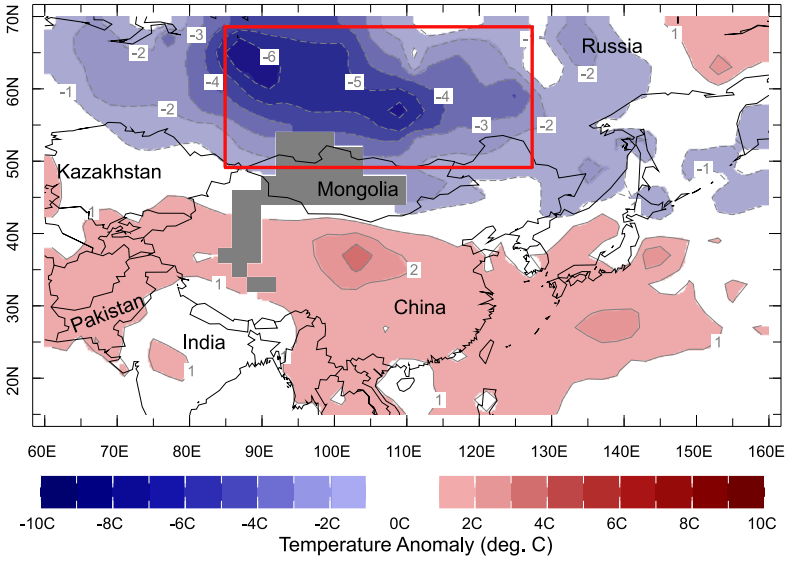

Fig. 71. Average surface air temperature anomaly (°C) for the period Nov 2000–Feb 2001. (Data from NOAA, Climate Prediction Center, CAMS.)

anomalies that extended from the Gulf of Guinea and crossed central and southern Africa into the central Indian Ocean (Fig. 66b). The pattern of dryness observed in December and January 2000–01 was followed by enhanced rainfall activity in February. Extreme heavy rainfall in the range 300–500 mm (not shown) inundated the central provinces of Mozambique, southern Malawi, north-central Zimbabwe, and southern Zambia. This pattern was consistent with an enhancement of convection over Indonesia, but also with the establishment of a circulation pattern similar to that in place in November 2000. However, consistent with the overall pattern of atmospheric circulation for the season, tropical cyclone activity was weak. However, it should be noted that Tropical Cyclone Dera, which formed over the Mozambique Channel on 9 March, brought very heavy rains and flooding to northern Mozambique and the west coast of Madagascar.

2) The Greater Horn

Long-term drought in portions of Kenya, Somalia, Mozambique, and Tanzania continued into 2001. Figure 67 shows annual precipitation anomalies for the Greater Horn of Africa in 2001. Except for Uganda, parts of eastern Kenya, and the tip of Somalia, which received normal or above-normal rainfall, the majority of East Africa experienced rainfall deficits of anywhere from 50 to more than 400 mm. At the end of the year, long-term drought conditions still prevailed across portions of northeastern Kenya, southern Somalia, and parts of southeastern Ethiopia, and rainfall totals were less than 50% of normal across most of the region.

Although the "long" rains that generally occur from March to May were near normal for the western areas of equatorial East Africa (e.g., Uganda, Burundi, Kenya, Rwanda), the seasonal rains were well below normal in northeastern Tanzania, eastern and northern Kenya, southern and eastern Ethiopia, and northeastern Kenya, which experienced its driest May since 1961. The short rains that usually begin in October, did not begin until November and consisted of sporadic short-lived events, which did little to alleviate the drought, which in some areas has persisted since 1998 (Lawrimore et al. 2001). Southeastern Kenya and northeastern Tanzania suffered especially from the much below normal November rainfall, which exacerbated residual dryness. Across southeastern Tanzania and northeastern Mozambique, no measurable rain fell in November. Despite some heavy rains in January 2001 (the heaviest in 40 years for parts of the region), the year concluded with annual rainfall totals well below normal for the third year in a row for much of East Africa.

3) Sahel rains

The Sahel receives approximately 90% of its mean annual rainfall during the June–September period.

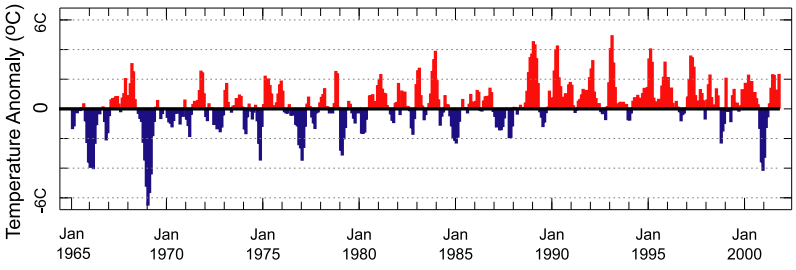

Fig. 72. Three-month running average temperature anomaly (°C) for the boxed region shown in Fig. 71. (Data from NOAA, Climate Prediction Center, CAMS.)

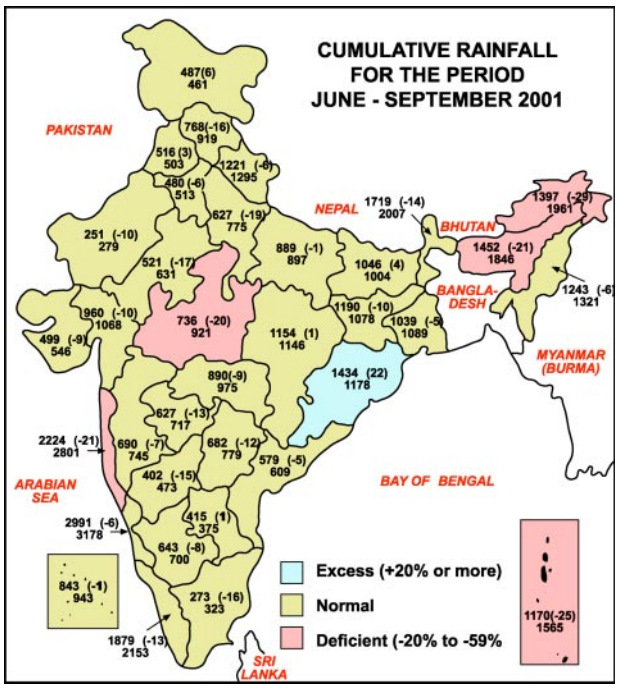

FIG. 73. Total Jun–Sep 2001 rainfall by meteorological subdivision. (Courtesy of the India Meteorological Department.)

This rainfall pattern is closely related to the intertropical convergence zone (ITCZ), which starts its northward migration in March and reaches its northernmost position near 15°N in August. Rainfall typically varies widely across the region, with long-term average totals reaching 1300 mm in the Guinean Highlands in the southwest, 700 mm in the southeast, and 100–300 mm in the north.

As in 2000 (Lawrimore et al. 2001), the Sahel, experienced a near-average rainy season overall during 2001 (Fig. 68). Area-averaged rainfall amounts ranged between 500 and 700 mm in the south, 300–500 mm in central Sahel, and 100–300 mm in the north (Fig. 69). These near-average rains were consistent with a return to normal of the global monsoon system. Near-average rains also prevailed in much of the Gulf of Guinea region. However, the Guinean Highlands to the west, were once again drier than normal, with rainfall totals ranging from 500 to 700 mm, more than 400 mm below the 1971–2000 mean. The eastern part of the Gulf of Guinea region, including eastern Nigeria and Cameroon was also drier than average, but rainfall deficits were only 100-400 mm below the climatological mean.

The atmospheric circulation during the 2001 season was also similar to that of 2000, and featured a moderately strong southerly and southwesterly flow of Atlantic tropical moisture at 925 hPa (not shown). The northward penetration of moisture was deeper across central Sahel. Strong northeasterly winds across northwestern Africa kept the moisture farther south in western Sahel. However, overall the low-level monsoonal flow was slightly enhanced at both 925 and 850 hPa (Fig. 70). At 850 hPa, an amplification of the St. Helen high pressure system, indicated by easterly wind anomalies 4 and 6 m s^{-1} along its equatorward flank, resulted in southwesterly to westerly wind anomalies averaging 1–2 m s^{-1}, which extended from northeastern South America and the eastern tropical Atlantic to southwestern Sahel. This monsoonal flow was comparable to the 2000 season and much weaker than in 1999 (Bell et al. 2000) when significantly above normal rainfall was observed in the Sahel. However, the low-level anomalous flow was associated with an area of midlevel cyclonic vorticity not extending past 15°N across much of the Sahel (Fig. 71), making it difficult for the African wave disturbances to develop. The area of enhanced cyclonic vorticity was confined over the Gulf of Guinea region. Accompanying these circulation features, an overall equatorward shift of the African easterly jet (AEJ) well south of 15°N across the Sahel and a near-average tropical easterly jet (TEJ; not shown) were evident. All these conditions are consistent with near-normal Sahel rainfall.

During 2001, the regional conditions that contributed to near-normal Sahel rains were linked to the return to normal of the global-scale monsoon system.

f. Asia

1) Harsh Siberian winter

The 2000–01 winter season was exceptionally cold across Siberia, Mongolia, and the far east of Russia (Fig. 71). In Mongolia, it was the second severe winter in a row with a repeat of dire consequences for livestock. In addition to its severity, the unusually cold winter is notable for its departure from a longer-term trend toward warmer conditions in the region (Fig. 72).

Climatologically, winter in the region generally extends from October to May. During the winter of 2000–01 unusually cold conditions developed over Siberia in November 2000 as an anomalous ridge in the upper-level flow developed west of the Ural Mountains with an accompanying, unusually deep downstream trough situated over eastern Asia. This flow pattern brought anomalously warm air to Europe while maintaining cold conditions over Siberia and Mongolia. This general pattern persisted for the next few months before finally breaking down in February of 2001, marking the end of the extreme cold in the region. The persistent stretch of cold coincided

with a strong negative phase of the Arctic Oscillation (AO). Although unusually warm conditions in Europe are not a feature generally associated with a negative AO, this was the strongest negative phase of the AO since 1995–96. In Siberia (i.e., boxed region in Fig. 71) the November–January 2001 period was the coldest in over 30 years with some areas recording the coldest winter since 1949.

Winter storms at the very start of 2001 brought significant snowfall to Mongolia, Manchuria, and the Korean Peninsula. Livestock mortality rates in Mongolia, already high due to the extreme cold, worsened as snow cover restricted access to grazing land on the country's vast steppes. By February 2001 nearly 850,000 livestock had reportedly died in Mongolia, twice the number of those lost at the same time the previous winter when roughly 10% of the total herd was lost. In the Chinese region of Inner Mongolia, heavy snow during early January 2001 blocked roads, isolating many small communities. The Chinese Red Cross indicated that the storms were the worst to impact the region in 50 years.

In Siberia and Russia's far east region the bitterly cold conditions were exacerbated by power and heating failures as high energy demand and high fuel prices limited power production. Cases of frostbite, hypothermia, and weather-related fatalities, although common in winter, were reported to be well above average.

Temperatures generally moderated throughout the region in February. Above-average temperatures during the boreal spring of 2001 (Fig. 72) enhanced snowmelt and contributed to flooding, especially in the Siberian region of Irkutsk and the Russian far east region of Yakutia. For the year 2001 as a whole, surface temperatures continued to be above the long-term (1961–90) mean for the region (Fig. 3).

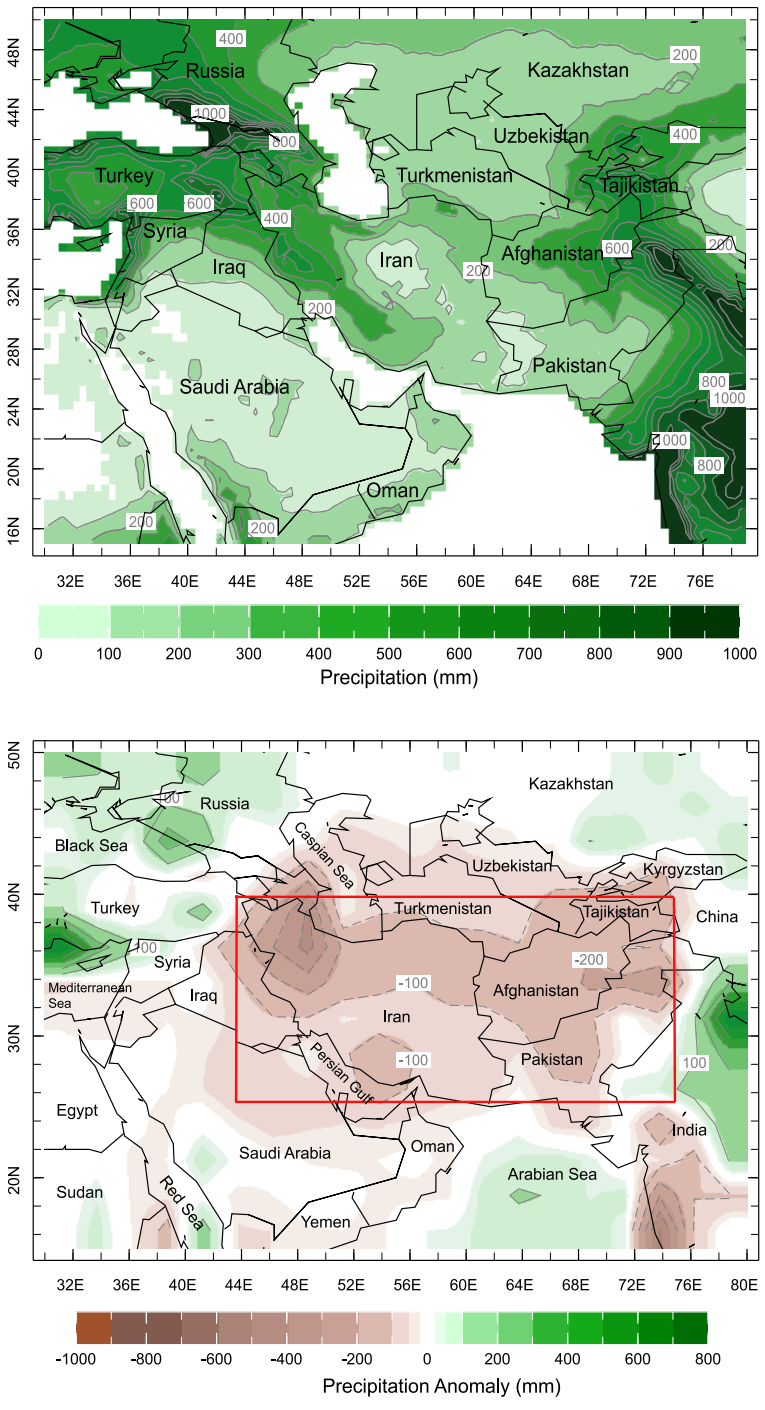

Fig. 74. (a) Climatological annual precipitation (mm) for 1961–90. Data from the University of East Anglia. (b) Precipitation anomaly (mm) for the year 2001. (Data from NOAA, Climate Prediction Center, CAMS_OPI.)

2) Asian southwest monsoon season

The Meteorological Department in India reported that 2001 marked the 13th consecutive normal (within 10% of the long-term average) summer monsoon with the cumulative, area-averaged precipitation totaling 92% of the 1961–90 mean (Fig. 73). The general characteristics of the 2001 mon-

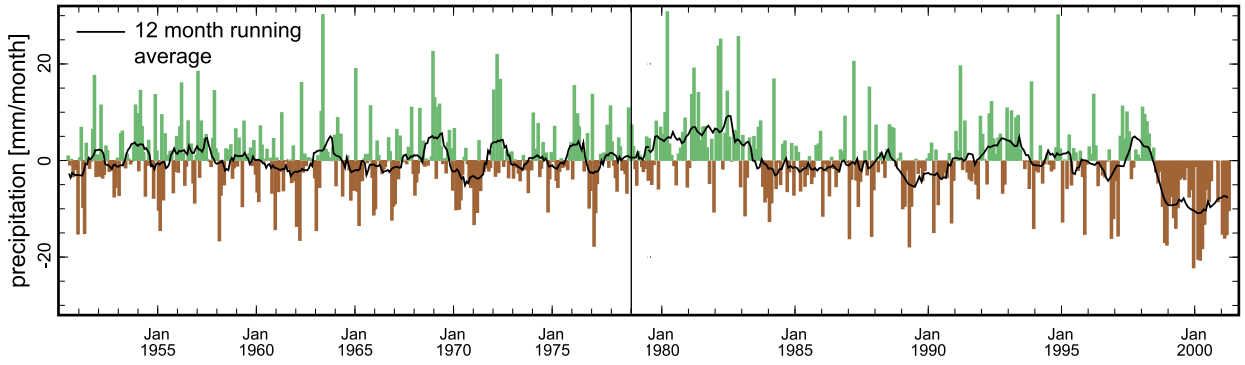

FIG. 75. Monthly precipitation anomaly (mm) averaged over boxed region shown in Fig. 74b for Jan 1950–Apr 2001. (Data for 1950–78 from the University of East Anglia; for 1979–2001 from NOAA, Climate Prediction Center, CAMS_OPI.)

soon were similar to those of the past two years with slightly below average June–September average rainfall (92% in 2000 and 96% in 1999). In addition, subdivisional data revealed that roughly two-thirds of all divisions received average to above-average rainfall, as has been the case since 1999. There were, however, some notable changes in the spatial distribution of rainfall in 2001.

Following widespread, above-average precipitation across much of India during the March–May period, the onset of the southwest monsoon in Kerala occurred on 23 May, one week earlier than average. The monsoon spread rapidly northward, encompassing all of India by 3 July, roughly 10 days ahead of its average progression. An early and vigorous monsoon brought abundant rainfall to the western states of Gujarat and Rajasthan during June and July, helping to ease a 2-yr drought. In northern Pakistan heavy July rainfall produced flash floods resulting in more than 100 fatalities while more moderate rainfall occurred in the eastern province of Punjab farther south. Anomalously low pressure in the northern Bay of Bengal during July resulted in very heavy rainfall in the state of Orissa with severe flooding in 22 of the state's 30 districts, destroying thousands of homes and affecting over 6 million people. Elsewhere, a widespread break in monsoon activity occurred during July, especially over the south-central sections of the peninsula and in the northeast states. Precipitation was sporadic during August with unusually dry conditions developing in much of Madhya Pradesh and Rajasthan while rainfall deficits persisted in parts of northeastern India in the state of Assam. The latter part of the monsoon season was somewhat more vigorous as more widespread precipitation developed in September, favoring eastern and southern areas as the monsoon underwent its southern retreat. Overall, the India Meteorological Department indicated 86% of the country received normal to excessive rainfall (within, and greater than 20% of the long-term average, respectively). Regions with the largest precipitation deficits for the June–September period (Fig. 73) were located in the northeast, north-central, and west coastal areas where precipitation was less than 80% of the long-term average.

In Southeast Asia the 2001 summer monsoon was mixed. June brought generally above average precipi-

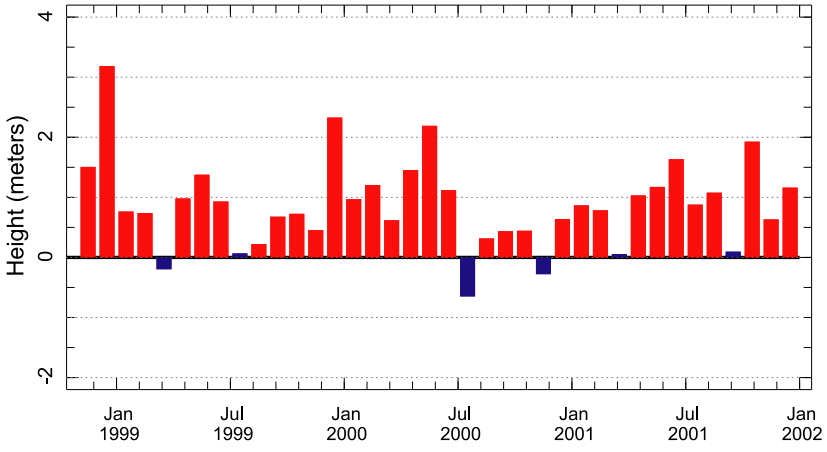

FIG. 76. Monthly standardized 250-hPa geopotential height anomaly for the boxed region in Fig. 74b for Nov 1998–Dec 2001. (Data from NCEP–NCAR reanalysis.)

tation with very heavy rainfall and severe local flooding in central Myanmar and southern Thailand. During July, rainfall was more erratic with precipitation well below average in many areas from south-central Thailand eastward across Cambodia to southern Vietnam. Roughly half of Cambodia's provinces, mainly in northern and western areas of the country, reported damage to rice crops due to the unusually dry conditions in July. Meanwhile, in northern Vietnam torrential rainfall associated with Typhoon Durian resulted in severe flooding in five highland provinces north of Hanoi.

A revived monsoon aided by tropical storm activity in some areas brought heavy rains to much of the Indo-China Peninsula during August. Tropical Storm Usagi crossed north-central Vietnam early in the month and tracked west across Laos into northern Thailand with attendant heavy rains resulting in severe flooding. Phetchabun was the hardest-hit province in Thailand with flash floods responsible for over 125 fatalities. Farther to the south and east, severe flooding occurred along the Mekong River in Cambodia and in the Mekong Delta in Vietnam. In these regions the flooding, although extensive, was not as severe as in 2000, which was the worst flooding observed in nearly 40 years (Lawrimore et al. 2001). Flooding was reported in 11 of Cambodia's 24 provinces as well as in 10 of the 12 delta provinces in Vietnam where more than 300 fatalities were reported. Flooding along the Mekong River generally peaked during September with water levels receding during the latter part of the month. Typhoon Lingling made landfall in south-central Vietnam during early November bringing another round of heavy rainfall to the region.

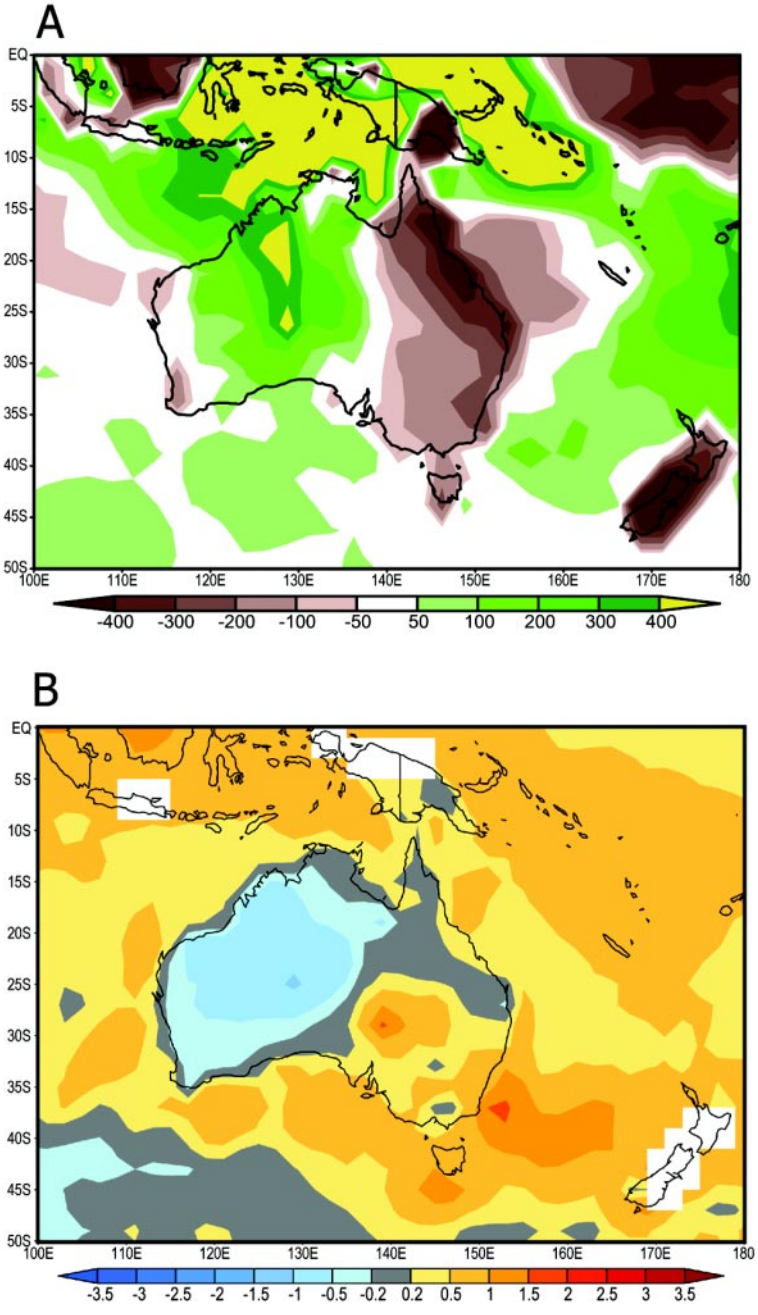

Fig. 77. (a) Annual CAMS precipitation anomalies (mm) for 2001 and (b) annual CAMS temperature anomalies (°C) for 2001.

3) Drought in Central and Southwest Asia

The climate of central and southwest Asia ranges from steppe to desert, with large areas of the region receiving little to no precipitation. The bulk of the precipitation that is received generally occurs between the months of November and April and is primarily associated with winter storms moving eastward from the Mediterranean with windward-facing slopes of the high mountains generally receiving the greatest amounts. This area includes the western Zagros Mountains in western Iran, the north slopes of the Albroz Mountains in northern Iran, and the slopes of the Hindu Kush in Afghanistan (Fig. 74a). In eastern Pakistan, the primary rainfall season occurs during boreal summer and is associated with the northernmost advance of the Asian monsoon.

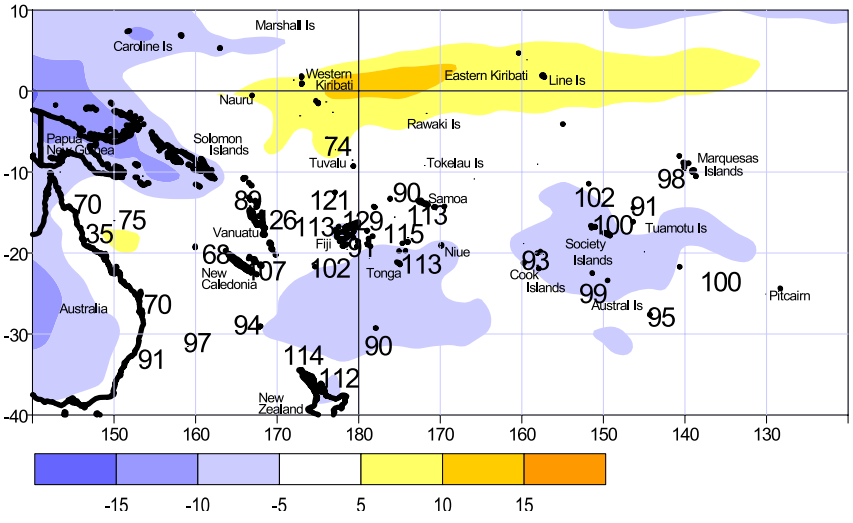

Fig. 78. OLR and rainfall anomalies for 2001. OLR anomalies, in W m^{-2}, are represented by hatched areas, and rainfall percentage of normal, shown by numbers. High radiation levels (yellow) are typically associated with clearer skies and lower rainfall, while cloudy conditions lower the OLR (blue) and typically mean higher rainfalls.

Widespread failure of the boreal winter precipitation in 2001 led to the third, and in some cases the fourth, consecutive year of drought in much of the region (Fig. 74b). Drought conditions extended from Iran eastward to Afghanistan and western Pakistan, while also affecting the southern states of Tajikistan, Uzbekistan, and Turkmenistan in the former Soviet Union. The drought was the worst in the region in at least 50 years (Fig. 75) with as many as 60 million affected.

Regionally, the impacts of the drought were severe. In Iran, 20 of the country's 28 provinces experienced shortfalls of precipitation during winter and spring 2001. The protracted drought left an estimated 37 million people, more than half the country's population, vulnerable to food and water insecurity according to a United Nations (UN) report. The most affected provinces were Fars, Keran, Khorasan, and Sistanva-Baluchistan. In Afghanistan widespread failure of rain-fed crops was reported in 2001 while irrigated agricultural output was significantly reduced due to a lack of water and failure of infrastructure. According to the UN's Food and Agricultural Organization, livestock in the country was depleted by 40% since 1998 owing to the drought. All of Pakistan's four provinces were affected although in the eastern plains of Pakistan (as well as in western India) the 2001 southwest monsoon brought above average rainfall and some relief. Elsewhere in Pakistan, however, the impact of the drought continued.

An anomalous ridge in the upper-level circulation was a persistent feature during the cold season in central and southern Asia over the past three years (Fig. 76). This pattern served to both inhibit the development of baroclinic storm systems in the region and to deflect eastward-propagating storms to the north of the drought-affected area. There is some evidence that this persistent and anomalous ridging pattern is associated with the combined effects of a prolonged La Niña and unusually warm surface temperatures in the western Pacific and eastern Indian Oceans (Barlow et al. 2002).

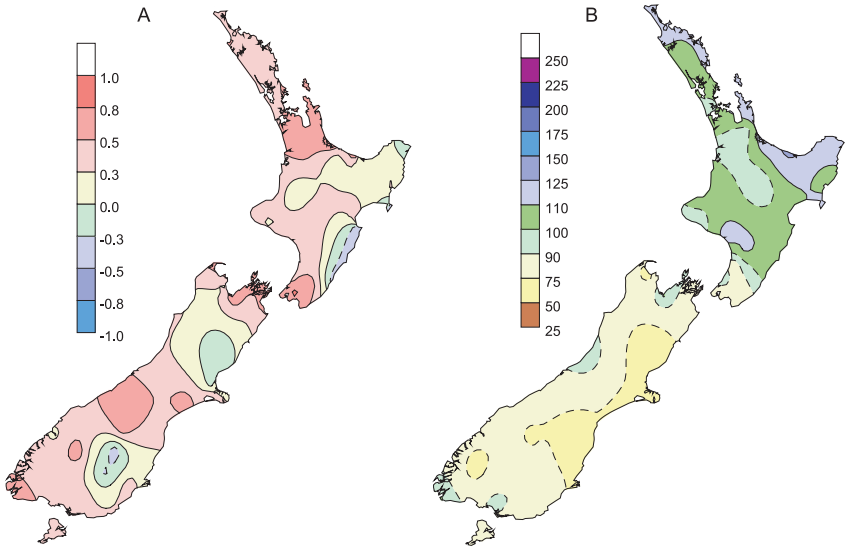

Fig. 79. (a) Jan–Dec 2001 mean temperature anomalies from the 1961–90 normal and (b) Jan–Dec 2001 percent of average precipitation from the 1961–90 normal.

g. Australasia and the South Pacific

1) Australia overview

A La Niña climate pattern dominated the weather over northern and central Australia in the early months of 2001, resulting in much above average rainfall. The waning of this pattern in autumn coincided with a return to more normal rainfall over most of the country. However, southern areas of the country experienced a mostly dry winter to early spring, associated with relatively weak midlatitude westerly flow over the Australian sector. Unusually cool conditions prevailed over the southern half in the period October–December, except along the east coast where serious bushfires broke out in New South Wales (NSW) near the end of December.

For the year as a whole, rainfall was well above normal over the western two-thirds of the continent (Fig. 77a) with a very wet 2000–01 summer in the north and west. Central Australia received much above average rainfall during January, March, June, October, and December. In contrast, much of eastern Australia experienced a dry 2001 (Fig. 77a), and the southwestern corner was particularly dry, with record low autumn and early winter rains. For the third consecutive year Australia as a whole had close to normal temperatures, however, the eastern half of the continent was generally warmer than normal, while wet conditions accompanied lower-than-normal temperatures in central and western areas (Fig. 77b).

2) January–May

January and February were exceptionally hot over extensive areas of south-central and southeastern Australia. In the first two weeks of January extreme heat affected a broad area of southern and inland Australia, with maximum temperatures at many locations approaching those of the renowned January 1939 heatwave. Maximum temperatures reached 47°C on several days, and over a widespread area, in the period 11–17 January with 48°C at Wudinna in south Australia on 13 January. At Oodnadatta, in far northern south Australia, the maximum temperature averaged just under 44°C for the first three weeks. Average January maxima were 4°–6°C above average over a broad area of south Australia, western NSW, and northwest Victoria. Unusually hot, and in many cases, dry conditions prevailed over essentially the same areas in February.

By contrast, heavy rain fell late in January around Alice Springs, which received 240 mm in four days, only 40 mm below the annual average. Flooding closed off most roads, and temporarily isolated Alice Springs. Heavy rain also soaked northern and eastern NSW. Many northeastern locations received over 200 mm in 24 h at the beginning of February, with peak falls up to 550 mm in 72 h. The Sydney metropolitan area received 150–250 mm of rain in 48 h, leading to flash flooding.

As the northern wet season ended and La Niña waned, conditions in April and May were mainly dry as high pressure predominated. Generally clear night skies led to below-average minimum temperatures in most areas. Southern Victoria, suffering from years of below-average rainfall, experienced heavy, though somewhat patchy, rain in late March and again in late April. In the latter event, some of the areas most affected by the drought that began in late in 1996 benefited most, notably the area west and southwest of Melbourne, which received over 150 mm in four days. Parts of the hilly country southeast and southwest of Melbourne received as much as 400 mm of rainfall during this time. However, dry conditions rapidly returned and the rains had no lasting impact on water storage. Southwestern Australia continued to experience dry conditions. Perth recorded its lowest ever September–April rainfall total of 98.4 mm (normal 258 mm). The previous record (over 124 yr of record) was 114 mm in 1957–58.

3) June–December

The period June through September was unusually dry and mild over much of southeastern Australia. In southwestern Australia, which is heavily dependent on winter rainfall, winter 2001 (June–August) was extremely dry, with many places experiencing record low rainfall. In Perth, despite one rainfall event totaling 88 mm late in July, this was the third driest winter on record, and followed an extremely dry nine months. In early September water restrictions were imposed on Perth residents, and on people in the inland Goldfields region who access water via a pipeline from the coast. By contrast, Broome (in northwest Australia) received over 90 mm of rain on 17 July, easily beating the previous wettest *monthly* July total of 72 mm in 1956.

The midnorth coast area of NSW also had a very dry winter, and warm, gusty winds fanned many bushfires in late winter and early spring (August–September). Scrub- and grass-fires were also more extensive than usual in the tropical savannah regions of the Northern Territory.

The period October–December was unusually cool over most of the southern half of Australia, with maximum temperatures in October and December averaging up to 3°–5°C below average over south-central Australia. Most of the country experienced above-average rainfall in October and November, with well

above average rainfall in the former month relieving the prospect of water restrictions in the Melbourne metropolitan area. Frequent tropical moisture inflows into central Australia in late November and through much of December produced extremely heavy rain and flooding in that area. Early in December as much as 260 mm fell within a week, in an area where the annual average rainfall is only about 250–300 mm yr^{-1}. At Giles, over central Australia near the western Australia–Northern Territory border, the December total rainfall of 338 mm was the highest recorded in any month.

In contrast to these conditions, the eastern coast from southern NSW to the northern Cape York Peninsula was warmer than normal over the last three months. The onset of persistent hot, dry northwesterly winds late in December resulted in disastrous bushfires over eastern New South Wales, in coastal districts and the adjacent ranges. Eastern Queensland experienced unrelenting heat in late December, many places having their hottest Christmas–New Year period since 1903. At Townsville, the December highest minimum temperature record of 28.1°C was broken four times in the week between Christmas and New Year.

4) Southwest Pacific and New Zealand

The year 2001 was one of contrasts across the Southwest Pacific. Important drivers of the annual pattern were the transition from La Niña to neutral ENSO conditions, the strength of the trade winds, and the distribution of warm and cool SST anomalies.

A noticeable shift from below- to above-average SSTs occurred from June onward over Kiribati, with a return to neutral ENSO conditions. Mean air temperatures were 0.3°–0.5°C above normal for the year in New Caledonia, Fiji, Tuvalu, Tonga, and parts of Vanuatu, and near average elsewhere.

The La Niña impact on rainfall distribution was evident in the annual anomaly pattern (Fig. 78), even after a return to neutral ENSO conditions, as enhanced trade winds east of the date line kept the South Pacific convergence zone (SPCZ) farther south and west than usual for much of the year. Below average rainfall was recorded in the central equatorial region (western and central Kiribati, Tuvalu, Tokelau, and the Northern Cooks), where the first half of the year was very dry. SSTs were below average in the areas where below-normal rainfall occurred. Annual rainfall was less than 75% of normal in some of these areas. Rainfall was also below normal in the southwest Coral Sea. Areas of enhanced rainfall and below-average outgoing longwave radiation occurred in the west, from Papua New Guinea to Tonga including the Solomons, and parts of Vanuatu and Fiji, with totals exceeding 120% of average on some islands. SSTs were above average in these areas.

The southwest Pacific tropical cyclone season of November 2000–April 2001 was the least active since that of 1994–95. It had the latest start for any season in at least 30 years. There were only five occurrences overall, with four occurring in just a few weeks between 20 February and 5 March. None resulted in severe damage or loss of life.

In New Zealand, anticyclonic conditions were more prevalent than normal across the South Island for the first nine months of the year. However pressures were much lower than normal in the Tasman Sea and across the North Island from October to December 2001. Overall for 2001, pressures were higher than normal across the South Island, and below average to the north of New Zealand, with more easterlies and northeasterlies in the north. Above-average SSTs contributed to generally higher than normal land temperatures, and contributed to stormy conditions from October to December.

The 2001 average temperature across New Zealand was 12.8°C, which was 0.3°C above normal (Fig. 79a). For New Zealand as a whole, there were eight warmer-than-normal months (including five exceptionally warm months: May, August, September, October, and December), and two very much cooler than normal months (January and July). Annual mean temperatures in 2001 were normal to above normal in most areas, except for a few eastern districts.

The circulation anomalies produced one of the driest years since records began in many eastern South Island areas (Fig. 79b). However, frequent troughs in the Tasman Sea and over the North Island for the last three months produced a warm and wet end, especially for the North Island. The year was also extremely dry in parts of Wellington (located at the south end of North Island). Precipitation was well below normal in southern Wairarapa (southern North Island), and below normal in most other South Island areas, where values were 60%–75% of normal in some areas. It was wetter than normal in parts of Northland, Coromandel, and Bay of Plenty (northern North Island). The severe austral summer (DJF)–autumn (MAM) drought was a major contributor to the extremely low South Island and southern North Island annual precipitation totals.

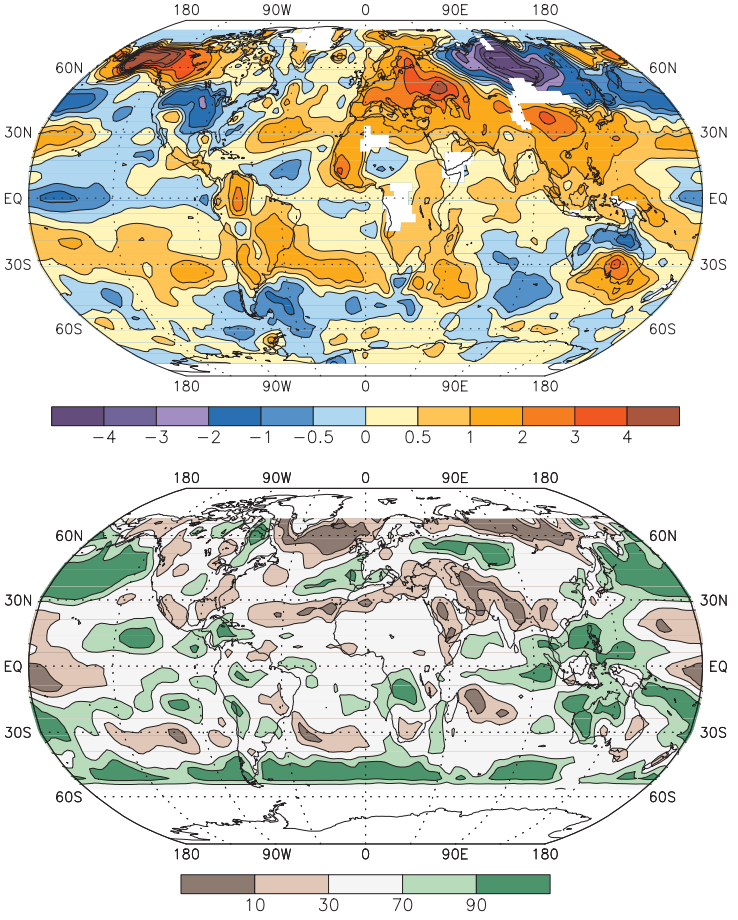

FIG. 80. Dec 2000–Feb 2001 surface temperature anomalies (top, °C) and precipitation percentiles based on a gamma distribution fit to the 1979–2000 base period (bottom). Temperature anomalies (1971–2000 base period) are based on station data over land and SST over water. Precipitation data are obtained from merge of rain gauge observations and satellite-derived precipitation estimates (Janowiak and Xie 1999). The analysis is omitted in data-sparse regions (white areas).

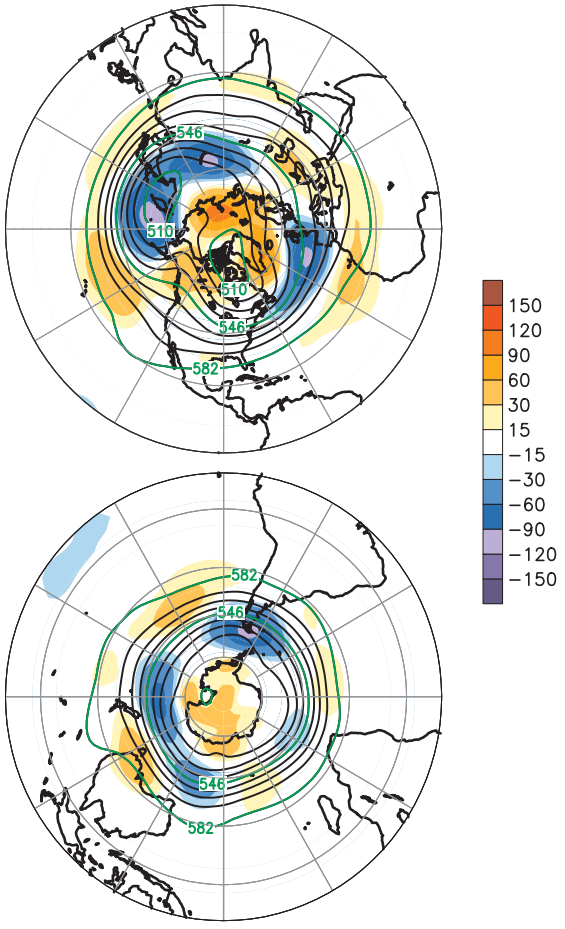

FIG. 81. Dec 2000–Feb 2001 Northern Hemisphere (top) and Southern Hemisphere (bottom) 500-hPa geopotential heights (contour interval is 9 dam) and anomalies (shading). Anomalies are departures from the 1979–2000 base period means.

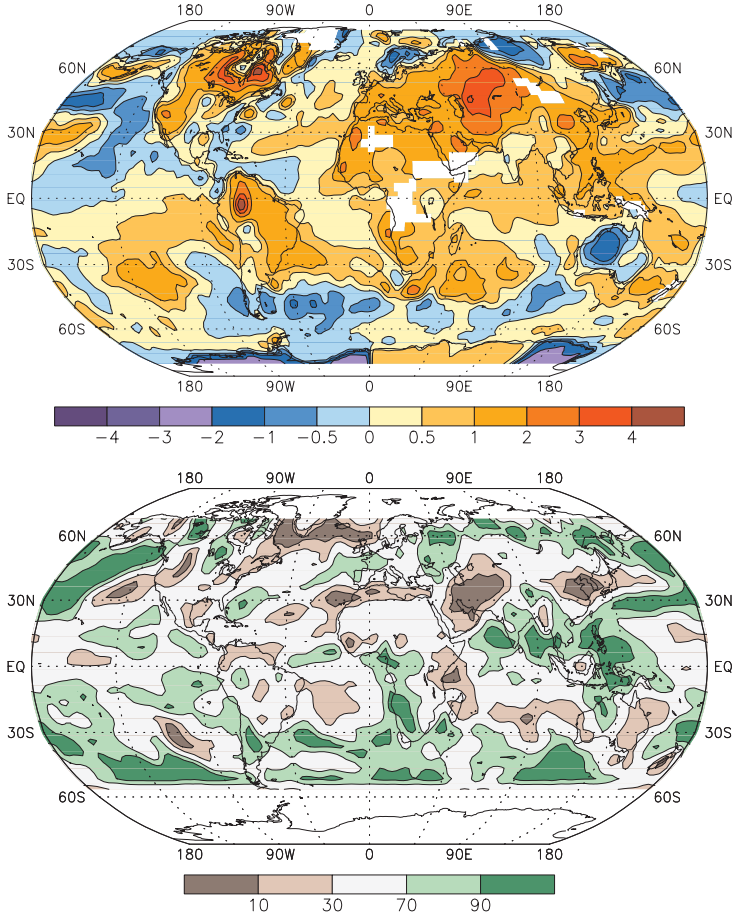

FIG. 82. Mar–May 2001 surface temperature anomalies (top, °C) and precipitation percentiles based on a gamma distribution fit to the 1979–2000 base period (bottom). Temperature anomalies (1971–2000 base period) are based on station data over land and SST over water. Precipitation data are obtained from a merge of rain gauge observations and satellite-derived precipitation estimates (Janowiak and Xie 1999). The analysis is omitted in data-sparse regions (white areas).

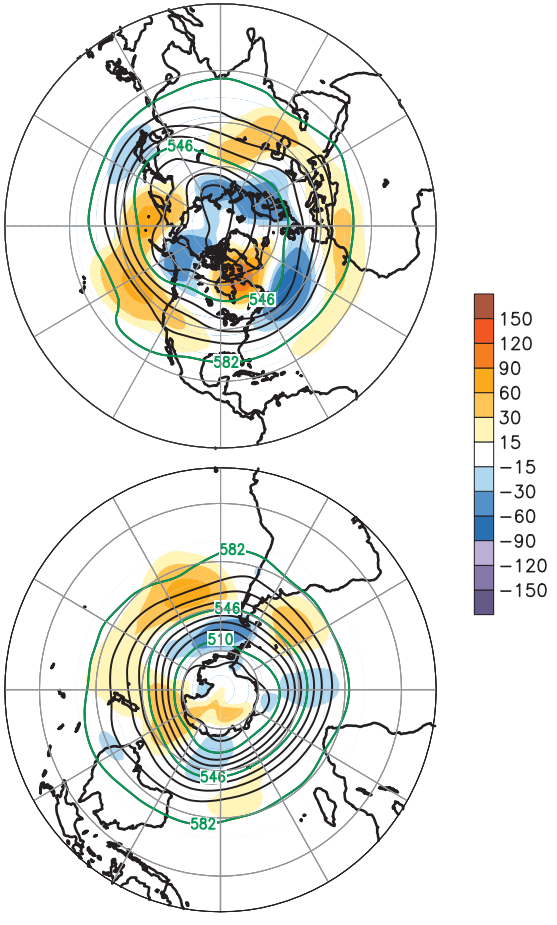

FIG. 83. Mar–May 2001 Northern Hemisphere (top) and Southern Hemisphere (bottom) 500-hPa geopotential heights (contour interval is 9 dam) and anomalies (shading). Anomalies are departures from the 1979–2000 base period means.

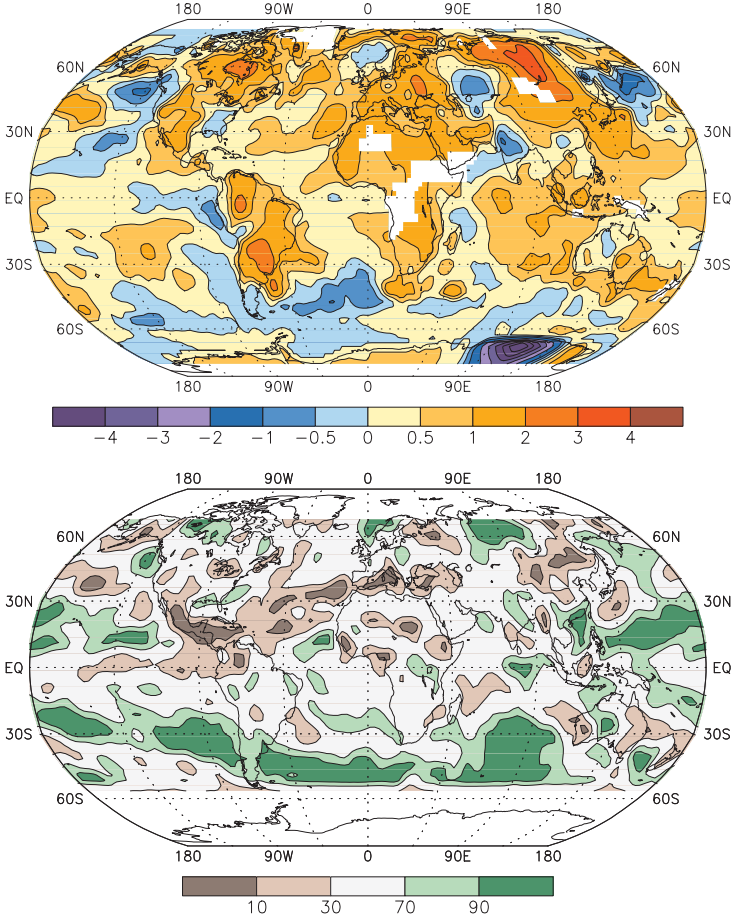

Fig. 84. Jun–Aug 2001 surface temperature anomalies (top, °C) and precipitation percentiles based on a gamma distribution fit to the 1979–2000 base period (bottom). Temperature anomalies (1971–2000 base period) are based on station data over land and SST over water. Precipitation data are obtained from a merge of rain gauge observations and satellite-derived precipitation estimates (Janowiak and Xie 1999). The analysis is omitted in data-sparse regions (white areas).

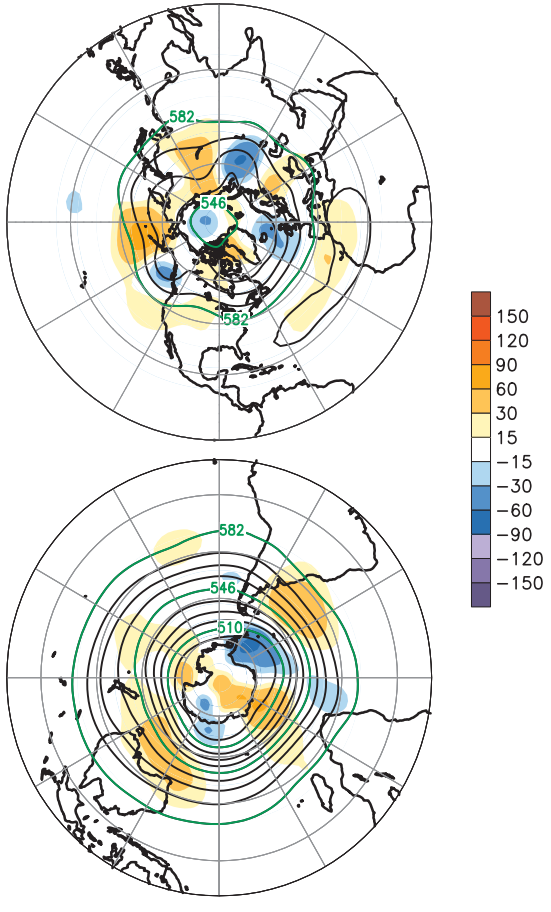

Fig. 85. Jun–Aug 2001 Northern Hemisphere (top) and Southern Hemisphere (bottom) 500-hPa geopotential heights (contour interval is 9 dam) and anomalies (shading). Anomalies are departures from the 1979–2000 base period means.

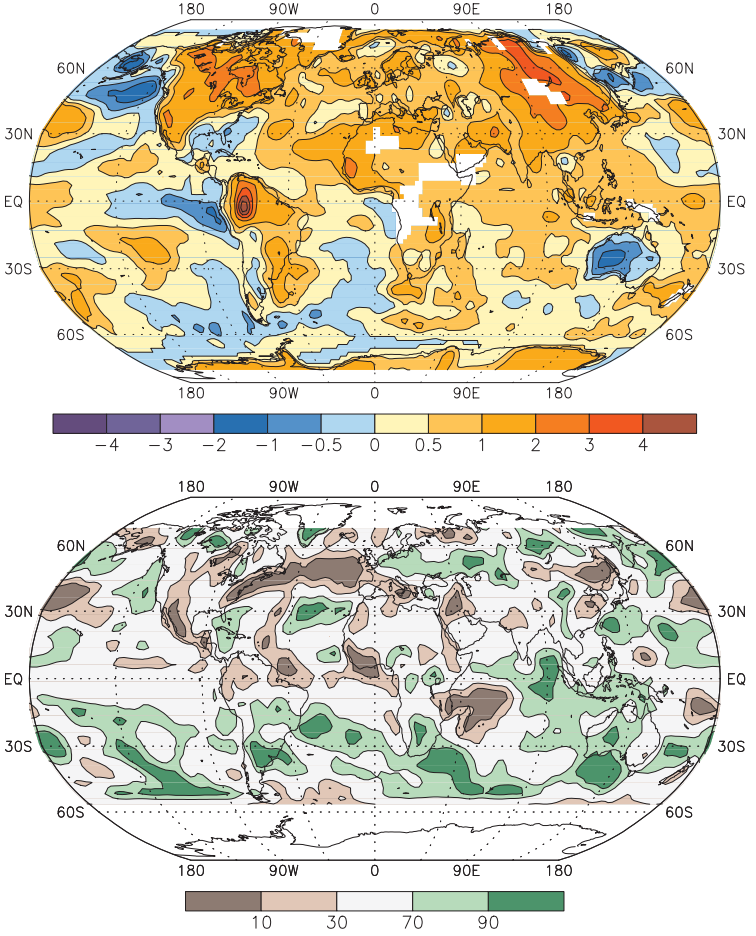

FIG. 86. Sep–Nov 2001 surface temperature anomalies (top,°C) and precipitation percentiles based on a gamma distribution fit to the 1979–2000 base period (bottom). Temperature anomalies (1971–2000 base period) are based on station data over land and sea surface temperature over water. Precipitation data are obtained from a merge of rain gauge observations and satellite-derived precipitation estimates (Janowiak and Xie 1999). The analysis is omitted in data-sparse regions (white areas).

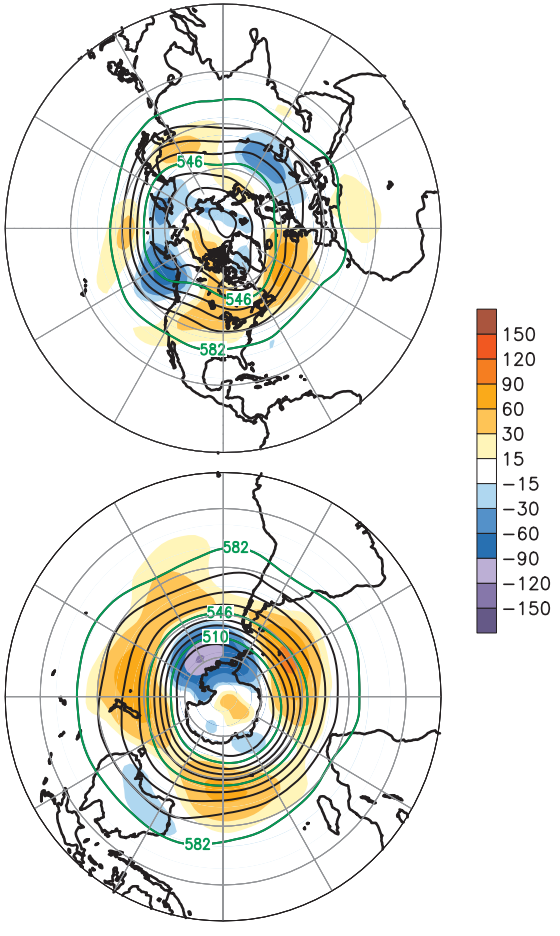

FIG. 87. Sep–Nov 2001 Northern Hemisphere (top) and Southern Hemisphere (bottom) 500-hPa geopotential heights (contour interval is 9 dam) and anomalies (shading). Anomalies are departures from the 1979–2000 base period means.

ACKNOWLEDGMENTS. This assessment would not have been possible without assistance and contributions from many scientists around the world. These scientists are named in the appendix and include a broad cross section of expertise from within the NOAA community, from other federal laboratories, from universities, and from other sites across the globe. We would like to thank them all for their timely and valuable input. We would also like to thank the anonymous reviewers whose comments and suggestions improved this article. This assessment was supported by a grant from the NOAA Office of Global Program's Climate Change Data and Detection Program.

APPENDIX: CONTRIBUTORS

Environment Canada, Ottawa, Canada
- David Phillips
- Bob Whitewood

National Climatic Data Center
- Scott Stephens
- Tom Peterson
- Trevor Wallis

Hadley Centre for Climate Prediction
- Nick Rayner

University of Alaska, Fairbanks
- George Divoki

NASA Goddard Institute of Space Studies (GISS)
- Jim Hansen

University of Illinois, Urbana–Champaign
- Bill Chapman

NOAA/Climate Monitoring and Diagnostics Laboratory/OAR
- B. Bodhaine
- J. Butler
- T. Conway
- E. Dlugokencky
- E. Dutton
- G. Dutton
- J. Elkins
- B. Hall
- B. Johnson
- D. Mondeel
- S. Montzka
- P. Novelli
- S. Oltmans
- T. Thompson

REFERENCES

Alexander, L. V., and P. D. Jones, 2001: Updated precipitation series for the U.K. and discussion of recent extremes. *Atmos. Sci. Lett.,* **1**(2), 142–150. [Available online from http://www.idealibrary.com/links/doi/10.1006/asle.2001.0025.]

Barlow, M., H. Cullen, and B. Lyon, 2002: Drought in central and southwest Asia: La Niña, the warm pool, and Indian Ocean precipitation. *J. Climate,* **15,** 697–700.

Bell, G. D., and M. Chelliah, 1999: The African easterly jet and its link to Atlantic basin tropical cyclone activity and the global monsoon system. *Proc. 23d Annual Climate Diagnostics Workshop*, Miami, FL, NOAA/NCEP, 215–218.

——, and Coauthors, 1999: Climate Assessment for 1998. *Bull. Amer. Meteor.* Soc., **80** (May), S1–S48.

——, and Coauthors, 2000: Climate Assessment for 1999. *Bull. Amer. Meteor.* Soc., **81** (May), S1–S50.

Bodhaine, B. A., B. G. Mendonca, J. M. Harris, and J. M. Miller, 1981: Seasonal variation in aerosols and atmospheric transmission at Mauna Loa Observatory. *J. Geophys. Res.*, **86**, 7395–7398.

Butler, J. H., S. A. Montzka, A. D. Clarke, J. M. Lobert, and J. W. Elkins, 1998: Growth and distribution of halons in the atmosphere. *J. Geophys. Res.,* **103** (D1), 1503–1511.

Chanin, M. L., and V. Ramaswamy, 1999: Trends in Stratospheric Temperatures. WMO Scientific Assessment of Ozone Depletion: 1998, Global Ozone Research and Monitoring Project—Rep. 44, Geneva, Switzerland, 5.1–5.59.

Chen, J., B. E. Carlson, and A. D. Del Genio, 2002: Evidence for strengthening of the tropical general circulation in the 1990s. *Science,* **295,** 838–841.

Christy, J. R., R. W. Spencer, and W. D. Braswell, 2000: MSU tropospheric temperatures: Dataset construction and radiosonde comparisons. *J. Atmos. Oceanic Technol.,* **17**, 1153–1170.

——, D. E. Parker, S. J. Brown, I. Macadam, M. Stendel, and W. B. Norris, 2001: Differential trends in tropical sea surface and atmospheric temperatures. *Geophys. Res. Lett.*, **28,** 183–186.

Ciais, P., P. P. Tans, and M. Trolier, 1995: A large northern-hemisphere terrestrial CO_2 sink indicated by the $^{13}C/^{12}C$ ratio of atmospheric CO_2. *Science,* **269,** 1098–1102.

Conway, T. J., P. P. Tans, L. S. Waterman, K. W. Thoning, D. R. Kitzis, K. A. Masarie, and N. Zhang, 1994: Evidence for interannual variability of the carbon cycle from the NOAA CMDL global air sampling network. *J. Geophys. Res.,* **99,** 22 831–22 855.

CPC, 2001a: *Climate Diagnostics Bulletin.* Vol. 01, No. 8, 85 pp.

CPC, 2001b: *Climate Diagnostics Bulletin.* Vol. 01, No. 10, 86 pp.

CPC, 2001c: *Climate Diagnostics Bulletin.* Vol. 01, No. 11, 89 pp.

Daniel, J. S., and S. Solomon, 1998: On the climate forcing of carbon monoxide. *J. Geophys. Res.,* **103,** 13 249–13 260.

Dlugokencky, E. J., E. G. Dutton, P. C. Novelli, P. P. Tans, K. A. Masarie, K. O. Lantz, and S. Madronich, 1996: Changes in CH_4 and CO growth rates after the eruption of Mt. Pinatubo and their link with changes in tropical tropospheric UV flux. *Geophys. Res. Lett.,* **23,** 2761–2764.

——, K. A. Masarie, P. M. Lang, and P. P. Tans, 1998: Continuing decline in the growth rate of the atmospheric methane burden. *Nature,* **393,** 447–450.

——, B. P. Walter, K. A. Masarie, P. M. Lang, and E. S. Kasischke, 2001: Measurements of an anomalous global methane increase during 1998. *Geophys. Res. Lett.,* **28,** 499–502.

Dutton, E. G., and B. A. Bodhaine, 2001: Solar irradiance anomalies caused by clear-sky transmission variations above Mauna Loa: 1958–99. *J. Climate,* **14,** 3255–3262.

——, J. J. DeLuisi, and A. P. Austring, 1985: Interpretation of Mauna Loa atmospheric transmission relative to aerosols, using photometric precipitable water amounts. *J. Atmos. Chem.*, **3,** 53–68.

Elkins, J. W., T. M. Thompson, T. H. Swanson, J. H. Butler, B. D. Hall, S. O. Cummings, D. A. Fisher, and A. G. Raffo, 1993: Decrease in the growth rates of atmospheric chlorofluorocarbons 11 and 12. *Nature,* **364,** 780–783.

Ellis, H. T., and R. F. Pueschel, 1971: Solar radiation: Absence of air pollution trends at Mauna Loa. *Science,* **172,** 845–846.

Gaffen, D. J., B. D. Santer, J. S. Boyle, J. R. Christy, N. E. Graham, and R. J. Ross, 2000: Multidecadal changes in the vertical structure of the tropical troposphere. *Science,* **287,** 1242–1245.

Goldenberg, S. B., and L. J. Shapiro, 1996: Physical mechanisms for the association of El Niño and West African rainfall with Atlantic major hurricanes. *J. Climate,* **9,** 1169–1187.

——, C. W. Landsea, A. M. Mestas-Nuñez, and W. M. Gray, 2001: The recent increase in Atlantic hurricane activity: Causes and implications. *Science,* **293,** 474–479.

GPCC, 1998: The Global Precipitation Climatology Centre. [Available online at http://www.dwd.de/research/gpcc.]

Gray, W. M., 1990: Strong association between West African rainfall and U.S. landfall of intense hurricanes. *Science,* **249,** 1251–1256.

Hansen, J. E., and M. Sato, 2001: Trends of measured climate forcing agents. *Proc. Natl. Acad. Sci.,* **98,** 14 778–14 783.

Holloway, T., H. Levy II, and P. Kasibhatla, 2000: The global distribution of carbon monoxide. *J. Geophys. Res.,* **12,** 123.

Horton, E. B., C. K. Folland, and D. E. Parker, 2001: The changing incidence of extremes in worldwide and central England temperatures to the end of the twentieth century. *Climatic Change,* **50,** 267–295.

Houghton, J. T., Y. Ding, D. J. Griggs, M. Noguer, P. J. van der Linden, D. Xiaosu, K. Maskell, and C. A. Johnson, Eds., 2001: *Climate Change 2001: The Scientific Basis.* Cambridge University Press, 892 pp.

Hurrell, J., S. J. Brown, K. E. Trenberth, and J. R. Christy, 2000: Comparison of tropospheric temperatures from radiosondes and satellites: 1979-1998. *Bull. Amer. Meteor. Soc.,* **81,** 2165–2177.

Jacka, T. H., and W. F. Budd, 1998: Detection of temperature and sea-ice extent changes in the Antarctic and Southern Ocean. *Ann. Glaciol.,* **27,** 553–559.

Jones, P. D., and D. Conway, 1997: Precipitation in the British Isles: An analysis of area-average data updated to 1995. *Int. J. Climatol.,* **17,** 427–438.

——, T. J. Osborn, K. R. Briffa, C. K. Folland, E. B. Horton, L. V. Alexander, D. E. Parker, and N. A. Rayner, 2001: Adjusting for sampling density in grid-box land and ocean surface temperature time series. *J. Geophys. Res.,* **106**, 3371–3380

Karlsdóttir, S., and I. S. A. Isaksen, 2000: Changing methane lifetime: possible cause for reduced growth. *Geophys. Res. Lett.*, **27,** 93–96.

Kasischke, E. S., and L. P. Bruhwiler, 2002: Emissions of carbon dioxide, carbon monoxide and methane from boreal forest fires in 1998. *J. Geophys. Res.*, in press.

Keeling, C. D., T. P. Whorf, M. Wahlen, and J. Vanderplicht, 1995: Interannual extremes in the rate of rise of atmospheric carbon dioxide since 1980. *Nature,* **375,** 666–670.

Landsea, C. W., 1993: The climatology of intense (or major) Atlantic hurricanes. *Mon. Wea. Rev.,* **121,** 1703–1713.

——, G. D. Bell, W. M. Gray, and S. B. Goldenberg, 1998: The extremely active 1995 Atlantic hurricane season: Environment conditions and verification of seasonal forecasts. *Mon. Wea. Rev.,* **126,** 1174–1193.

——, R. A. Pielke, A. M. Mestas-Nuñez, and J. A. Knaff, 1999: Atlantic Basin hurricanes: Indices of climate changes. *Climate Change,* **42,** 89–129.

Lawrimore, J., and Coauthors, 2001: Climate Assessment for 2000. *Bull. Amer. Meteor. Soc.,* **82** (May), S1–S55.

Lelieveld, J., P. J. Crutzen, and C. Brühl, 1993: Climate effects of atmospheric methane. *Chemosphere,* **26,** 739–768.

Levine, J. S., 1999: The 1997 fires in Kalimantan and Sumatra, Indonesia, gaseous and particulate emissions. *Geophys. Res. Lett.,* **26,** 815.

Maloney, E. D., and D. L. Hartmann, 2000: Modulation of hurricane activity in the Gulf of Mexico by the Madden–Julian Oscillation. *Science,* **287,** 2002–2004.

Mo, K. C., 2000: The association between intraseasonal oscillations and tropical storms in the Atlantic Basin. *Mon. Wea. Rev.,* **128,** 4097–4107.

Montzka, S. A., J. H. Butler, R. C. Myers, T. M. Thompson, T. H. Swanson, A. D. Clarke, L. T. Lock, and J. W. Elkins, 1996: Decline in the tropospheric abundance of halogen from halocarbons: Implications for stratospheric ozone depletion. *Science,* **272,** 1318–1322.

——, ——, J. W. Elkins, T. M. Thompson, A. D. Clarke, and L. T. Lock, 1999: Present and future trends in the atmospheric burden of ozone-depleting halogens. *Nature,* **398,** 690–694.

——, C. M. Spivakovsky, J. H. Butler, J. W. Elkins, L. T. Lock, and D. J. Mondeel, 2000: New observational constraints for atmospheric hydroxyl on global and hemispheric scales. *Science,* **288,** 500–503.

Novelli, P. C., K. A. Masarie, and P. M. Lang, 1998: Distributions and recent changes of carbon monoxide in the lower troposphere. *J. Geophys. Res.,* **103,** 19 015–19 033.

Parker, D. E., T. P. Legg, and C. K. Folland, 1992: A new daily Central England Temperature series, 1772-1991. *Int. J. Climatol.,* **12,** 317–342.

Peterson, T. C., and R. S. Vose, 1997: An overview of the Global Historical Climatology Network temperature database. *Bull. Amer. Meteor. Soc.,* **78,** 2837–2849.

Reed, R. J., D. C. Norquist, and E. E. Recker, 1977: The structure and properties of African wave disturbances as observed during Phase III of GATE. *Mon. Wea. Rev.,* **105,** 317–333.

Reynolds, R. W., and T. M. Smith, 1994: Improved global sea surface temperature analyses using optimum interpolation. *J. Climate*, **7,** 929–948.

Rudolf, B., H. Hauschild, W. Rueth, and U. Schneider, 1994: Terrestrial precipitation analysis: Operational method and required density of point measurements. *Global Precipitations and Climate Change,* M. Desbois and F. Desalmond, Eds., NATO ASI Series I, Vol. 26, Springer-Verlag, 173–186.

Shapiro, L. J., and S. B. Goldenberg, 1998: Atlantic sea surface temperatures and tropical cyclone formation. *J. Climate*, **11**, 578–590.

Simpson, R. H., 1974: The hurricane disaster potential scale. *Weatherwise*, **27**, 169–186.

Smith, T. M., R. W. Reynolds, R. E. Livezey, and D. C. Stokes, 1996: Reconstruction of historical sea surface temperature using empirical orthogonal functions. *J. Climate,* **9,** 1402–1420.

Stendel, M., J. R. Christy, and L. Bengtsson, 2000: Assessing levels of uncertainty in recent temperature time series. *Climate Dynamics,* **16**(8), 587–601.

Wotawa, G., P. C. Novelli, M. Trainer, and C. Granier, 2001: Interannual variability of summertime CO concentrations in the Northern Hemisphere explained by boreal forest fires in North America and Russia. *Geophys. Res. Lett.,* **28,** 4575.